

Late Paleozoic Felsic Volcanics in Southern New Brunswick and
Related Uranium Mineralization

By
Taryn Rosemary Gray Hons. B.Sc.

A Thesis Submitted to
Saint Mary's University, Halifax, Nova Scotia
in Partial Fulfillment of the Requirements for
the Degree of Master of Applied Science.

August, 2010, Halifax, Nova Scotia

Copyright Taryn Rosemary Gray, 2010

Approved:

Dr. Jaroslav Dostal
Professor Emeritus

Approved:

Dr. Jacob Hanley
Assistant Professor

Approved:

Dr. Robert Singer
Professor

Approved:

Dr. Marcos Zentilli
Professor Emeritus

Date:

August 4, 2010



Library and Archives
Canada

Published Heritage
Branch

395 Wellington Street
Ottawa ON K1A 0N4
Canada

Bibliothèque et
Archives Canada

Direction du
Patrimoine de l'édition

395, rue Wellington
Ottawa ON K1A 0N4
Canada

Your file *Votre référence*
ISBN: 978-0-494-68828-1
Our file *Notre référence*
ISBN: 978-0-494-68828-1

NOTICE:

The author has granted a non-exclusive license allowing Library and Archives Canada to reproduce, publish, archive, preserve, conserve, communicate to the public by telecommunication or on the Internet, loan, distribute and sell theses worldwide, for commercial or non-commercial purposes, in microform, paper, electronic and/or any other formats.

The author retains copyright ownership and moral rights in this thesis. Neither the thesis nor substantial extracts from it may be printed or otherwise reproduced without the author's permission.

In compliance with the Canadian Privacy Act some supporting forms may have been removed from this thesis.

While these forms may be included in the document page count, their removal does not represent any loss of content from the thesis.

AVIS:

L'auteur a accordé une licence non exclusive permettant à la Bibliothèque et Archives Canada de reproduire, publier, archiver, sauvegarder, conserver, transmettre au public par télécommunication ou par l'Internet, prêter, distribuer et vendre des thèses partout dans le monde, à des fins commerciales ou autres, sur support microforme, papier, électronique et/ou autres formats.

L'auteur conserve la propriété du droit d'auteur et des droits moraux qui protègent cette thèse. Ni la thèse ni des extraits substantiels de celle-ci ne doivent être imprimés ou autrement reproduits sans son autorisation.

Conformément à la loi canadienne sur la protection de la vie privée, quelques formulaires secondaires ont été enlevés de cette thèse.

Bien que ces formulaires aient inclus dans la pagination, il n'y aura aucun contenu manquant.


Canada

Late Paleozoic Felsic Volcanic Rocks in Southern New Brunswick and
Related Uranium Mineralization

By
Taryn Rosemary Gray Hons. B.Sc.

A Thesis Submitted to
Saint Mary's University, Halifax, Nova Scotia
in Partial Fulfillment of the Requirements for
the Degree of Master of Applied Science.

August, 2010, Halifax, Nova Scotia

Copyright Taryn Rosemary Gray, 2010

Approved: Dr. Jaroslav Dostal
Professor Emeritus

Approved: Dr. Jacob Hanley
Assistant Professor

Approved: Dr. Robert Singer
Professor

Approved: Dr. Marcos Zentilli
Professor Emeritus

Date: August 4, 2010

Late Paleozoic Felsic Volcanic Rocks in Southern New Brunswick and Related Uranium Mineralization

by Taryn Rosemary Gray Hons. B.Sc.

Abstract

Three units of Late Paleozoic felsic volcanics within southern New Brunswick were examined geochemically and petrographically to determine their genetic history and economic potential. The Late Devonian Harvey and Piskahegan Groups are predominantly composed of peraluminous volcanics, and were previously considered coeval since they contain similar stratigraphy, and formed during the same pulse of igneous activity. The younger, Viséan aged Cumberland Hill formation is characterized by peralkaline trachytes and rhyolites, forming through extensive fractional crystallization of alkali basaltic magma, likely derived from a mantle plume. The Harvey, and to a lesser extent, Piskahegan Group display excellent economic potential, enriched in uranium and rare earth elements. Cumberland Hill exhibited significantly lower concentrations of economic elements, slightly elevated in incompatible trace elements, including uranium. This study determined Harvey and Piskahegan are not genetically related, it also refined the genetic history and economic potential of southern New Brunswick.

August 4, 2010

ACKNOWLEDGEMENTS

I would like to start by thanking Dr. Jaroslav Dostal for providing me with an interesting topic that combined my love for geochemistry and allowed me to apply it to a new realm of geology that I previously had little experience with. Dr. Dostal taught me the importance of the big picture and looking outside oneself to find the answers. I do not think a person could find a warmer, more genuine supervisor. I am very thankful for all he taught me, and expanding my horizons into the world of petrology and economic based geological problems.

I would also like to thank Henry Schwarcz for getting me involved in geology, and leading me to work with Dr. Dostal, a former student of his, who he spoke very highly of. As a second year undergrad studying psychology of all things, I stumbled into the office of a very revered geochemist, although I did not know this at the time. During my interview for a summer research assistant, he captivated me with talks of climate records derived from teeth; I was hooked. Had it not been for that interview, and Dr. Henry Schwarcz taking a chance on me, I would never have found geology. For this, and his continued friendship, I am always grateful.

Several people also played an important role intellectually in the completion of this thesis. Thank you to Dr. Jacob Hanley for all the times I dropped into your office to ask you questions, your assistance with the LA-ICP-MS melt inclusion analyses, and of course the careful editing of Chapter 3 and comments on the rest of the thesis. I would also like to thank Marcos Zentilli for his time editing my grant proposals, and for acting as my external examiner; your continued input has greatly aided my thesis. Thank you to

Duncan Keppie, and Marcel Guillong for your contributions to Chapters 5 and 3 respectively; your comments improved both manuscripts. A special thanks to Malcolm McLeod, not only for his intellectual input to Chapter 5, but also for his continued support throughout this project. Lastly, thank you to Greg Shellnut for completing the zircon analysis and your input into Chapter 4.

I would also like to thank my family and friends for always encouraging me and helping through this academic journey. To my parents, words could not express how grateful I am to have such loving, patient and supportive parents. You dealt with my changing disciplines, jobs and moving thousands of kilometres away in pursuit of education, I love you both very much. To Pete, what can I say? You made all the crazy journey's with me and we're just getting started. Thanks for being my best friend, and always being there for me, I love you. Lastly, to all the geo friends I've met along the way, thanks for making these the best years of my life and sharing a few pints with me.

Lastly, I would like to thank the several sources of funding I received for this Project. Without their generosity, this research would not have been possible:

- (1) Natural Sciences and Engineering Research Council of Canada (NSERC)
Research Capacity Development Fellowship
- (2) Society of Economic Geologists Student Research Grant
- (3) Mineralogical Association of Canada Travel and Research Grant
- (4) George Frederic Matthew Research Grants in Geology, Museum of New Brunswick

TABLE OF CONTENTS

Abstract	iii
ACKNOWLEDGEMENTS	iv
CHAPTER 1: INTRODUCTION	1
1.1. INTRODUCTION TO THE PROBLEM	1
1.2. CENTRAL RESEARCH QUESTIONS	2
1.3. GENERAL THESIS OUTLINE	2
CHAPTER 2: METHODS	4
2.1. SAMPLE PREPARATION AND FIELD WORK	4
2.2. PETROGRAPHY	4
2.3. MAJOR AND TRACE ELEMENT GEOCHEMISTRY	5
2.4. ¹⁴⁷Sm/¹⁴⁴Nd RADIOGENIC ISOTOPES	5
2.5. Lu-Hf ZIRCON ISOTOPES	6
2.6. $\delta^{18}\text{O}$ QUARTZ ISOTOPES	7
CHAPTER 3: MAGMATIC ENRICHMENT OF URANIUM, THORIUM AND RARE EARTH ELEMENTS IN LATE PALEOZOIC RHYOLITES OF SOUTHERN NEW BRUNSWICK, CANADA: EVIDENCE FROM SILICATE MELT INCLUSIONS	9
3.1. ABSTRACT	9
3.2. INTRODUCTION	10
3.3. GEOLOGICAL SETTING	12
3.4. ANALYTICAL METHODS	15
3.5. RESULTS	17
3.5.1. Description of Melt Inclusions.....	17
3.5.2. Melt inclusion and whole-rock compositions.....	19
3.6. DISCUSSION	21
3.6.1. Comparison of Harvey and Piskahegan: the role of fractionation.....	21
3.6.2. Significance of U/Th ratios and changes in U and Th content of the melts	23
3.6.3. Controls on LILE, REE and HFSE abundance	25
3.6.4. The effect of boundary layers on melt inclusion composition	27
3.6.5. Comparisons to other volcanic- and caldera-associated U deposits	28
3.6.6. Melt inclusions as an exploration tool	29
3.7. CONCLUSION	31
3.8. ACKNOWLEDGEMENTS	32
3.9. CHAPTER 3 APPENDIX	33
3.10. SUMMARY OF CONTRIBUTIONS	47
CHAPTER 4: REVISED PETROGENIC HISTORY OF LATE PALEOZOIC RHYOLITES OF THE HARVEY FORMATION, NEW BRUNSWICK, CANADA	48
4.1 ABSTRACT	48
4.2 INTRODUCTION	49
4.3 GEOLOGIC SETTING	50

4.4 METHODS	53
4.4.1. Sample Preparation and Field Work	54
4.4.2. Major and Trace Element Analysis	54
4.4.3. $^{147}\text{Sm}/^{144}\text{Nd}$ Radiogenic Isotopes	54
4.4.4. $^{206}\text{Pb}/^{238}\text{U}$ Geochronologic Dating	55
4.4.5. Hf zircon isotopes	56
4.4.6. $\delta^{18}\text{O}$ Quartz Isotopes.....	56
4.5. ALTERATION AND THE POSSIBLE EFFECT ON CHEMICAL COMPOSITION	56
4.6. RESULTS	57
4.6.1. Geochronology- $^{206}\text{Pb}/^{238}\text{U}$ ICP-MS	58
4.6.2. Geochemistry- major element.....	58
4.6.3. Geochemistry-trace element.....	60
4.6.4. Petrology- major and minor elements.....	62
4.6.5. ϵ_{Nd} isotopes.....	62
4.6.6. $\delta^{18}\text{O}$ Quartz.....	63
4.6.7. ϵ_{Hf} isotopes	64
4.7. DISCUSSION	65
4.7.1. Harvey felsic volcanics comparison.....	65
4.7.2. Relationship to Piskahegan	66
4.7.3. Similarity to Topaz Rich Rhyolites	68
4.8. CONCLUSIONS	69
4.9. ACKNOWLEDGEMENTS	69
4.10. CHAPTER 4 APPENDIX	70
4.11. SUMMARY OF CONTRIBUTIONS	84
CHAPTER 5: GEOCHEMISTRY OF LATE PALEOZOIC PERALKALINE FELSIC VOLCANIC ROCKS, CENTRAL NEW BRUNSWICK: URANIUM POTENTIAL	85
5.1. ABSTRACT	85
5.2. INTRODUCTION	85
5.3. GEOLOGICAL SETTING	87
5.4. GEOCHEMISTRY	88
5.5. PETROGENESIS	92
5.6. ECONOMIC POTENTIAL	94
5.7. CONCLUSIONS	95
5.8. ACKNOWLEDGEMENTS	96
5.9. CHAPTER 5 APPENDIX	96
5.10. SUMMARY OF CONTRIBUTIONS	106
CHAPTER 6: CONCLUSIONS	108
6.1. ADDRESSING THE CENTRAL RESEARCH QUESTIONS	108
6.2. ENVIRONMENTAL IMPLICATIONS	112
CHAPTER 7: REFERENCES	114
CHAPTER 8: APPENDIX	128
8.1. ADDITIONAL FIGURES	128

8.2. ADDITIONAL TABLES..... 131

CHAPTER 1: INTRODUCTION

1.1. Introduction to the Problem

The Maritimes Basin of southern New Brunswick is known to contain felsic volcanic and volcanoclastic rocks, resulting from a period of intense tectonic activity during the Mid-Devonian to Late Permian (Belt, 1968; Kuan, 1970; Pajari, 1973; Bradley, 1982; Beuthin; 1994). This area has been continually investigated for its economically viable ore deposits throughout much of the last century creating profitable mining industries harvesting tin, indium, tungsten, molybdenum and gold (Pouliot et al., 1978; Yang et al., 2003; Sinclair et al., 2006). Although uranium mineralization was discovered during historic metal exploration, only recently has it become economically viable with the expansion of nuclear energy resources in the late twentieth century. As a result, limited research has been conducted on the genesis of the deposits or the geochemical signatures of uranium host rocks within the area.

The Late Devonian (McGregor & McCutcheon, 1988; Tucker et al., 1998) Harvey and Piskahegan Groups of southern New Brunswick were previously documented to contain U mineralization within felsic rhyolites (Strong, 1980; Brack, 1982; McLeod and Johnson, 2007). Previous studies (see Kuan, 1970; van de Poll, 1972; Pajari, 1973; Gemmell, 1975; Beaudin et al. 1980; Ruitenberg & McCutcheon, 1985; Payette & Martin, 1986b) have indicated the Harvey and Piskahegan Groups can be lithologically correlated despite displaying distinct geochemical characteristics and subtle regional variability. The younger, Viséan (St. Peter, 2002) Cumberland Hill Formation (Fm) also contains U mineralization within felsic volcanics, although of a less significant grade than

either Harvey or Piskahegan. Through both geochemical and petrographic investigations, these localities will be utilized to examine the genetic history, geochemistry and economic potential of southern New Brunswick felsic volcanics.

1.2. Central Research Questions

When this thesis first began, the primary focus was to determine whether or not the felsic volcanic deposits, Harvey and Piskahegan of southern New Brunswick were genetically related. From here, a diverse geochemical and petrographic research design was implemented to solve a variety of other intriguing questions related to uranium mineralization in southern New Brunswick. Three additional central research questions guided this scientific investigation then on.

1. What was the original geochemical composition of the Harvey Group and how did it evolve (i.e. partial melting, fractional crystallization, crustal contamination, lithospheric interaction etc.)?
2. How does the geochemistry of the Cumberland Hill Formation compare to other formations within southern New Brunswick? How does this influence our current understanding of the geological history of the Maritimes?
3. What economic potential lies within the uranium deposits of Southern New Brunswick?

1.3. General Thesis Outline

The body of this thesis aims to answer the aforementioned research questions and continually builds on knowledge in the subject area. Chapter three investigated the

original melt geochemistry of peraluminous felsic volcanics of the Harvey and Piskahegan Groups through the analysis of melt inclusions, hosted within quartz. This study offers the first of many lines of geochemical evidence that the two groups are geochemically unrelated, in contrast to previous work (see Kuan, 1970; van de Poll, 1972; Pajari, 1973; Gemmell, 1975; Beaudin et al. 1980; Ruitenberg & McCutcheon, 1985; Payette & Martin, 1986b). The enormous economic U potential within felsic volcanics of southern New Brunswick is also further illustrated within this study.

Chapter four investigated the genetic history and geochemical characteristics of whole-rock samples (n=27) within the Harvey Group. Since the age of the Harvey Group was previously unknown, Piskahegan and Harvey were predominantly correlated, and assumed coeval, based on stratigraphy alone. This study advances our current understanding of how the Harvey Group formed, and further exemplifies that Harvey and Piskahegan are distinct deposits.

Lastly, chapter five investigated whole-rock samples (n=15) from the younger, peralkaline rhyolites and trachytes of the Cumberland Hill Fm. While difficult to infer from geochemistry alone, this study offered valuable insight into the possible petrogenic history of the Maritimes. The uranium potential of these region was also exemplified through comparison to the Streltsovka Caldera, the largest hydrothermal, peralkaline uranium deposit in the world.

All of the chapters in this body of work were separately completed as a manuscript for publication. As a result, some introductory material may seem redundant, since each chapter is designed to stand-alone.

CHAPTER 2: METHODS

Methods discussed extensively within the bodies of Chapters 3, 4, and 5 are not discussed below. Any additional details not discussed in methods covered in the aforementioned chapters will be covered herein.

2.1. Sample Preparation and Field Work

During the summer 2008, fieldwork including reconnaissance field investigation, detailed mapping of selected areas, and sample collection was completed in southern New Brunswick. Twenty-seven samples were obtained from the Harvey Group (Cherry Hill– n=18, Harvey Mountain– n=5, York Mills– n=5), 110 samples from the Piskahegan Group (Albert– n=2, Bailey Rock– n=4, Big Scott Mountain– n=16, Kleef –n=3, Little Mount Pleasant– n=10, McDougall Brook Granite– n=20, Mount Pleasant Mine Site– n=1, Scoullar Mountain– n=27, Seelys– n=25, South Oromocto– n=2) and 15 samples from the Cumberland Hill Fm. Whole-rock samples were expedited to Saint Mary's University, Halifax, Nova Scotia for further processing. All samples were cut into slabs (1 cm width) to prepare for thin sectioning and subsequently chipped and powdered (Dalhousie University, Halifax) for geochemical analysis.

2.2. Petrography

A slab from representative samples were sent to Vancouver Petrographics where twenty-seven polished thin sections were obtained for petrographic characterization and microprobe analyses. Thin sections were stained to readily distinguish between albitic plagioclase and potassium feldspar. Representative samples from each group were

examined utilizing both a petrographic and transmitted light microscope to identify the minerals, and textures present within the samples.

2.3. Major and Trace Element Geochemistry

Standard sample preparation procedures were used for geochemical analysis using a Philips PW2400 X-Ray fluorescence spectrometer (XRF) at the G.G. Hatch Stable Isotope Laboratory, Ottawa, Ontario. Each sample was fused (Claisse Fluxer) and pressed (Carver press) prior to placement in the Philips PW2510 sample changer. The XRF was controlled by Philips SuperQ/Quantitative and SemiQ/Qualitative (v. 2.1D) software, enabling the quantifiable output of 28 major (wt. %) and minor elements (ppm), loss of ignition (L.O.I.) values, and major compounds (wt. %). The XRF operates at detection limits of 0.01% (or better) for major elements and L.O.I.

Various samples from Harvey and Piskahegan were analyzed by fusion using a Perkin Elmer Optima 3000 inductively coupled plasma mass spectrometer (ICP-MS) to determine trace element concentrations. Samples were analyzed at Activation Laboratories, Ancaster, Ontario according to standard procedures (Hoffman, 1992).

2.4. $^{147}\text{Sm}/^{144}\text{Nd}$ Radiogenic Isotopes

Four samples (NB07-2, -11, -21, -28) were analyzed for Sm/Nd isotopic ratios using a Finnigan MAT 262V thermal ionization -mass spectrometer (TIMS) at Memorial University, Newfoundland. Samples chosen for analysis contained low Rb (<1075 ppm) and Sr (<950 ppm) concentrations, few inclusions and were relatively homogenous. Approximately 0.05-0.2g of powdered sample was dissolved in concentrated HF and HNO₃ acids, and spiked with $^{150}\text{Nd}/^{149}\text{Sm}$ prior to acid digestion (5 days). Once the

sample evaporated, the remaining material is taken up into 2N HCl for 2 days, dried again, and taken up into 2N HCl. Samples are subsequently loaded into cationic exchange chromatography utilizing AG50W–X8 resin to accumulate rare earth element (REE) fractions. After purification, the Sm and Nd fractions are isolated with a secondary column loaded with Eichrom© Ln resin and analyzed using a multicollector Finnigan Mat 262 mass spectrometer operating in static mode. Once analyzed, the values are normalized to $^{146}\text{Nd}/^{144}\text{Nd} = 0.7219$, calibrated to the JNdi-1 standard ($^{143}\text{Nd}/^{144}\text{Nd} = 0.512115$, Tanaka et al., 2000), and accurate to $<0.002\%$ (Nd), and $<0.1\%$ ($^{147}\text{Sm}/^{144}\text{Nd}$ ratio). Subsequent to analysis, ϵ_{Nd} values were calculated based on the present day chondrite uniform reservoir (CHUR; $^{147}\text{Sm}/^{144}\text{Nd} = 0.1967$ and $^{143}\text{Nd}/^{144}\text{Nd} = 0.512638$), and age equations were modeled using the De Paolo mantle model, and the known ^{147}Sm decay constant (6.54×10^{-12} years; Steiger and Jäger, 1977).

2.5. Lu-Hf Zircon Isotopes

In situ zircon Hf isotope analyses were carried out using a New Wave UP 213 laser-ablation microprobe, attached to a Nu Plasma multi-collector ICP-MS, coupled with a fixed detector array of 12 Faraday cups and 3 ion counters at the Institute of Earth Sciences, Academia Sinica in Taipei. The New Wave UP 213 laser system delivered a beam of 213 nm UV light from a frequency-quintupled (5th harmonic) Nd: YAG laser. Analyses were carried out with a beam diameter of 55 μm , 5 Hz repetition rate, and energies of ~ 0.4 mJ/pulse. Typical ablation times were 80–120 s, with background collected 30 s prior to ablation. Instrumental conditions, data acquisition, and analytical procedures were similar to Griffin et al. (2000).

For this study, masses 172, 175, 176, 177, 178, 179 and 180 were simultaneously examined in static-collection mode and normalized to $^{179}\text{Hf}/^{177}\text{Hf} = 0.7325$, using an exponential correction for mass bias. All isobaric interferences of ^{176}Lu and ^{176}Yb on ^{176}Hf were corrected, and the recommended $^{176}\text{Lu}/^{175}\text{Lu}$ and $^{176}\text{Yb}/^{172}\text{Yb}$ ratios of 0.02669 (De Bièvre and Taylor, 1993) and 0.5865 were used for the data reproduction. The reproducibility of the Hf isotope analyses is demonstrated by 28 Hf analyses on the 50 ppb solution of the AMES Hf metal, with the mean value for $^{176}\text{Hf}/^{177}\text{Hf}$ equalling 0.282152 ± 18 (2σ), identical to the recommended value of 0.282151 ± 13 (Munker et al., 2001). All results were calibrated to zircon standards, Mud Tank and 91500 (Woodhead and Hergt, 2005; Griffin et al., 2006, Weidenbeck et al., 1995), with typical within run precision (2σ) of ± 0.000030 on the $^{176}\text{Hf}/^{177}\text{Hf}$ analysis.

The $\epsilon_{\text{Hf}(T)}$ values were calculated using chondritic ratios of $^{176}\text{Hf}/^{177}\text{Hf}$ (0.282772) and $^{176}\text{Lu}/^{177}\text{Hf}$ (0.0332) as derived by Blichert-Toft and Albarede (1997). These values were reported relative to $^{176}\text{Hf}/^{177}\text{Hf} = 0.282163$ for the JMC475 standard. The $^{176}\text{Hf}/^{177}\text{Hf}$ value of 0.282152 ± 18 were obtained for the AMES Hf metal, considered isotopically indistinguishable to the JMC475 standard.

2.6. $\delta^{18}\text{O}$ Quartz Isotopes

Six samples were chosen based on the large abundance of quartz phenocrysts to analyze for $\delta^{18}\text{O}$. Samples were chipped to obtain individual mineral grains, and 15mg of quartz was isolated using a binocular microscope. Samples were analyzed at the Queen's University Stable Isotope and ICP-MS Lab for analysis of $\delta^{18}\text{O}$ in quartz using the

conventional BrF₅ method of Clayton and Mayeda (1963) and run on a dual inlet Finningan Mat 252 Isotope Ratio Mass Spectrometer. All values reported in standard delta notation relative to VSMOW, and were reproducible to 0.3‰.

$$\delta^{18}\text{O} = \left(\frac{{}^{18}\text{O}/{}^{16}\text{O}_{\text{sample}} - {}^{18}\text{O}/{}^{16}\text{O}_{\text{standard}}}{{}^{18}\text{O}/{}^{16}\text{O}_{\text{standard}}} \right) \times 1000$$

CHAPTER 3: MAGMATIC ENRICHMENT OF URANIUM, THORIUM AND RARE EARTH ELEMENTS IN LATE PALEOZOIC RHYOLITES OF SOUTHERN NEW BRUNSWICK, CANADA: EVIDENCE FROM SILICATE MELT INCLUSIONS

Submitted to Economic Geology, April 7, 2010

Accepted May 27, 2010

TARYN R. GRAY^{1*}, JACOB J. HANLEY¹, JAROSLAV DOSTAL¹, MARCEL GUILLONG^{2,+}

¹Department of Geology, Saint Mary's University, Halifax, Nova Scotia, B3H 3C3, Canada

²Department of Earth Sciences, ETH Zurich, Clausiusstrasse 25, Zürich, Switzerland

⁺ current address: ARC Centre of Excellence in ore Deposits (CODES), University of Tasmania, Hobart, Tasmania, 7001

*corresponding author <Taryn.Gray@smu.ca>

3.1. Abstract

The major and trace element geochemistry of silicate melt inclusions was investigated within Late Paleozoic felsic rhyolites from the Piskahegan and Harvey Groups of southern New Brunswick, Canada in order to provide further insight into the genetic history of the volcanic- and caldera-related U mineralization that occurs in the region. Glassy melt inclusions analyzed by laser ablation ICP-MS and electron microprobe show enrichment in most incompatible trace elements but a marked depletion in Ba, Sr, and Eu compared to whole-rock. At Harvey, melt trapped in early quartz phenocrysts (“pre-eruptive” inclusions) and in late quartz aggregates (“syn-eruptive” inclusions) within the groundmass of the rhyolites was significantly more fractionated than melt trapped in quartz phenocrysts at Piskahegan. Fractionation was associated with the crystallization of feldspar and resulted in progressive enrichment of the melt in U, Th, B, LILE, LREE and other metals, and an increase in the U/Th ratio of the melt. A higher degree of melt

fractionation combined with post-magmatic leaching may have been prerequisites for mineralization at Harvey. Since whole-rocks are highly susceptible to alteration, melt inclusion analysis may be the only method capable of providing constraints on melt chemistry/evolution in such ancient volcanic terrains and may enable the evaluation of the economic potential of such terrains if the initial U and Th concentration, and U/Th ratio of the volcanic products impact the ultimate mineralizing potential of the system.

3.2. Introduction

In volcanic- and caldera-associated U deposits, metal-bearing magmas are derived from either a deep mantle source (Locardi, 1985; Treuil, 1985), or partial melting of mid-lower crustal rocks (Chen and Fang, 1985). Since peraluminous rhyolites, as well as granites are almost always of crustal origin (Douce, 1999), the latter hypothesis is more likely but still debated. The enrichment of U, Th and REE can be further facilitated by subsequent fractionation of the mantle- or crustal-derived melt or by assimilation of additional U-, Th-, and REE-enriched crustal rocks during ascent and emplacement, and later through extraction, leaching and redistribution of ore metals by interaction of mineralized volcanics with exsolved magmatic fluid or heated meteoric water (Chen and Fang, 1985).

In the late Devonian Harvey and Piskahegan Groups in southern New Brunswick, the processes that led to U and Th enrichment in the mineralized felsic volcanic rocks are poorly understood. Evidence from similar volcanic U-related deposits indicates that in addition to primary magmatic enrichment processes related to the eruption of U-Th-bearing volcanics, secondary magmatic enrichment processes tend to dominate near

intrusive centers (e.g., Rexpar, Canada; Preto, 1978) and may involve the exsolution and circulation of magmatic-hydrothermal fluids from the volcanic sequence. Whereas, distal to the intrusive centers, metamorphic or meteoric water circulation control enrichment (e.g., Anderson, United States; Rytuba and Glazman, 1979). It is often difficult in such environments to determine the relative importance of primary and secondary processes in generating the mineralization. First, the interpretation of the genetic history of a volcanic rock sequence using whole-rock geochemistry and mineral chemistry alone can be misleading because whole-rocks represent mixtures of variable proportions of crystals and silicate liquid. Second, many trace elements, notably the large ion lithophile elements (LILE), light rare earth elements (LREE), U and Th are prone to differential remobilization during alteration over a wide range of conditions (e.g., Schiano, 2003; Lowenstern, 2003; Dawood et al., 2004; Davidson et al., 2007). In contrast to whole-rocks, determination of the trace element concentrations of glassy melt inclusions can be done reliably using *in-situ* analytical techniques to yield reliable information about the magmatic phase composition at the time of melt entrapment in a given host phase, and its evolutionary path by primary magmatic processes (e.g., crystal fractionation, mixing and assimilation) provided that no post-entrapment modification has occurred (e.g., Webster et al., 1995; Chabiron et al., 2001, 2003; Halter, 2002; Heinrich, 2003). Determination of the trace element content of melt inclusions may also serve as a means to evaluate how post-solidus alteration has modified the original chemistry of the coeval volcanic rocks.

In order to determine how differing levels of U and Th enrichment in ore-forming magmas were achieved at Harvey and Piskahegan, and to evaluate the influence of any

post-magmatic processes (i.e. leaching), glassy silicate melt inclusions within rhyolites at both localities were investigated to constrain the magmatic phase composition at the time of entrapment. While previous investigations (Payette and Martin, 1986a) examined major element composition within melt inclusions of Harvey, trace element analyses of the inclusions were not obtained. Mineralized rhyolites are highly enriched in U, containing up to ~1500 ppm U at Harvey and Piskahegan (Brack, 1982; N. Downey, pers. commun.). The analysis of melt inclusions makes it possible to determine if sufficient magmatic enrichment occurred to account for the observed mineralization directly (i.e., derived from the parent magma), or whether they were enriched by some other mechanism.

3.3. Geological Setting

The late Devonian Harvey and Piskahegan Groups are located in southern New Brunswick, on the eastern edge of the Maritimes Basin, approximately 40km southeast and 50km south of Fredericton respectively (Fig. 1). The 12 km-thick Maritimes Basin formed during the Mid-Devonian in the final phase of the growth of Pangaea and remained tectonically active until the early Permian (*c.f.* Gibling et al., 2009). Repeated subsidence, basin inversions (with associated faulting), and two major basin extensional phases led to four distinct pulses of igneous activity within the region. These occurred during the Middle Devonian (390–385 Ma), Late Devonian (375–370 Ma), Latest Devonian to Early Tournaisian (365–354 Ma), and Late Tournaisian–Early Viséan (339–250 Ma) as determined through the examination of igneous rocks of Middle Devonian–

Early Carboniferous age from the southern margin of the Magdalen basin in Cape Breton Island and northern mainland Nova Scotia (Dunning et al., 2002). The Piskahegan Group was deposited in 363.4 ± 1.8 Ma (Tucker et al., 1998) while the Harvey Group is believed to be synchronous with Piskahegan based on stratigraphy (Payette and Martin, 1986b; McCutcheon et al., 1997).

Harvey and Piskahegan contain U mineralization within rhyolitic rocks (McLeod and Johnson, 2007). The mineralization style is classified as volcanic- and caldera-related U, and localized within felsic volcanics, and intercalated clastic sediments (*c.f.* Gandhi and Bell, 1996; IAEA, 2009). Such mineralization can be either synvolcanic or epigenetic, strongly structurally-controlled, and can be found in all stratigraphic levels of the volcanic complex. Volcanic- and caldera-related U deposits are typically low grade and several deposits may be present in a given region or volcanic complex (e.g., Streltsovka caldera, Russia, Chabiron et al., 2001, 2003, Nash, 2010; Gan-Hang volcanic belt, China, Finch et al., 1993; Dornot deposit, Mongolia, Mironov, 1993; Nopal deposit, Mexico, Goodell, 1981). In these mineralized systems, and as is displayed at Harvey and Piskahegan, uraninite typically occurs with molybdenite, fluorite, quartz, and sulphides.

The Harvey Group is subdivided into three formations: York Mills, Cherry Hill, and Harvey Mountain (Kuan, 1970; Beaudin et al., 1980), composed predominantly of sedimentary rocks (red sandstone and siltstone) within York Mills, and felsic volcanogenic sediments in all formations including laminated rhyolites, ash flow and ash-fall tuffs (ignimbrites), and pyroclastic breccia (Fig. 1). The 75-100m thick Harvey Mountain is composed of laminated rhyolites, pyroclastic breccia and ash-fall tuffs. The

rhyolites are aphanatic and devitrified, with well-defined alteration indicated by the presence of grey-green spherulite (3-4mm) layers (Payette and Martin, 1986b), with the glass replaced by a mica-rich material (illite and quartz; Kuan, 1970; Pajari, 1973). A summary of the major and accessory mineral phases present within Harvey Mountain can be found in Table 1. The Cherry Hill Formation is the predominant host of U mineralization, composed of quartz-feldspar porphyry, with 2 poorly welded ash-flow sheets (5 m and 100 m thick) at the base (Kuan, 1970; Beaudin et al., 1980). The quartz-feldspar porphyry contains about 20% phenocrysts (up to 3 mm in diameter) of quartz and feldspars set in a groundmass composed of devitrified welded shards. These rocks also contain pumice and lithic fragments. Recent exploration identified three mineralized ignimbritic units with associated clay alteration, silicification and hematization, grading up to 0.447% U_3O_8 over 0.6 m, and 0.24% U_3O_8 over 1.2 m within Harvey (Capella, 2007).

The Piskahegan Group represents one of only a few caldera sequences in Canada of the pre-Cenozoic that has preserved exocaldera, intracaldera and late-caldera fill sequences (McCutcheon et al., 1997). The exocaldera sequence contains the Bailey Rock rhyolites, the only formation identified to contain suitable melt inclusions hosted in quartz phenocrysts. The Bailey Rock Formation is composed of quartz-feldspar-phyric lava flow with abundant K-feldspar phenocrysts, with quartz, plagioclase and hornblende pseudomorphs (Table 1). Devitrification and flow banding can be observed, however the groundmass is generally recrystallized (McCutcheon et al., 1997). Previous exploration has identified spatially associated mineralized volcanogenic sandstone and conglomerates

with associated chlorite, hematite, and fluorite alteration grading up to 0.036% U₃O₈ over 1.22 m within the Carrow Formation, underlying the Bailey Rock rhyolites (McNamara, 1978).

3.4. Analytical Methods

Major and minor element analysis of whole-rock was performed on fused glass disks using a Philips PW2400 X-Ray fluorescence spectrometer (XRF) at the University of Ottawa, G.G. Hatch Stable Isotope Laboratory. Trace element analysis was performed using a Perkin Elmer Optima 3000 inductively coupled plasma mass spectrometer (ICP-MS) at Activation Laboratories, Ancaster, Ontario.

Representative rhyolite samples from Harvey (NB07-18, NB07-31) and Piskahegan (NB07-39, NB07-78) were chosen for melt inclusion analysis. Approximately 15 melt inclusions of varying size (between 40 and 150 µm) per slide were chosen for geochemical analysis. Selected inclusions (>40 µm) were absent of solid phases of ambiguous origin (i.e., that may be accidentally trapped, or formed during recrystallization), did not contain any visible signs of post-entrapment modification, and were large enough and trapped at sufficiently low degrees of undercooling to eliminate the influence of diffusion-related concentration gradients on trapped melt composition (i.e., boundary layer effects).

Major and minor elements in silicate melt inclusions from each sample were analyzed using a JEOL JXA 8200 Superprobe electron microprobe (EMP) comprised of 5 wavelength-dispersive spectrometers, a Noran (133eV resolution) energy dispersive spectrometer, and a cathodoluminescence photomultiplier. An accelerating voltage of

15kV and a 20s on-peak counting time was applied for the analysis of all elements, except F which required a 40s on-peak counting time. Calibration of analyte sensitivities and confirmation of analytical accuracy was performed using a variety of natural mineral standards (fluorapatite, garnet, sanidine, tugtupite, kaersutite, Durango apatite) and silicate glass standards (Coso Obsidian, Astimex Obsidian). Fluorine was analyzed using a TAPH crystal since it is the most sensitive crystal available that does not have peak overlap problems between F $K\alpha$ and Fe $L\alpha$ lines. Several large inclusions (~70-100 μm) were analyzed multiple times, never in the same location, to determine the influence of beam diameter and current on alkali and halogen mobility. It was determined that a beam current of 2.03×10^{-8} A, coupled with a large beam diameter (3 μm) was optimal for all elements, excluding Na_2O for which concentrations reported are ~20% lower than concentrations obtained by LA-ICP-MS. Reduction of beam current was shown to improve Na_2O accuracy but compromised F concentrations. Since F cannot be determined accurately by LA-ICP-MS, but Na_2O can, we chose to optimize for F determination (2.03×10^{-8} A, 3 μm).

Major and trace element concentrations were quantified by laser ablation ICP-MS (LA-ICP-MS) at the Swiss Federal Institute of Technology (ETH Zurich). Heinrich et al. (2003) outline the details of the analytical routine used. Ablation was performed using a prototype 193 nm ArF excimer laser ablation system similar to GEOLAS, with the laser operating at an energy density of 25-35 J/cm^2 , with a pulsed beam, and energy-homogenized beam profile (Gunther et al., 1997). Melt inclusions were ablated through step-wise increasing of the ablation pit diameter (from 10-110 μm) such that the final pit

size was slightly larger than the maximum inclusion dimension. After collecting ~50 s of background signal with the laser turned off, the inclusions required 10 to 30 s of ablation time to collect the melt inclusion + host quartz signal. Ablated aerosols were transported into an ELAN DRC quadrupole ICP-MS operated in dual detector mode using the conditions similar to those described in Pettke et al. (2004). Mass spectrometer dwell time was 10 ms for all elements. Quantification of trace element concentrations followed procedures outlined in Longerich et al. (1996), Heinrich et al. (2003), and Halter et al. (2002), and was performed using the software SILLIS (Guillong et al., 2008). Groups of 16 analyses were collected, bracketed by 2 analyses before and after the external standard (SRM 610 from NIST) to apply a linear instrument drift correction. The Al₂O₃ content of the melt inclusions, determined by EMP, was very consistent in assemblages of inclusions from single samples and used as the internal standard to quantify trace element concentrations in melt inclusions from raw LA-ICP-MS data.

3.5. Results

3.5.1. Description of Melt Inclusions

Porphyritic rhyolite samples contain melt inclusions in early quartz phenocrysts and later quartz-rich matrix (Fig. 2A, B, E). Melt inclusions ranged from 25-300 μm in diameter at Harvey, and 30-200 μm in Piskahegan. The inclusions often exhibited negative crystal shapes and are primary in origin. Analyzed inclusions ranged from 40-150 μm, were completely glassy and clear (colorless to pale brown), free from devitrification and recrystallization, and devoid of daughter crystals, accidental solids, or bubbles. In the unlikely event that tiny fluid bubbles were present in the samples

analyzed, their total volume would have contributed negligibly to the overall LA-ICP-MS signal. Melt inclusions were classified into the following categories: (i) early (in quartz phenocryst; “pre-eruptive”) glass + vapour bubble (Fig. 2C); (ii) early glass + bubble (1-8 μm) + solids (Fig. 2D), and (iii) late (in matrix quartz) “syn-eruptive” glass + vapour bubble (2 μm) + aqueous fluid bubbles (6 μm ; Fig. 2E). The fluid bubbles were trapped within the melt during inclusion formation (a free volatile phase), while the vapour bubbles were produced post entrapment via contraction as the inclusion cooled. The fluid bubbles are not considered shrinkage bubbles as they are too finely dispersed and are present in variable amounts in each inclusion, showing that heterogeneous entrapment occurred (Fig. 2G, H). Analyses of the “syn-eruptive” inclusions were restricted to those without visible fluid bubbles. We can not preclude the possibility that a few bubbles, masked by the larger vapour bubble, were present in some analyzed inclusions. However, we consider that the data obtained through LA-ICP-MS do not represent mixtures of a volumetrically minor fluid and dominant melt phases since the relatively very small size of the fluid bubbles would prevent them having any significant influence on the overall bulk element concentrations. On the other hand, the presence of a fluid phase at eruption, prior to, or at the time of entrapment (Fig. 2E) of “syn-eruptive” melt is significant in terms of the overall evolution of the magmatic-hydrothermal system because it implies metals may have already been scavenged by a fluid phase at the time the melt was trapped. Therefore, concentrations of U, Th and other incompatible elements in the “syn-eruptive” melts are minimums, with the original magmatic concentrations being possibly higher than those reported here (see below).

3.5.2. *Melt inclusion and whole-rock compositions*

Based on the EMP and LA-ICP-MS data, melt inclusions in the rhyolites containing a high-K calc-alkaline rhyolitic liquid with concentrations (normalized to 100 wt. %) of SiO₂ in the melt averaging 74 wt. % in Harvey and Piskahegan, with whole-rock concentrations slightly higher at 78 wt. % in Harvey and 80 wt. % in Piskahegan (Table 2). Melt inclusions at both Harvey and Piskahegan contain significantly lower concentrations of MgO and TiO₂, and slightly lower CaO and Na₂O compared to whole-rock. This may reflect the accumulation of plagioclase feldspar, mafic silicates and oxides, or the presence of mafic rock inclusions (xenoliths ?) within the host rocks to the inclusion-bearing phenocrysts. Only P₂O₅, and Al₂O₃ are elevated in the Harvey “syn-eruptive” melt inclusions compared to bulk host rocks (Table 2). The geochemical characteristics of the whole-rock compared to melt inclusions imply the melt was more evolved, with whole-rock diluted by phenocrysts. Based on discrimination diagrams for tectonic granitoids (e.g., Rb vs. Y+Nb or Y+Ta, Ta vs. Yb; Pearce et al., 1984), the pre-eruptive phase of the rhyolite has a composition consistent with within-plate granitoids (i.e., continental rifting) but the relative proportions of mantle-derived and crustal-derived source volume is not known.

Previous work (Payette and Martin, 1986a) showed highly variable F concentrations in melt inclusions from Harvey, ranging widely from below detection limits to ~ 2 wt. %. These results could not be reproduced in the current study, possibly due to analytical error in the earlier study associated with F-Fe peak overlap. Several inclusions analyzed by Payette and Martin (1986a) were acknowledged to contain solid phases, that, if

accidentally trapped, may have artificially elevated F concentration. Concentrations of F in the “pre-eruptive” melt inclusions analyzed in the current study were very consistent from inclusion to inclusion and averaged 0.28 ± 0.14 wt. % (n=13, 1σ) and 0.23 ± 0.17 wt. % (n=11, 1σ) in the two samples at Harvey, compared to 0.38 ± 0.08 wt. % (n=12, 1σ) and 0.21 ± 0.10 wt. % (n=8, 1σ) in the two samples from Piskahegan (Table 2). The Cl content of the melt inclusions is also consistent and very homogeneous at both study locations, averaging 0.18 ± 0.03 wt. % (n=11, 1σ) and 0.05 ± 0.06 wt. % (n=13, 1σ) in the Harvey samples, compared to 0.11 ± 0.02 wt. % (n=12, 1σ) and 0.14 ± 0.02 wt. % (n=8, 1σ) at Piskahegan (Table 2). The H₂O contents of the inclusions at Harvey and Piskahegan are low, consistent with an already partially degassed rhyolite melt at the time of entrapment. Estimated H₂O contents of approximately 1-1.5 wt. % assumed that water comprises the difference between 100% and the totals of major and minor elements determined by EMP (Table 2; Anderson, 1973; Sommer, 1977)

Normalized abundance (continental crust-normalized; Rudnick and Gao, 2004) diagrams (Fig. 3) show that silicate melt inclusions at both Harvey and Piskahegan are slightly enriched in most incompatible trace elements and significantly depleted in Ba, Sr, and Eu compared to whole-rock. This is most notable at Harvey where Ba, Sr and Eu contents in the melt inclusions are orders of magnitude lower than bulk rhyolite (Fig. 3). There is slight enrichment of HREE relative to LREE in both the whole-rocks and melt inclusions from both deposits. Overall, trace element patterns are similar at both localities; however Harvey melt inclusions show higher overall trace element contents and greater depletion in Ba, Eu and Sr than Piskahegan. Late, “syn-eruptive” melt

inclusions at Harvey show much higher LILE and U, Th contents compared to early “pre-eruptive” melt inclusions.

3.6. Discussion

3.6.1. Comparison of Harvey and Piskahegan: the role of fractionation

Harvey and Piskahegan have been interpreted as genetically related based on stratigraphy (Kuan, 1970; Pajari, 1973; Gemmell, 1975; Beaudin et al., 1980). While this appears unlikely based on melt inclusion geochemical trends, it is possible to argue that Harvey represents a more evolved volcanic suite based on high concentrations of incompatible elements and elevated U/Th ratio. In order to explicitly determine the genetic relationship between Harvey and Piskahegan, additional geochemical investigations will be required to ascertain the nature of the source material, and the petrogenetic chronology of Harvey.

However, the melt inclusion data do allow for a comparison of the relative magmatic evolution (i.e., melt fractionation) of Harvey and Piskahegan rhyolites at the time melt inclusions were trapped in early quartz phenocrysts, prior to eruption. Differences in the degree of fractionation within the liquids of each environment are best exemplified by the behavior of highly incompatible trace element concentrations (e.g., B, Cs) and incompatible ore metals U and Th (Fig. 4). Since B and Cs behave incompatibly during crystallization, and are only slightly more compatible in exsolving volatile phases than in coexisting in granitic magmatic systems (Pichavant, 1981; London, 1988; Audétat and Pettke, 2003), changes in their concentrations in melt are highly sensitive to only crystal fractionation. Using the calculation method of Audétat and Pettke (2003), and assuming

plagioclase and alkali feldspar were the fractionating mineral phases, we estimated the degree of fractionation of melts trapped in inclusions from each environment. Based on the Cs content of the “pre-eruptive” melt, we determined the degree of fractionation to be between 70 and 92% at Piskahegan, and at least 95% at Harvey for all melt inclusions analyzed. The concentration of Cs and other highly incompatible elements in “syn-eruptive” melt inclusions at Harvey is about an order of magnitude higher than in the “pre-eruptive” inclusions, corresponding to a degree of fractionation exceeding 99%.

Increasing concentrations of Cs and B correlate positively with U and Th, as do several other pathfinder elements including Cu, As, W, and S and incompatible elements (Cr, Nb, Ti). This indicates that all these elements experienced enrichment in the melt due to crystal fractionation, and were not artificially elevated through sampling of fluid bubbles. Notably, this process influences the U/Th ratio whereby increasing U relative to Th results in increasing U/Th ratio with increasing fractionation. Significantly elevated values of Th exist on average in the “syn-eruptive” inclusions (118 ± 21 ppm, 1σ , $n=7$) compared to Harvey (45 ± 6.4 ppm, 1σ , $n=42$) and Piskahegan melt (37 ± 8.0 ppm, 1σ , $n=35$), and especially in contrast to the non-mineralized whole-rocks of Harvey (45 ppm, 1σ , $n=2$) and Piskahegan (37 ppm, 1σ , $n=1$). The “syn-eruptive” (76 ± 12 ppm, 1σ , $n=7$) and “pre-eruptive” (20 ± 2.0 ppm, 1σ , $n=42$) values of Harvey are also elevated in U compared to non-mineralized whole-rock (9.0 ppm, 1σ , $n=2$), with a less significant difference exhibited in Piskahegan melt (11 ± 3.6 ppm, 1σ , $n=35$) and non-mineralized rock (6.0 ppm, 1σ , $n=1$). Overall, both Harvey and Piskahegan melt inclusions are

notably enriched in U and Th compared to whole-rock, with Harvey “syn-eruptive” inclusions highly enriched. The U/Th ratios in Harvey vary from 0.52-0.92 (average= 0.66 ± 0.15 , 1σ , $n=7$) in the “syn-eruptive” inclusions, compared to a range of 0.28-0.56 (average= 0.45 ± 0.06 , 1σ , $n=42$) in “pre-eruptive” inclusions, and 0.14-0.84 in non-mineralized whole-rock (average= 0.49 ± 0.50 , 1σ , $n=2$). The U/Th ratio is less variable in Piskahegan, ranging from 0.22-0.41 (average= 0.29 ± 0.4 , 1σ , $n=35$) in “pre-eruptive” inclusions and 0.23 ($n=1$) in non-mineralized whole-rock.

3.6.2. Significance of U/Th ratios and changes in U and Th content of the melts

A continual increase in the U/Th ratio over time at Harvey was related to the evolution of the rhyolitic magma. It is impossible to comment on the relative concentrations of U in the initial source magmas for the Harvey and Piskahegan volcanics since melt inclusions were trapped in quartz after significant fractionation had already occurred. Changes in U, Th and U/Th ratio are related to fractionation, but interestingly, the increase in U and Th observed between the “pre-“ and “syn-eruptive” melt inclusions was not of the same magnitude as observed for the LILE. The concentrations of U and Th increase by a factor of 3-4, whereas Cs and B increase by only an order of magnitude. This suggests that U and Th either behaved much more compatibly than Cs and B during mineral fractionation, or that the metals partitioned into a volatile (fluid) phase, thereby reducing the amount of these metals in the melt. The latter hypothesis is justified on the basis of petrographic evidence (Fig. 2) that shows that the “syn-eruptive” melt was saturated in a fluid phase at the time of entrapment in the matrix quartz. The presence of the fluid phase (Fig. 2 D, E) indicates we analyzed the coexisting melt phase from which the fluid separated.

Therefore, the concentration of fluid compatible trace elements within the “syn-eruptive” melt essentially represents a minimum, likely higher prior to fluid separation in the lava, since some elements were extracted when the fluid separated. Recent experimental evidence also shows that (i) U is highly soluble in magmatic hydrosaline fluids at relatively oxidizing conditions, and (ii) U solubility under such conditions greatly exceeds Th solubility, resulting in preferential transport of U relative to Th during fluid exsolution and fluid-melt interaction (Bali et al., 2009).

While primary magmatic fractionation clearly affected the total and relative abundance of U and Th in the melts at Harvey and Piskahegan differently, syn- to post-magmatic processes involving fluid leaching of ore metals also resulted in differential transport of U over Th. At Harvey, a complete lack of correlation between U and Th in the whole-rocks (Gray et al., in prep) is observed, while Piskahegan displays a linear, positive correlation between U and Th. Additionally, U is highly enriched in some mineralized rocks at Harvey, ranging from 330-1560 ppm (n=6), with a U/Th ratio of 7.6-49 (n=6; N. Downey, pers. commun.). Non-mineralized samples drilled within the same area as mineralized samples exhibit significantly lower U concentrations (17.2- 148 ppm, n=28), and U/Th ratios (0.39-3.0, n=28). This is in contrast to other rocks in both the York Mills and Harvey Mountain Formations are enriched in Th, relative to U (Gray et al., in prep), possibly representing U-depleted source rocks that were extensively leached (c.f. Dawood, 2004).

Examination of the “syn-eruptive” inclusions identified small bubbles of fluid, interpreted as a fluid that separated from the melt during crystallization of the rhyolitic

magma prior to or during eruption. This indicates that volatiles are capable of interacting with partially crystallized lava, and provides evidence that leaching of metals from these fluids could occur over a wide range in temperature, starting at high temperatures, culminating with low temperatures due to interaction with meteoric water circulation. Therefore, the eventual leaching of U and Th glass from highly evolved melt inclusions could enable a significant concentration of metals to be supplied to meteoric fluids, in addition to the metals may have been initially removed from the melt during fluid-melt interaction at higher temperatures.

3.6.3. Controls on LILE, REE and HFSE abundance

While incompatible trace elements, especially LILE and HFSE, are highly enriched in melt inclusions compared to whole-rock, both Harvey and Piskahegan exhibit negative Eu, Sr, and Ba anomalies in melt inclusions and whole-rock. The preferential depletion of these elements indicates that the crystallization of feldspars within the melt (Fig. 3; Table 1; Hildreth, 1979; Cullers and Graf, 1984). Harvey displays significant variation in feldspar composition throughout the major formations, with relatively few feldspar phenocrysts exhibited within the oldest York Mills, rare to abundant K-feldspar and plagioclase (up to 2 mm) found in Cherry Hill, and abundant, coarse-grained K-feldspar, and rare albite found within the uppermost Harvey Mountain Formation (Payette and Martin, 1986b). Piskahegan is also highly zoned, with significant K-feldspar and plagioclase accumulations present in the uppermost (late) caldera formations, decreasing in the underlying sequences (McCutcheon et al., 1997). However, the Bailey Rock Formation contains significant K-feldspar ($\leq 20\%$), and plagioclase, despite its lower

stratigraphic position. Since whole-rocks do not show these extreme Eu, Sr and Ba depletions (Fig. 3) when compared to the melt inclusions, the whole-rocks cannot be considered representative of bulk liquid compositions and must represent samples from formations that contain significant accumulations of feldspar crystals.

Melt inclusions in Harvey show enrichment in HREE compared to LREE, while Piskahegan shows a relatively flat REE pattern. Initially, we considered that differences in REE chemistry may be related to accessory phases (Table 1). Rare microphenocrysts of apatite, titanomagnetite and zircon occur within the Bailey Rock rhyolites of Piskahegan (McCutcheon et al., 1997), while only zircon was identified at Harvey (Table 1; Payette and Martin, 1986b). Considering the mineral-melt partition coefficients for relevant trace elements in these systems (Mahood and Hildreth, 1983; Stix and Gorton, 1990; Streck and Grunder, 1997), it is possible that U and Th would have preferentially partitioned into zircon, while La and Ce partitioned into titanomagnetite, apatite and zircon. However, since the partition coefficient for U between zircon and melt is significantly higher than Th, zircon fractionation would have resulted in a progressive lowering of the U/Th ratio in the melt. This is in contrast to the observed compositions of melt inclusions at both localities that show a progressive increase in U/Th ratio with time (Figure 4). Therefore, zircon could not have significantly influenced U and Th abundance.

Similarly, titanomagnetite appeared to be a potential LREE fractionating phase present at Piskahegan but absent at Harvey. But HREE enrichment is characteristic of the Harvey rocks in which this mineral is absent, and apatite and zircon abundance the same in both locations (Table 1). Like U and Th, differences in REE composition of the Harvey

and Piskahegan rocks must not be related to accessory phase crystallization. This is in agreement with Taylor (1981) who indicated that HREE enrichment is unable to occur through crystal-liquid equilibrium processes alone, and hypothesized that F-rich volatiles may interact with the melt to cause this enrichment. Increases in F concentration have been demonstrated to yield a positive correlation with HREE and a negative correlation with LREE suggesting that F forms stable complexes with HREE (Mineyev et al., 1963). This hypothesis has been demonstrated both empirically (Kerrick and Fryer, 1979; Taylor and Fryer, 1980; Webster et al., 1989) and experimentally (Flynn and Burnham, 1978) whereby Cl-bearing fluids increase the concentration of LREE, Na, Fe, Ti, Mn, Zn, Nb, and Zr, while F or CO₂-bearing fluids enhance the abundance of HREE, Al, Na, Li, Rb, Cs, Ta, Th, and U. However, since the F-rich peralkaline granites (Taylor, 1981) fail to exhibit enrichment of HREE, and trapped melt phases at Harvey and Piskahegan have similar F concentrations (~0.2-0.3 wt. %) despite differing REE patterns, it is evident that F did not significantly influence the concentrations of HREE in these 2 environments. On the basis of the arguments above, we suggest the differences in REE signatures between Harvey and Piskahegan likely reflects differences in the original magmatic source for each suite.

3.6.4. The effect of boundary layers on melt inclusion composition

Previous research (e.g. Harrison and Watson, 1984; Bacon, 1989; Lu et al., 1995) has suggested that the presence of a boundary layer adjacent to forming melt inclusions can facilitate preferential enrichment and depletion of elements with variable diffusive

coefficients. However, some studies argue that this process is reduced for inclusions $>40\mu\text{m}$ while others suggest that boundary layers have little effect on overall trace element concentrations in trapped melts except in cases where diffusion-controlled crystal growth predominates (see Bacon et al., 1992; Lowenstern, 1995; Baker, 2008). A recent study by Baker (2008) indicated that a test of homogeneity dependant on melt inclusion size can be conducted to determine if inclusions were influenced by boundary layer effects. In the study areas, ratios of elements with variable diffusivities (e.g., Zr/Cs) in the melt inclusions of variable size were relatively constant. It was concluded that boundary layer effects did not impact the studied inclusions and that observed (measured) compositions are homogeneous, ultimately representing the composition of the bulk melt.

3.6.5. Comparisons to other volcanic- and caldera-associated U deposits

The Streltsovka Caldera is the largest U deposit in the world, containing over 280000 tons of U_3O_8 (grade = 0.2% U; IAEA, 2009). Despite being significantly elevated in F (~1.77 wt. %) compared to the peraluminous Harvey and Piskahegan deposits, the rhyolitic melt inclusions of the Streltsovka Caldera display similar trace element signatures. Streltsovka melt inclusions are peralkaline, high F, moderate to high SiO_2 , low FeO, and TiO_2 , with moderate Na_2O and K_2O . The exhibited geochemical trends are similar, with slightly enriched LREE, and depleted HREE compared to Piskahegan and Harvey melt inclusions (Fig. 3C; Chabiron et al., 2001). This provides further evidence that concentration of F within a melt does not explicitly control the concentrations of

HREE as commonly indicated (see Mineyev et al., 1963; Flynn and Burnham, 1978; Kerrich and Fryer, 1979; Taylor and Fryer, 1980; Webster et al., 1989).

The relative enrichment of REE in melt compared to whole-rock implies the melt of Harvey, just like Streltsovka, was saturated during trapping and experienced significant fractionation since crystallization occurred (Chabiron et al., 2001). Piskahegan did not exhibit REE enrichment in melt inclusions compared to whole-rock, and therefore minimal fractionation occurred after trapping of the magma. This provides further evidence that a variable genetic history occurred between Harvey and Piskahegan.

Overall, the REE geochemical signature of the Streltsovka melt inclusions most closely resembles the “syn-eruptive” inclusions of Harvey, with both exhibiting REE enrichment, and negative Eu and Ba anomalies in melt inclusions. Interestingly, both Harvey “syn-eruptive” (76 ± 18 ppm), and melt inclusions (34 ± 10 ppm), are enriched in U compared to Streltsovka melt inclusions (17 ± 4 ppm), while the concentration of U within mineralized samples is significantly elevated at Streltsovka (~ 2000 ppm) compared to Harvey (~ 1500 ppm). Although both deposits are highly enriched in U, it is evident that significant U was lost from Harvey, facilitated by intense alteration (i.e. by meteoric water circulation, regional metamorphism).

3.6.6. Melt inclusions as an exploration tool

Through comparison of U and Th concentrations within melt inclusions and whole-rock samples, it is evident that the analysis of melt inclusions holds promise as an exploration tool for volcanic- and caldera-related U deposits. Melt inclusions from known economic U deposits (Fig. 3C) show highly elevated U, Th and REE contents with

negative Eu anomalies. The compositions of melt inclusions at Harvey and Piskahegan are very comparable to known economic U deposits, with the Harvey “syn-eruptive” inclusions even more significantly enriched in U, Th, and REE than other sites. These chemical characteristics can be identified easily through the analysis of melt inclusions and it may be favorable to target volcanic sequences with unusually high U and Th contents contained in melt inclusions (Figure 4).

Whole-rock values, on the other hand, will be misleading due to the effects of alteration and differential remobilization of U and or Th. This is evident in the barren volcanics at Harvey and Piskahegan which have similar U, Th and U/Th ratios, despite marked differences in the U grade of mineralization at each locality (Figure 4). Multiple studies have indicated that U can be removed from volcanics during primary degassing (Goodell and Trentham, 1980) or by post magmatic processes including groundwater (Goodell and Trentham, 1980) and acid leaching (Whitfield et al., 1959; Larsen, 1961). Non-mineralized samples at Harvey depict a lower U/Th ratio than either mineralized whole-rocks or melt inclusions, and overall, whole-rock enrichments in barren rhyolites at Harvey and Piskahegan are similar, despite the enrichment in U in the mineralization at these two deposits being so markedly different. Therefore, even if a deposit contains mineralization, it may be overlooked if the exploratory drilling fails to intersect the mineralized section. By performing melt inclusion analyses in conjunction with whole-rock geochemistry, it may be possible to differentiate between those volcanic suites that exhibited the greatest level of primary magmatic enrichment and therefore, have the greatest potential to contain high grade mineralization since it is the volcanic materials

themselves that source the U and Th in the deposits by interaction with a continuum of high-temperature magmatic to lower-temperature meteoric/metamorphic fluids. On the other hand, determination of U/Th ratios in melt inclusions as a means to predict the ultimate U/Th ratio of the deposits is less reliable, since in addition to primary decoupling of U from Th during magmatic fractionation, U is remobilized more readily than Th by acidic fluids. Acid soluble U can be derived from multiple sources including, metamict minerals, adsorbed ions on crystal surfaces, acid soluble minerals with elevated U, and hydrothermal fluids that are introduced through cracks or grain boundaries (Larsen and Phair, 1954; Brown et al., 1956; Neuerburg, 1956). This is especially prevalent in rocks with high SiO₂ concentrations as a greater proportion of the U is acid-soluble, and therefore easily leached (Whitfield et al., 1959).

Exploration should focus on identifying highly evolved (fractionated) melt inclusions as they contain the highest values of both U and Th. This study suggests that crystallization of feldspars that do not sequester any strongly incompatible trace elements (including Th and U), leading to increases in the overall concentration of U and Th in the melt that were higher at Harvey than in temporally similar melt stages at Piskahegan.

3.7. Conclusion

The analyses of melt inclusions from Harvey and Piskahegan indicate that the magmatic-hydrothermal genetic history cannot be determined from whole-rock data alone. While the major and trace element geochemical trends are similar in whole-rock, the melt inclusion trace element signatures are extremely varied between the two

deposits, with Harvey significantly more enriched in U, Th, Cs, B, and LREE than Piskahegan. This implies these suites did not evolve from the same magmatic source, or at the very least Harvey represents a more fractionated magma, indicated by the variable U/Th ratios, and trace element signatures. In order to conclusively determine the genetic source of Harvey and Piskahegan, additional geochemical work will be required.

Much higher grade U mineralization at Harvey may be related to the higher pre- and “syn-eruptive” melt concentrations. After initial enrichment by magmatic fractionation, U contained in the volcanic products was likely remobilized by a magmatic fluids, or low temperature meteoric/metamorphic fluids. Additional evidence for remobilization is exhibited by the prevalent alteration within some samples, and the occurrence of vein-hosted U mineralization. Volcanic products at Piskahegan, in contrast, did not attain the same degree of fractionation (and therefore, enrichment in U and Th) and may not have experienced significant post-magmatic U remobilization. Whole-rock analyses do not adequately portray the melt evolution of these systems, since non-mineralized and mineralized whole rocks at Harvey and Piskahegan are shown to display similar U/Th ratios and bulk U and Th concentrations, despite marked differences in U grades shown by the localities.

3.8. Acknowledgements

Fieldwork expenses were supported by a grant from the Geological Survey Branch of the New Brunswick Department of Natural Resources (JD). Analytical work was funded in part by the Natural Sciences and Engineering Research Council of Canada (NSERC) Discovery Grant (JD), Society of Economic Geologists Student Research Grant (TRG),

Mineralogical Association of Canada Travel and Research Grant (TRG), and the George Frederic Matthew Research Grant in Geology (TRG). The Swiss Science Foundation is acknowledged for its continued support of the LA-ICP-MS facility in the Department of Earth Sciences, ETH Zurich. We thank Malcolm McLeod, New Brunswick Department of Natural Resources, Geological Survey for his continued support, as well as Dan MacDonald, Dalhousie Microprobe Facility, and Darren LeFort for their assistance with microprobe work.

3.9. Chapter 3 Appendix

All the figures are located in a consecutive manner, in the general style required for manuscript submission to peer-reviewed journals.

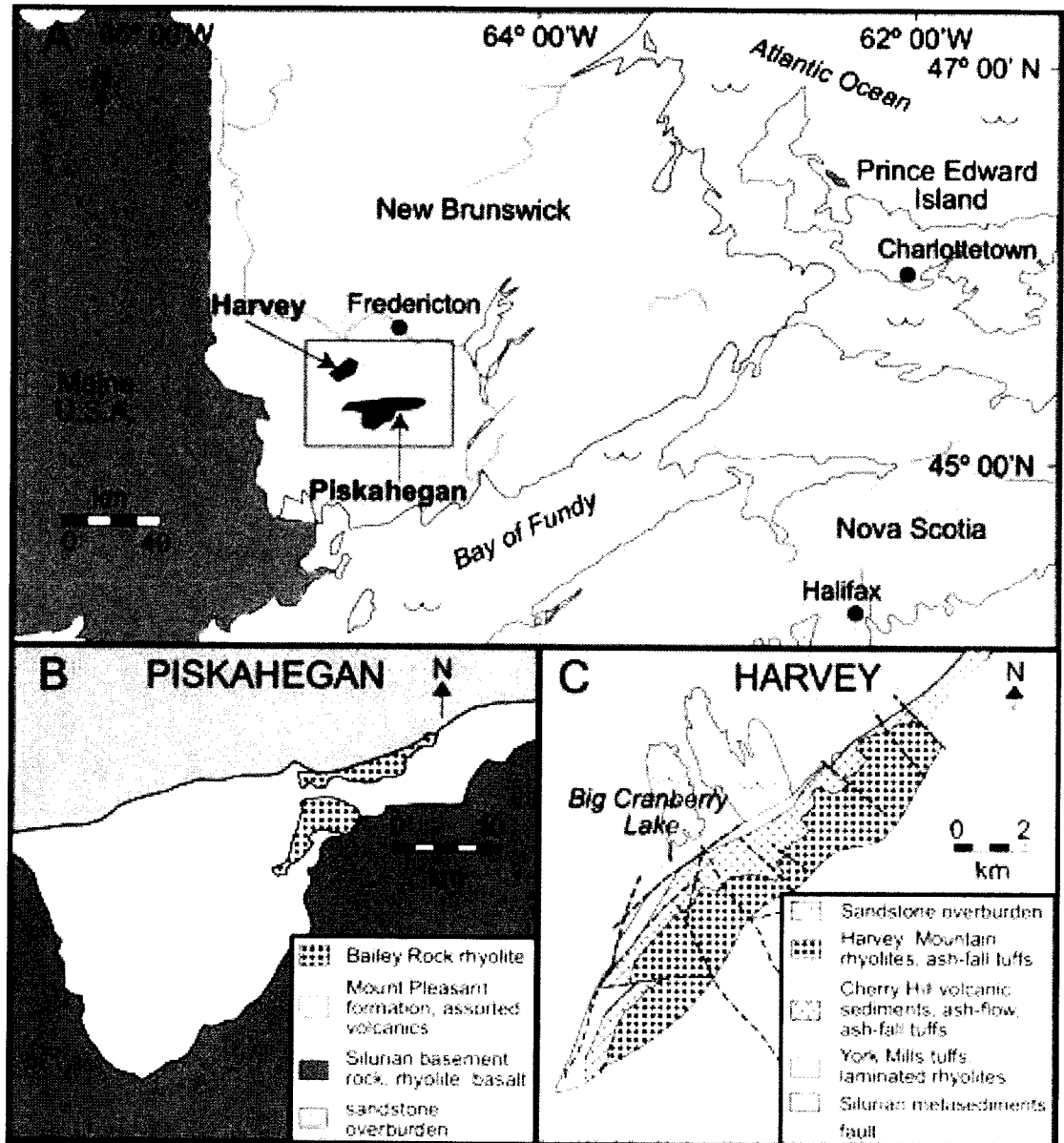


Figure 3.1. Map of study locations. (a) Location of Harvey and Piskahegan within the Atlantic Provinces, Canada, (b) Piskahegan, analyzed samples are located within the Bailey Rock rhyolite formation (modified from McCutcheon et al., 1997), and (c) Harvey, analyzed samples are located in the Cherry Hill, and Harvey Mountain rhyolite formations (modified from Payette and Martin, 1986b).

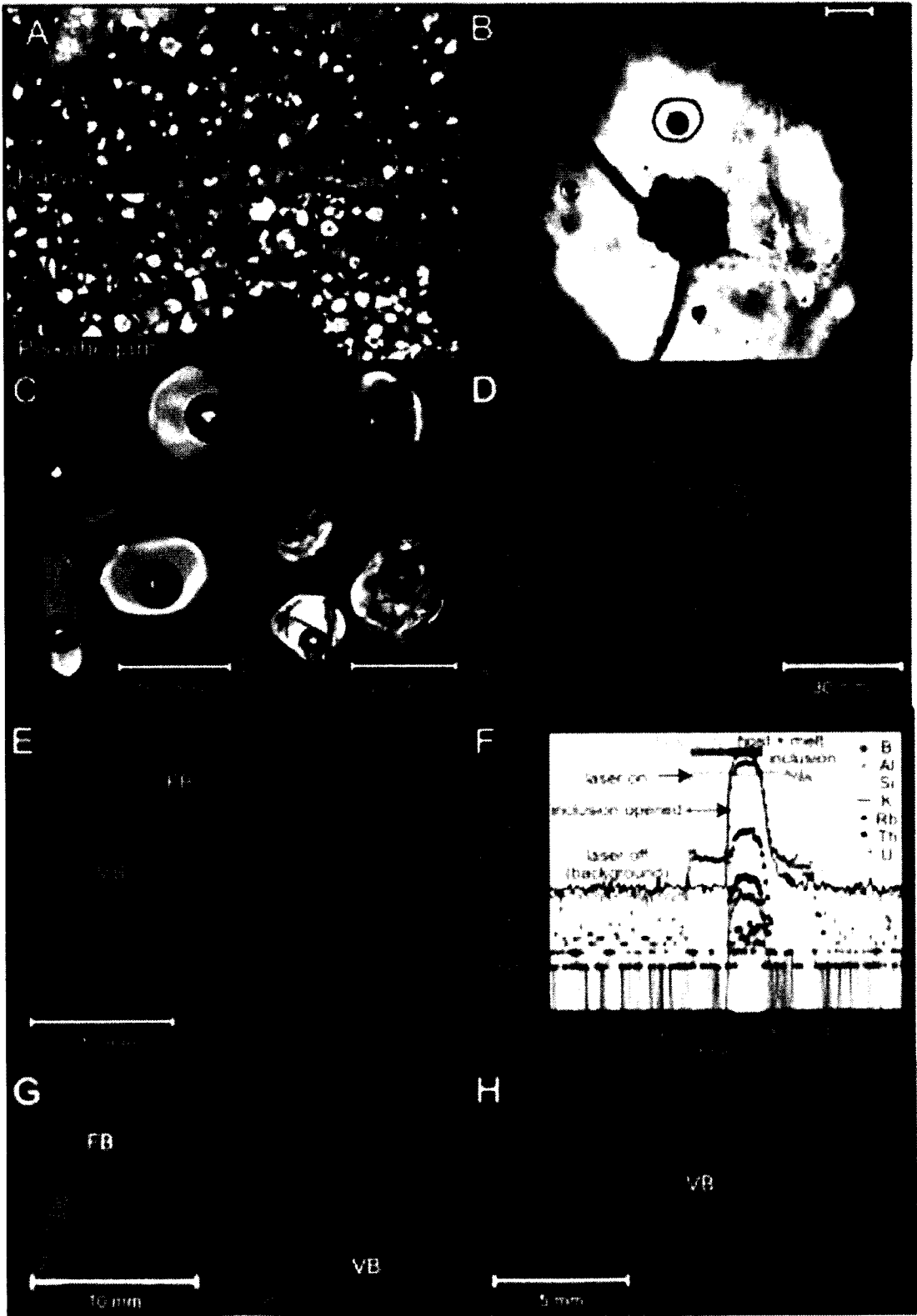


Figure 3.2. Types of melt inclusions and their host. A. porphyritic rhyolite sample with quartz phenocrysts, B. melt inclusions within a quartz phenocryst C. melt inclusion type 1, glass + bubble, and melt inclusion type 2, glass + bubble + daughter phases, D. “syn-eruptive” melt inclusion in matrix, E. bubbles of fluid trapped within the melt, and F. signal from the LA-ICP-MS indicating various elements measured within the inclusion, G. Melt inclusions with variable amounts of fluid bubbles indicating heterogeneous entrapment, H. Clean (fluid bubble free) “syn-eruptive” melt inclusion. QZ = quartz, FB = fluid bubble, VB = vapour bubble

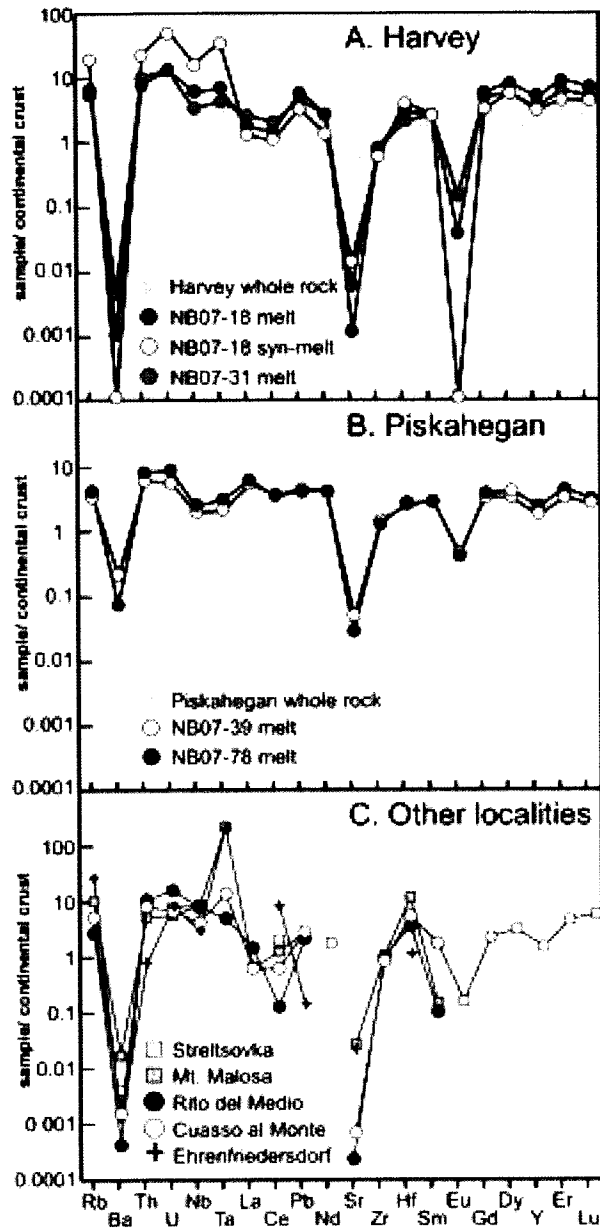


Figure 3.3. Average continental crust-normalized multi element plot of melt inclusions and whole-rock. A. Harvey, whole-rock(n=2), Cherry Hill NB07-18 melt (n=21), and “syn-eruptive” melt (n=7), and Harvey Mountain, NB07-31 melt (n=21). Neither NB07-18, nor NB07-31 whole-rocks were analyzed by ICP-MS, therefore representative

samples from the Cherry Hill and Harvey Mountain Formations were averaged, and used to reflect the whole-rock geochemical trend of Harvey. B. Piskahegan, whole-rock (n=1), and Bailey Rock NB07-39 (n=25), NB07-78 (n=10) melt. C. Melt inclusions from other localities: Mount Malosa (n=7); Cuasso al Monte (n=2); Ehrenfriedersdorf (n=1); Rito del Medio (n=2; Zajacz et al., 2008), and Streltsovka (n=40; Chabiron et al., 2001). Values required for normalization were obtained from Rudnick and Gao (2004).

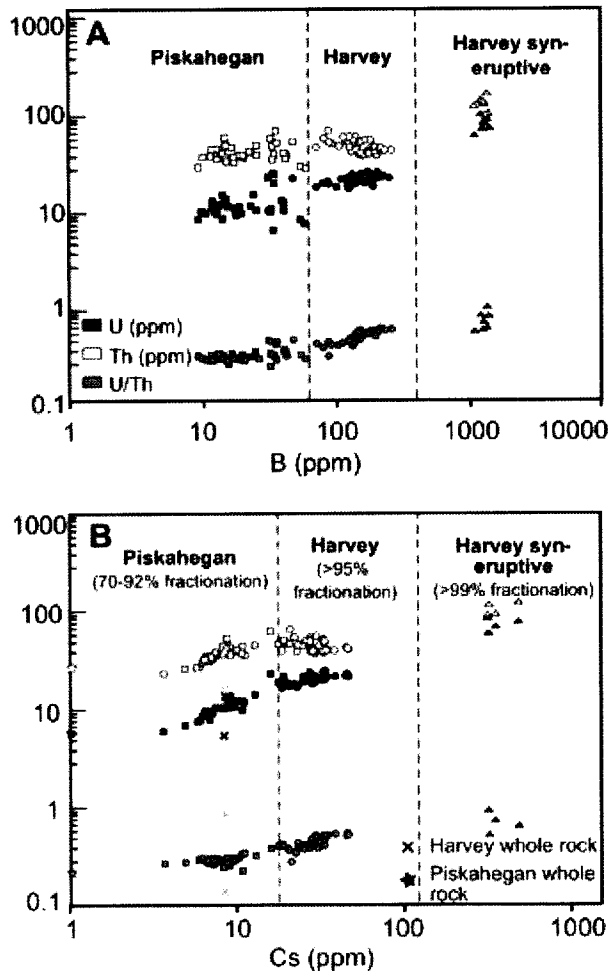


Figure 3.4. Fractionation trends involving Cs, B, U and Th at Harvey and Piskahegan, as evidenced from melt inclusions. Whole-rock values are indicated for 1 host rhyolite at

Piskahegan and 2 samples of rhyolite from Harvey, and are similar to one another. A. Concentration of B relative to incompatible trace elements in quartz-hosted melt inclusions. B. Concentration of Cs relative to incompatible trace elements in quartz-hosted melt inclusions. Approximate fractionation values (% fractionation of the liquid) for the Piskahegan “pre-eruptive” melt, Harvey “pre-eruptive” melt and Harvey “syn-eruptive” melt are shown, and were estimated using the method of Audétat and Pettke (2003) utilizing the Cs content of the melt inclusions, determined by LA-ICP-MS.

Mineral	Bailey Rock	Cherry Hill	Harvey Mountain
	25-35% phenocrysts, remainder is groundmass, Kfs>Qz>Pl>HBL	15% phenocrysts, remainder is felsic groundmass Qz>Kfs>Pl	10-15% phenocrysts, remainder is felsic groundmass Qz>Kfs>Pl
Modal Abundance			
quartz	0.1- 3.0mm phenocrysts	0.1-3mm phenocrysts	0.1-2mm phenocrysts
k-feldspar	1.0-12mm phenocrysts	<2mm phenocrysts	<2mm phenocrysts
plagioclase	1.8mm phenocrysts	rare phenocrysts	rare phenocrysts
biotite	N/A	rare altered biotite	rare altered biotite
	0.2-1.50mm pseudomorphs (Ap, Zrn, Ti-Mag) in plagioclase	N/A	N/A
amphibole	replaced amphibole	N/A	N/A
chlorite	N/A	present in cavities	present in cavities
flourite	N/A	rare	
calcite	N/A	replaced glass shards in groundmass	N/A
illite	rare microphenocrysts in amphibole	rare microphenocrysts	rare microphenocrysts
apatite	rare microphenocrysts in amphibole	rare microphenocrysts	rare microphenocrysts
zircon	rare microphenocrysts in amphibole	N/A	N/A
titanomagnetite			

Table 3.1. Summary of major and accessory minerals within Piskahegan and Harvey. Descriptions of phenocrysts represent summaries of current and previous work on Piskahegan (McCutcheon et al., 1997) and Harvey (Payette and Martin, 1986a, b; Kuan, 1970; Pajari, 1973). Abbreviations used: Hbl = hornblende, Kfs = K-feldspar, Pl = plagioclase, Qx = quartz

Harvey-Cherry Hill

	NB07-11	NB07-18	NB07-18 Melt inclusions**														
	Whole rock (n=11)	Microprobe Average (n=11)	1	2	3	4	5	6	7	8	9	10	11	12	13	14	15
SiO ₂ (wt%)	77.0	74.8	71.9	72.5	72.8	72.7	72.1	72.7	72.3	73.1	73.3	72.7	72.6	72.3	73.8	73.9	73.8
TiO ₂	0.6	0.06	0.07	0.07	0.05	0.09	0.07	0.10	0.08	0.07	0.05	0.06	0.05	0.06	0.04	0.04	0.05
Al ₂ O ₃	12.0	15.0	14.4	14.4	14.4	14.4	14.4	14.4	14.4	14.4	14.4	14.4	14.4	14.4	14.5	14.5	14.5
FeO	2.00	0.511	1.63	1.34	1.65	1.32	1.14	1.31	1.39	1.26	1.06	1.40	1.25	1.40	1.00	0.95	1.01
MnO	0.11	0.02	0.03	0.03	0.02	0.03	0.01	0.01	0.02	0.02	0.02	0.03	0.03	0.02	0.02	0.02	0.02
MgO	1	-	0.01	0.01	0.01	0.01	0.10	0.01	0.02	0.01	0.00	0.01	0.01	0.01	0.00	0.00	0.00
CaO	1.7	0.26	0.71	0.72	0.70	0.69	0.47	0.67	0.96	0.72	0.64	0.69	0.61	0.71	0.61	0.60	0.63
Na ₂ O	3.1	2.9	3.8	3.9	3.7	3.8	4.1	3.8	3.5	3.5	3.5	3.6	3.9	3.8	3.7	3.7	3.7
K ₂ O	2.2	6.3	5.7	5.4	5.6	5.3	6.0	5.4	5.5	5.3	5.4	5.5	5.6	5.4	5.6	5.5	5.3
P ₂ O ₅	0.11	-	0.00	0.01	0.06	0.01	0.01	0.00	0.00	-	0.00	0.00	0.01	0.00	0.00	-	0.01
H ₂ O	-	0.96	1.7	1.7	1.7	1.7	1.7	1.7	1.7	1.7	1.7	1.7	1.7	1.7	1.7	1.7	1.7
F	0.13	0.23	-	-	-	-	-	-	-	-	-	-	-	-	-	-	-
S	-	0.01	-	-	-	-	-	-	-	-	-	-	-	-	-	-	-
Cl	-	0.18	-	-	-	-	-	-	-	-	-	-	-	-	-	-	-
Total	100	100	100	100	100	100	100	100	100	100	100	100	100	100	100	100	100
Biphenyl	-	-	165	150	271	130	155	140	126	147	194	182	211	150	206	240	177
Sc	-	-	4.1	4.2	1.9	3.8	4.4	4.1	4.9	3.7	1.9	2.9	1.3	4.9	1.2	1.6	2.4
V	54	-	-	-	-	-	-	-	-	-	-	-	-	-	-	-	-
Cr	70	-	8.3	1.7	-	1.56	-	-	-	-	-	-	-	2.6	2.6	-	3.3
Co	6.0	-	1.9	4.4	0.79	2.8	1.8	-	-	-	0.44	0.10	4.0	-	0.10	-	-
Ni	-	0.54	0.68	0.54	-	0.22	-	-	-	-	-	-	-	2.0	0.39	-	-
Cu	20	0.61	1.4	1.4	1.6	0.64	1.2	6.0	1.6	1.7	2.2	1.1	5.6	2.4	0.70	1.1	1.1
Au	54	30	27	31	25	26	26	30	31	33	26	35	27	35	37	26	26
Pb	168	484	453	519	407	515	441	509	486	547	499	511	477	613	653	481	481
Sr	101	0.29	0.44	0.32	0.53	0.38	0.39	0.49	0.36	0.22	0.27	0.40	0.72	0.29	0.45	0.53	0.23
Y	31	154	152	138	141	153	166	184	164	145	147	140	160	150	150	133	133
Zr	294	175	161	177	164	152	199	187	156	145	143	161	160	143	136	134	134
Nb	39	81	73	74	58	77	64	85	79	80	76	74	70	82	82	72	72
Mo	-	3.5	2.7	2.3	3.1	3.3	3.9	2.5	1.8	3.2	2.9	2.1	2.4	2.7	2.4	2.4	2.4
Ag	-	-	0.01	0.05	-	0.09	-	0.17	-	-	0.06	-	-	-	0.09	0.09	0.09
Sn	5.0	22	18	24	16	19	14	19	19	21	20	26	18	30	32	20	20
Sb	4.5	0.37	0.77	0.67	0.46	0.51	0.53	0.53	1.0	0.70	0.61	0.57	0.92	0.68	0.77	0.60	0.60
Cs	8.6	29	28	34	23	30	23	28	29	33	30	36	28	45	46	30	30
Ba	184	0.37	0.52	0.26	0.92	0.39	0.56	0.22	-	-	0.44	0.16	0.42	0.42	0.66	0.35	0.35
La	33	34	31	17	41	39	44	46	28	19	48	21	33	15	15	20	20
Ce	80	96	89	51	110	90	119	100	83	55	68	61	93	46	42	57	57
Pr	7.6	12	12	7.1	15	12	15	15	11	7.9	9.1	7.9	12	5.9	5.8	7.9	7.9
Nd	29	54	53	30	62	52	62	63	47	33	41	33	55	25	26	33	33
Sm	6.9	19	19	12	20	19	21	22	17	12	16	12	20	9.4	8.9	13	13
Eu	0.93	0.04	0.04	0.01	0.06	0.02	0.04	0.07	-	-	0.04	-	-	0.03	-	0.02	0.02
Gd	6.1	22	23	15	23	22	24	25	23	17	21	15	22	13	14	17	17
Tb	3.1	4.1	4.4	3.3	4.2	4.2	4.7	5.2	4.4	3.0	4.3	3.1	4.6	2.8	2.8	3.2	3.2
Dy	6.8	26	30	23	28	29	31	32	28	23	27	23	29	22	21	23	23
Ho	3.4	5.5	5.8	4.9	5.4	5.7	6.1	7.1	6.4	5.0	5.8	4.8	5.9	5.0	4.7	5.0	5.0
Er	4.1	17	18	15	16	17	19	19	17	18	16	16	19	16	16	16	16
Tm	0.62	2.3	2.4	2.3	2.3	2.3	2.5	2.5	2.7	2.5	2.4	2.2	2.6	2.3	2.4	2.2	2.2
Yb	4.0	15	17	16	14	16	18	17	14	16	18	15	18	18	18	18	18
Lu	0.58	2.1	2.3	2.3	1.9	2.2	2.3	2.1	2.3	2.5	2.5	2.3	2.4	2.4	2.7	2.0	2.0
Hf	8.3	9.2	8.9	8.8	8.7	8.6	10.9	10.2	8.6	9.2	9.7	9.7	8.5	10	9.5	8.6	8.6
Ta	2.7	6.3	6.7	7.4	5.5	6.1	6.1	6.5	6.1	7.4	6.8	7.3	5.8	9.1	9.2	6.8	6.8
W	6.6	5.7	6.2	7.8	5.3	6.0	5.6	7.0	6.9	7.1	7.1	7.8	6.9	8.9	10	7.5	7.5
Au	-	-	-	0.02	-	0.01	-	-	-	-	0.09	0.16	-	0.05	-	-	0.01
Pt	17	62	62	70	50	66	60	50	64	73	63	73	64	78	78	67	67
Bi	17	1.4	1.2	1.6	1.2	1.4	1.2	1.2	1.2	1.6	1.4	1.7	1.4	1.9	2.0	1.4	1.4
Th	16	38	39	40	38	37	44	43	39	38	39	40	39	43	41	36	36
U	17	19	19	21	17	19	14	18	18	21	20	21	18	22	22	18	18
U/Th	0.85	0.49	0.48	0.53	0.44	0.52	0.42	0.43	0.46	0.53	0.51	0.53	0.47	0.51	0.52	0.51	0.51

Table 3.2. Table 2. Major Compounds and Trace Element Concentrations of Melt Inclusions Hosted in Quartz Phenocrysts, and Whole-Rock. *Representative samples from Harvey (Cherry Hill, NB07-11 and Harvey Mountain, NB07-21) were used as trace element data (obtained through ICP-MS) was unavailable for these samples. **All values were obtained through ICP-MS and normalized with the SILLS program using average microprobe data. All major compound values were normalized to 100%, H₂O content within inclusions was not directly measured and assumed to equal the difference between the sum of oxides subtracted from 100 wt. %. F was analyzed using a 3µm beam diameter and a 1x10⁻⁸A beam current, utilizing silicate Coso Obsidian (Analyzed= 1.0±0.09 wt. %, Expected= 1.13 wt. %), Astimex Obsidian (Analyzed= 0.08±0.04 wt. %, Expected= 0.07 wt. %) and mineral standards, Durango Apatite (Analyzed= 3.10±0.18 wt. %, Expected= 3.22 wt.%). - symbol indicates no data available, or value below detection limits

NB07-18 Melt inclusions**													NB07-21 Whole rock (n=1)	NB07-31 Microprobe average (n=13) [†]	
	16	17	18	19	20	21	syn1	syn2	syn3	syn4	syn5	syn6	syn7		
SiO ₂ (wt%)	74.3	73.6	73.0	73.4	73.4	72.7	72.5	73.0	76.1	75.5	75.9	75.4	75.3	80.0	80.4
TiO ₂	0.06	0.07	0.04	0.04	0.07	0.12	0.17	0.09	0.13	0.23	0.12	0.24	0.14	0.07	0.04
Al ₂ O ₃	14.5	14.5	14.5	14.5	14.5	14.5	14.5	14.5	14.5	14.5	14.5	14.5	14.5	11.0	11.4
FeO	0.48	1.23	1.23	0.92	1.22	1.39	1.47	1.26	1.40	1.48	1.39	1.75	1.27	0.28	0.714
MnO	0.01	0.02	0.03	0.02	0.03	0.04	0.12	0.11	0.13	0.14	0.13	0.17	0.12	0.01	0.06
MgO	0.00	0.03	0.00	0.00	0.01	0.01	0.04	0.05	0.03	0.44	0.03	0.07	0.04	0.11	0.01
CaO	0.31	0.68	0.65	0.84	0.73	0.88	3.38	1.01	0.65	1.11	0.79	-	-	0.06	0.24
Na ₂ O	3.8	3.7	4.0	3.5	3.9	3.9	2.0	2.4	2.0	1.8	2.1	2.3	2.5	1.5	2.0
K ₂ O	5.8	5.5	5.8	6.0	5.5	5.5	4.0	4.7	4.3	3.9	4.4	4.4	5.0	6.6	5.1
P ₂ O ₅	0.00	0.01	0.02	0.00	0.01	0.33	0.22	0.09	-	0.15	-	-	-	0.07	-
H ₂ O	0.78	0.78	0.78	0.78	0.78	0.78	1.6	0.82	0.79	0.78	0.77	1.1	1.1	-	1.18
F	-	-	-	-	-	-	-	-	-	-	-	-	-	0.05	0.28
S	-	-	-	-	-	-	-	-	-	-	-	-	-	-	0.02
Cl	-	-	-	-	-	-	-	-	-	-	-	-	-	-	0.03
Total [†]	100	100	100	100	100	100	100	100	100	100	100	100	100	100	100
B (ppm)	176	137	215	220	145	202	1276	1376	1229	1090	1381	1415	1298	-	-
Sc	3.5	4.4	2.1	1.3	3.1	6.5	14	9.9	6.7	7.7	17	-	9.0	-	-
V	-	-	-	-	-	1.5	-	-	-	-	9.6	-	-	-	-
Cr	28	2.9	2.9	0.99	3.0	57	183	54	-	-	138	-	-	-	-
Co	3.4	7.6	3.7	164	7.0	0.23	-	1.9	1.2	3.8	-	-	-	-	-
Ni	18	1.5	0.84	0.22	1.6	-	-	-	-	-	-	-	-	-	-
Cu	2.3	2.9	0.67	0.87	6.4	11	29	24	18	35	121	-	-	-	-
Zn	28	25	33	32	26	24	252	341	289	323	278	210	327	14	479
Rh	489	479	575	639	515	461	1459	1653	1616	1362	1498	1629	1872	479	479
Sr	0.90	0.30	0.35	0.23	0.73	-	-	4.6	-	-	-	-	-	-	430
Y	143	158	143	132	156	164	30	44	31	160	328	20	33	81	81
Zr	143	180	127	130	151	172	109	154	144	133	77	90	141	117	117
Nb	75	79	77	82	78	72	188	207	176	172	172	159	236	26	26
Mo	4.1	3.3	2.1	2.5	2.3	4.2	-	4.6	-	-	59	-	12	-	-
Ag	-	0.14	0.08	0.10	0.43	-	-	1.2	-	-	-	-	-	-	-
Sn	5.4	20	27	29	24	11	79	73	72	64	72	124	62	13	13
Sb	1.8	0.55	0.83	0.67	0.63	0.98	6.3	14	9.0	6.7	-	11	11	6	6
Cs	30	28	39	46	33	-	-	-	-	324	320	355	489	8	8
Ba	1.1	0.17	0.11	0.18	0.90	-	-	-	-	-	-	-	-	153	153
La	26	43	15	14	23	34	15	17	17	71	16	16	16	40	40
Ce	34	94	48	41	69	95	54	57	60	86	57	62	60	59	59
Pr	9.4	12	6.2	5.4	9.4	11	6.4	8.3	5.6	12	4.9	5.1	7.0	10	10
Nd	41	51	27	23	41	51	23	31	18	55	18	16	13	40	40
Nm	15	19	10	9.3	16	18	-	15	7.3	21	16	-	9.2	10	10
Eu	-	-	0.03	-	-	-	-	-	-	-	-	-	-	0.07	0.07
Gd	20	22	17	12	21	23	4.2	2.1	3.2	33	5.3	11	16	11	11
Tb	4.0	4.2	3.1	2.6	3.9	4.7	1.5	1.0	2.8	4.3	5.1	2.1	3.4	2.2	2.2
Dy	25	28	21	20	26	30	5.2	18	6.7	37	27	-	33	15	15
Ho	5.3	5.9	4.8	4.2	5.6	5.8	1.7	4.3	2.9	5.7	5.2	-	1.8	3.0	3.0
Er	18	17	15	14	17	18	9.1	7.2	3.9	15	13	5.6	9.4	9.3	9.3
Tm	2.3	2.5	2.2	2.2	2.6	2.3	0.52	0.92	0.32	2.3	3.8	-	0.65	1.40	1.40
Yb	17	17	15	16	16	15	7.7	9.0	9.2	16	34	-	9.0	8.2	8.2
Lu	2.1	2.3	2.3	2.4	2.4	2.1	0.71	0.52	0.8	3.4	1.3	-	1.2	1.2	1.2
Hf	8.9	10	8.6	9.2	9.1	11	17	17	4.4	16	9.0	22	10	5.6	5.6
Ta	7.4	7.0	7.9	9.2	7.1	5.6	14	40	41	30	37	27	36	3.9	3.9
W	8.6	5.9	7.5	9.5	6.5	6.5	64	105	96	36	151	83	91	1.5	1.5
Au	-	-	0.03	0.02	-	-	-	-	-	-	-	-	-	-	-
Pb	71	64	72	79	65	65	14	34	76	41	38	22	20	36	36
Bi	1.1	1.2	1.6	1.9	1.4	1.3	-	-	-	1.0	-	3.4	-	0.50	0.50
Th	41	40	40	42	38	37	127	151	128	113	91	98	120	38	38
U	19	19	21	23	19	17	68	83	93	58	64	68	77	5.2	5.2
U/Th	0.47	0.48	0.54	0.56	0.51	0.46	0.53	0.55	0.74	0.52	0.92	0.73	0.64	0.14	0.14

Figure 3.2. Continued 1

Harvey - Harvey Mountain

NBO7-31 Melt inclusions**

	1	2	3	4	5	6	7	8	9	10	11	12	13	14	15	16	17
SiO ₂ (wt%)	74.2	74.1	74.4	73.1	74.3	74.2	73.6	73.7	73.3	74.7	73.9	73.4	73.8	73.1	74.7	73.3	74.4
TiO ₂	0.06	0.05	0.11	0.10	0.04	0.05	0.07	0.05	0.05	0.09	0.15	0.07	0.07	0.06	0.08	0.08	0.06
Al ₂ O ₃	14.1	14.1	14.1	14.1	14.1	14.1	14.1	14.1	14.1	14.1	14.0	14.0	14.0	14.0	14.0	14.0	14.0
FeO	1.19	1.12	1.11	1.49	1.34	1.18	1.39	1.20	1.19	1.25	1.46	0.98	0.95	1.80	1.28	0.96	1.19
MnO	0.02	0.02	0.03	0.03	0.03	0.03	0.03	0.03	0.03	0.02	0.03	0.02	0.02	0.03	0.03	0.02	0.04
MgO	0.02	0.02	0.03	0.03	0.03	0.02	0.04	0.06	0.06	0.03	0.05	0.03	0.02	0.03	0.04	0.02	0.02
CaO	0.70	0.67	0.38	0.71	0.30	0.48	0.49	0.70	0.73	0.67	0.76	0.54	0.78	0.96	0.39	0.29	0.68
Na ₂ O	2.9	2.9	2.9	3.1	2.7	2.9	2.9	3.2	3.2	2.8	3.0	2.7	3.5	3.3	3.2	3.2	3.0
K ₂ O	5.2	5.4	3.0	5.7	5.1	5.1	5.7	5.3	5.2	4.6	5.6	5.1	5.7	5.6	5.1	5.1	5.6
P ₂ O ₅	0.01	0.01	0.01	0.01	0.03	0.01	0.02	0.02	0.05	0.01	-	0.01	-	0.01	-	0.01	-
H ₂ O	1.6	1.7	1.7	1.7	1.7	1.7	1.7	1.7	1.7	1.7	1.0	1.1	1.1	1.1	1.0	1.1	1.0
F	-	-	-	-	-	-	-	-	-	-	-	-	-	-	-	-	-
S	-	-	-	-	-	-	-	-	-	-	-	-	-	-	-	-	-
Cl	-	-	-	-	-	-	-	-	-	-	-	-	-	-	-	-	-
Total	100	100	100	100	100	100	100	100	100	100	100	100	100	100	100	100	100
H (ppm)	123	133	70	88	47	117	111	124	118	81	129	134	134	164	153	132	182
Sc	2.9	2.5	2.3	3.3	2.8	3.0	3.1	2.7	3.4	3.3	3.4	2.7	2.2	2.6	3.3	2.6	1.9
V	-	-	-	-	-	-	-	-	-	-	1.1	-	2.4	0.29	-	0.18	-
Cr	-	-	-	-	-	-	5.9	6.2	-	5.9	18	-	4.6	7.3	5.4	3.8	14
Co	-	-	0.47	0.23	0.81	-	0.07	-	0.18	0.13	-	-	132	-	1147	736	-
Ni	1.2	-	1.6	0.98	2.8	-	-	1.17	1.16	-	-	2.7	0.61	9.7	3.2	6.6	-
Cu	5.7	5.0	2.9	4.1	5.7	2.4	1.2	2.9	4.1	6.3	12	4.4	3.8	11	8.1	5.7	6.7
As	42	37	32	35	45	34	39	36	36	28	27	29	34	37	28	29	39
Rb	314	318	433	332	527	498	493	471	473	479	388	473	339	363	491	446	486
Sr	1.85	1.88	2.54	1.35	1.31	0.80	2.10	1.30	1.19	2.08	6.1	3.5	0.57	1.3	2.1	1.9	0.76
Y	114	111	94	104	115	123	108	106	103	108	75	116	117	138	80	38	140
Zr	125	130	136	156	142	148	134	141	139	184	190	147	132	120	142	142	112
Nb	40	43	36	36	41	43	43	37	43	43	25	40	45	55	43	39	56
Mo	2.1	5.2	2.8	3.6	3.1	3.7	3.1	2.3	2.9	4.6	3.8	3.6	2.6	2.9	2.8	2.6	5.9
Ag	-	-	-	0.42	0.82	0.28	0.17	0.14	0.38	0.44	1.3	0.16	1.1	0.50	0.71	0.43	0.65
Sb	20	19	14	23	9	20	18	17	19	16	11	18	19	23	19	17	17
Sn	-	1.1	1.2	0.82	0.86	0.51	0.87	0.40	0.78	0.70	3.4	0.38	1.2	3.6	6.0	1.7	0.66
Cs	30	30	23	26	28	28	28	28	28	27	19	24	34	33	26	26	54
Ba	1.7	1.2	2.6	1.2	-	-	0.46	1.5	1.2	1.0	8.2	2.9	0.19	1.8	1.1	1.1	-
La	53	33	67	54	34	42	32	39	37	55	79	44	42	28	33	34	26
Ce	97	90	153	140	92	112	88	99	95	124	193	90	91	76	81	83	76
Pr	12	11	18	16	9	13	10	11	12	15	19	11	11	10	10	9.2	11
Nd	42	46	71	63	52	51	43	46	44	55	63	44	42	40	38	33	42
Sm	14	13	16	13	6.9	15	10	13	14	16	12	15	12	14	9.2	8.0	13
Eu	-	-	-	-	-	-	-	-	-	0.13	0.36	0.05	0.06	0.03	-	0.06	0.13
Gd	19	16	19	14	12	15	17	14	15	16	19	15	16	15	11	7.3	18
Tb	10	2.7	2.6	3.1	2.6	3.2	2.7	2.6	2.7	2.4	2.3	2.9	2.7	3.3	2.4	1.4	3.3
Dy	22	19	18	16	18	18	19	18	17	19	13	20	22	21	13	11	26
Ho	3.4	4.2	3.6	3.5	3.4	4.4	3.9	3.7	3.9	3.8	2.5	4.3	3.8	4.6	2.8	2.1	5.3
Er	13	13	10	10	8.4	12	13	14	10	10	9.2	11	15	13	7.1	6.6	15
Tm	1.9	1.6	0.87	1.6	1.4	1.9	1.4	1.6	1.6	2.0	1.3	2.3	1.7	2.3	1.3	1.0	2.1
Yb	11	12	12	9.1	15	16	14	12	10	9.1	10	13	13	14	12	7.1	14
Lu	3.8	1.7	1.6	1.5	2.0	1.6	1.6	1.5	1.4	1.3	1.4	1.5	1.7	1.9	1.2	1.0	2.7
Hf	5.8	6.8	4.3	7.3	5.9	7.7	9.0	6.1	7.5	8.2	7.0	7.1	7.1	6.9	7.9	7.5	7.4
Ta	6.4	5.1	2.7	4.4	3.3	5.0	5.3	5.9	5.2	4.1	2.6	4.4	5.3	5.8	4.6	4.5	6.4
W	6.6	8.6	4.0	5.5	1.6	9.0	7.3	6.3	7.3	5.5	1.6	7.2	5.3	8.7	8.1	6.2	6.9
Au	-	-	-	-	-	-	-	-	-	-	-	-	-	-	-	0.16	0.03
Pb	59	55	41	55	53	54	58	52	51	43	45	54	56	58	44	44	58
Bi	0.78	1.6	1.6	1.2	1.6	1.4	1.0	1.4	1.3	1.2	1.5	0.94	1.4	1.0	1.3	1.1	2.0
Th	55	49	45	49	49	55	54	48	50	54	39	50	48	51	49	50	51
U	23	21	17	19	21	23	21	21	20	18	16	20	20	23	21	21	24
U/Th	0.38	0.44	0.38	0.38	0.42	0.42	0.38	0.44	0.41	0.34	0.41	0.39	0.41	0.45	0.42	0.41	0.48

Figure 3.2. Continued 2

	Harvey - Harvey Mountain					Pikabegun - Bailey Rock									
	NB07-31 Melt inclusions**				NB07-39 Whole rock (n=11)	NB07-39 Microprobe average (n=12)	NB07-39 Melt inclusions**								
	18	19	20	21			1	2	3	4	5	6	7	8	9
SiO ₂ (wt%)	75.0	75.2	75.2	76.0	77.0	75.8	72.9	73.2	72.5	73.2	71.2	72.5	73.1	72.8	73.3
TiO ₂	0.10	0.08	0.12	0.12	0.24	0.16565931	0.1	0.1	0.2	0.1	0.1	0.2	0.1	0.2	
Al ₂ O ₃	14.0	14.0	14.0	14.0	12.0	14.2	14.1	14.1	14.1	14.1	14.1	14.1	14.1	14.1	14.1
FeO	1.26	0.93	1.25	0.79	1.70	0.67	1.36	1.27	1.84	1.73	1.63	1.60	1.31	1.36	1.05
MnO	0.03	0.03	0.02	0.03	0.02	0.028109825	0	0	0	0	0	0	0	0	0
MgO	0.07	0.03	0.08	0.04	0.13	0.105835199	0	0	0.1	0.1	0.1	0.1	0.1	0	0
CaO	0.99	0.37	0.67	0.77	0.14	0.376798571	0.7	0.7	0.6	0.7	1.6	0.7	0.5	0.8	0.4
Na ₂ O	2.6	2.9	2.8	2.7	2.6	2.5	3.3	3.3	3.3	3.0	3.6	3.4	3.4	3.1	3.4
K ₂ O	4.9	5.1	4.3	4.5	5.6	6.1	6.4	6.2	6.3	6.0	6.5	6.3	6.3	6.4	6.3
P ₂ O ₅	0.02	0.04	0.01	0.04	0.05	-	0	0	0	0	0	0	0	0.1	0
H ₂ O	1.1	1.1	1.1	1.1	-	0.7	1.1	1.1	1.1	1.1	1.1	1.1	1.1	1.1	1.1
F	-	-	-	-	-	0.38	-	-	-	-	-	-	-	-	-
S	-	-	-	-	-	-	-	-	-	-	-	-	-	-	-
Cl	-	-	-	-	-	0.11	-	-	-	-	-	-	-	-	-
Total	100	100	100	100	100	100	100	100	100	100	100	100	100	100	100
H (ppm)	88	131	102	88	-	-	19	40	10	33	54	10	12	14	42
Sc	3.4	0.9	2.7	2.6	-	-	3.8	4.1	4.0	4.7	4.6	3.6	3.8	3.4	4.6
V	16	-	-	1.7	15	-	1.4	1.6	1.2	1.7	2.5	1.6	1.4	0.8	1.3
Cr	5.9	3.7	-	17	-	-	-	8.3	-	7.8	-	-	1.9	-	4.3
Co	-	-	2283	11	3	-	0.9	0.4	2.4	466	0.5	2.5	0.3	3	4.3
Ni	18	-	1.5	32	-	-	0.3	-	-	-	1.4	0.7	0.3	1.8	0.4
Cu	10	12	6.9	7.0	-	-	1.6	3.3	1.1	6.1	13	3	3.1	2	4
As	308	33	28	41	-	-	6	13	6	8	6	6	6	8	6
Rb	404	439	416	422	224	-	802	316	297	332	293	330	290	330	290
Sr	5.3	1.8	1.6	3.3	37	-	19	17	23	17	29	20	23	9.1	22
Y	140	113	94	112	68	-	62	63	61	66	51	61	55	111	55
Zr	177	130	195	180	357	-	273	219	257	270	309	236	253	431	260
Nb	29	39	30	30	22	-	25	26	25	26	24	23	24	36	24
Mo	-	1.9	1.1	4.3	-	-	3.0	3.1	2.7	4.0	3.8	3.4	3.5	6.2	2.8
Ag	-	0.64	0.47	-	-	-	-	0.2	0	0.1	-	-	0	-	0.1
Sn	11	17	12	15	5	-	9	11	8	12	11	8	7	10	8
Sb	1.4	-	-	-	5.6	-	-	-	-	-	-	-	0	-	0.3
Cs	21	23	21	20	7	-	7	11	7	8	6	7	7	9	7
Ba	1.2	1.1	1.1	1.1	499	-	60	64	109	60	200	75	109	17	95
La	61	38	115	71	106	-	93	89	105	142	75	89	165	155	82
Ce	139	93	154	155	156	-	199	198	191	214	167	192	186	339	179
Pr	53	11	17	17	22	-	21	21	20	21	18	20	19	39	19
Nd	58	37	68	73	78	-	75	74	73	78	61	71	66	154	67
Sm	18	15	17	16	16	-	15	14	11	15	11	12	11	25	11
Eu	0.33	0.18	-	-	2	-	0.5	0.6	0.4	0.6	0.8	0.5	0.4	0.4	0.5
Gd	52	12	14	17	14	-	11	12	11	14	11	12	11	27	12
Th	7.2	1.0	2.2	2.7	2.4	-	1.8	1.8	1.7	1.8	1.5	1.8	1.6	3.7	1.8
Dy	40	21	17	19	13	-	11	12	11	11	10	11	11	24	10
Ho	4.6	4.2	2.5	3.7	2.8	-	2.3	2.1	2.1	2.4	1.7	2.2	2.2	4.8	2.1
Er	12	15	1.9	8.6	8	-	7	7	6	7	6	7	5	13	6
Tm	1.5	1.6	1.3	1.4	1.3	-	1.0	1.0	0.8	1.0	0.9	1.0	0.9	1.9	0.7
Yb	34	11	6.7	11	7	-	6	6	7	7	5	7	7	11	6
Lu	1.4	2.1	1.4	1.7	0.9	-	1.0	1.3	0.9	0.9	0.7	0.8	0.9	1.2	0.8
Hf	8.9	7.4	6.8	7.2	9.3	-	9.6	7.9	9.5	8.9	8.6	8.4	7.9	13.8	9.2
Ta	3.6	4.8	3.2	3.2	2.0	-	2.2	2.6	2.2	1.9	1.7	2.3	2.4	3.6	2.1
W	8.1	4.9	4.6	4.3	0.6	-	1.5	1.7	3.0	2.3	3.5	2.2	1.8	3.6	1.8
Au	-	-	-	-	-	-	-	-	-	-	-	-	-	0.1	-
Pb	44	44	38	40	27	-	43	44	40	45	45	42	194	44	44
Ir	0.68	1.4	0.59	2.5	0.2	-	0.5	0.6	0.5	0.4	0.2	0.4	0.4	0.7	0.5
Rh	64	47	46	47	26	-	34	36	35	36	27	34	31	52	33
L	18	17	17	18	6	-	9	12	9	10	8	9	9	14	9
U/Th	0.28	0.37	0.37	0.39	0.22662	-	0.3	0.3	0.3	0.3	0.3	0.3	0.3	0.3	0.3

Figure 3.1. Continued 3

Pitakegan- Bailey Rock Rhyolite

NB07-39 Melt inclusions**

	10	11	12	13	14	15	16	17	18	19	20	21	22	23	24	25
SiO ₂ (wt%)	72.8	72.6	72.7	74.4	72.8	74.2	75.0	74.4	73.6	73.9	74.1	73.8	74.3	74.4	74.1	74.0
TiO ₂	0.16	0.10	0.21	0.18	0.37	0.21	0.14	0.30	0.19	0.22	0.20	0.19	0.18	0.14	0.18	0.22
Al ₂ O ₃	14.1	14.1	14.1	13.9	13.9	13.9	13.9	13.9	13.9	13.9	13.9	13.9	13.9	13.9	13.9	13.9
FeO	1.69	1.62	1.58	1.72	1.97	1.55	1.56	1.55	2.03	1.73	1.44	1.74	1.56	1.41	1.77	1.54
MnO	0.05	0.03	0.03	0.03	0.03	0.03	0.03	0.03	0.03	0.03	0.03	0.03	0.03	0.03	0.03	0.03
MgO	0.08	0.06	0.07	0.07	0.09	0.06	0.05	0.07	0.07	0.06	0.06	0.06	0.07	0.04	0.06	0.07
CaO	0.71	0.51	0.69	0.81	0.81	0.72	0.75	0.69	0.56	0.75	0.60	0.68	0.67	0.48	0.69	0.73
Na ₂ O	3.4	3.5	3.2	2.9	3.4	3.0	2.8	3.0	3.3	3.1	3.4	3.3	3.0	3.4	3.3	3.2
K ₂ O	6.4	6.4	6.3	6.0	6.6	6.3	5.8	6.2	6.6	6.3	6.3	6.3	6.3	6.2	6.0	6.3
P ₂ O ₅	0.01	0.03	0.04	0.01	0.05	0.02	0.01	0.01	0.01	0.01	0.01	0.01	0.02	0.01	0.06	0.03
H ₂ O	1.1	1.1	1.1	-	-	-	-	-	-	-	-	-	-	-	-	-
F	-	-	-	-	-	-	-	-	-	-	-	-	-	-	-	-
S	-	-	-	-	-	-	-	-	-	-	-	-	-	-	-	-
Cl	-	-	-	-	-	-	-	-	-	-	-	-	-	-	-	-
Total	100	100	100	100	100	100	100	100	100	100	100	100	100	100	100	100
H (ppm)	32	41	60	32	34	25	-	-	18	13	17	17	13	13	13	9.1
Sc	4.6	4.4	4.1	5.1	6.3	5.6	4.2	3.9	4.4	4.0	4.0	4.5	3.8	4.2	5.0	4.7
V	1.5	2.0	2.8	1.0	3.0	1.9	-	0.76	1.2	1.3	1.3	1.1	2.0	0.37	0.36	1.7
Cr	1.9	9.2	8.7	-	5.6	-	-	-	2.4	3.1	1.7	2.7	-	-	4.1	-
Co	1.6	0.25	1.9	26	0.55	0.74	-	0.49	1.4	0.60	7.4	7.2	0.88	0.50	0.54	1.0
Ni	0.76	1.1	0.65	-	0.48	-	0.77	-	0.51	0.80	0.56	1.9	-	0.61	5.6	1.5
Cu	5.2	5.1	1.5	4.6	8.5	2.7	1.2	2.5	5.6	2.4	4.4	1.2	0.78	6.0	11	2.3
As	6.1	11	5.0	6.5	2.9	4.0	3.3	4.5	6.4	4.7	6.0	6.3	5.4	9.9	6.3	4.0
Rb	289	336	328	356	288	303	323	288	315	285	275	296	270	309	319	264
Sr	22	13	34	12	34	15	9.5	21	15	18	22	15	25	11	8.3	27
Y	56	60	49	90	49	68	83	60	60	60	52	60	54	66	94	50
Zr	234	268	330	299	479	337	360	254	263	275	250	251	265	231	275	311
Nb	23	25	23	31	23	29	35	22	26	23	22	24	24	27	32	24
Mo	3.2	3.2	2.4	3.5	2.5	3.2	3.9	2.1	2.3	2.7	2.5	4.0	3.2	3.8	3.1	3.9
Ag	0.05	0.22	-	-	0.22	0.17	0.38	-	0.08	0.24	0.11	0.09	0.09	0.09	0.08	0.16
Sb	7.0	12	9.4	10	4.7	7.0	10.8	3.2	7.7	6.1	5.9	7.0	5.9	8.9	8.1	5.8
Sn	-	-	-	-	-	0.29	-	-	0.12	-	0.05	-	-	-	0.12	-
Cs	7.0	11	5.0	11	3.7	6.7	9.1	7.3	7.7	6.6	6.4	7.5	7.0	9.2	8.4	6.0
Ba	105	59	256	45	111	52	110	50	103	121	38	134	37	25	202	202
La	83	85	74	146	63	125	147	86	137	84	78	88	76	99	157	77
Ce	168	194	157	283	134	207	305	180	196	182	170	196	166	221	307	166
Pr	19	19	16	31	14	22	31	19	21	19	18	20	17	23	33	17
Nd	68	69	62	115	58	80	115	63	71	70	62	71	65	82	129	62
Sm	13	14	10	18	11	14	16	11	14	14	11	13	11	14	24	13
Eu	0.57	0.58	0.43	0.39	0.71	0.49	0.52	0.38	0.37	0.53	0.44	0.31	0.56	0.26	0.44	0.69
Gd	11	10	8.5	18	7.2	11	19	10	12	11	10	11	10	12	19	9.3
Tb	1.7	1.7	1.6	2.7	1.6	2.0	3.0	1.8	3.8	1.9	1.5	1.9	1.5	2.1	3.1	1.6
Dy	10	12	11	16	7.6	12	19	11	11	11	10	12	10	12	18	10
Ho	2.0	2.2	2.2	3.2	1.8	2.5	3.8	2.0	2.3	2.3	2.0	1.9	1.9	2.6	3.9	2.0
Er	6.2	6.5	6.6	11	6.5	7.3	10	6.1	6.6	6.1	5.8	6.8	5.0	6.4	10	5.8
Tm	0.87	1.0	0.81	1.3	0.71	0.90	1.1	0.88	0.90	0.73	0.83	1.0	0.88	1.1	1.4	0.83
Yb	5.7	8.0	4.9	8.8	4.0	5.0	9.3	5.2	6.2	6.7	6.0	6.4	6.6	7.2	9.0	5.2
Lu	0.90	1.2	0.62	0.87	0.79	1.1	1.4	0.5	1.0	0.66	0.83	0.90	0.82	1.2	1.3	0.86
Hf	8.1	7.0	9.2	11	12	9.2	15	10	8.9	7.5	8.5	8.4	7.9	8.5	11	9.0
Ta	2.2	2.7	2.4	2.7	1.7	2.1	2.8	2.4	2.5	2.3	2.0	2.3	2.1	2.7	2.8	2.0
W	1.7	2.5	2.2	2.3	0.6	2.0	1.5	2.0	2.1	1.9	1.6	1.7	1.8	2.6	2.2	1.3
Au	-	-	-	-	-	-	-	-	-	-	-	-	-	-	0.06	-
Pb	41	47	34	43	39	43	50	40	44	44	41	40	38	42	50	39
Bi	0.48	0.64	3.5	0.64	0.09	0.38	0.58	0.54	0.48	0.31	0.35	0.43	0.65	0.5	5.5	0.48
Th	32	26	26	43	23	35	43	33	35	33	30	36	30	36	44	27
U	10	12	6.8	10	5.9	9.4	11	9.2	10	9.1	8.7	10	8.0	11	10	7.6
U/Th	0.30	0.33	0.26	0.22	0.26	0.27	0.25	0.28	0.29	0.28	0.29	0.28	0.26	0.30	0.24	0.29

Figure 3.1. Continued 4

Piskanegean-Bulky Rock Rhyolite											
NB07-78 Microprobe average (n=8)	NB07-78 Melt inclusions**										
	1	2	3	4	5	6	7	8	9	10	
SiO ₂ (wt%)	74.9	70.7	70.3	71.5	71.3	71.3	70.0	70.9	70.8	71.8	71.8
TiO ₂	0.15	0.13	0.17	0.17	0.17	0.07	0.21	0.18	0.08	0.07	0.12
Al ₂ O ₃	14.7	14.1	14.1	14.1	14.1	14.1	14.1	14.1	14.1	14.1	14.1
FeO	0.269	1.40	1.62	1.34	1.45	1.27	1.48	1.64	1.69	1.23	1.18
MnO	0.03	0.03	0.03	0.02	0.03	0.03	0.03	0.03	0.03	0.03	0.02
MgO	0.02	0.05	0.06	0.05	0.05	0.05	0.05	0.05	0.05	0.07	0.04
CaO	0.57	0.70	0.77	0.60	0.78	0.59	0.61	0.83	0.86	0.68	0.58
Na ₂ O	3.2	3.3	3.4	3.2	3.0	3.0	3.4	3.0	3.4	3.0	2.9
K ₂ O	6.2	6.0	5.9	5.5	5.6	5.9	6.5	5.8	5.5	5.6	5.8
P ₂ O ₅	-	0.01	0.01	0.01	0.02	0.05	0.01	0.01	0.01	0.01	0.01
H ₂ O	1.3	3.5	3.5	3.5	3.5	3.5	3.5	3.5	3.5	3.5	3.5
F	0.21	-	-	-	-	-	-	-	-	-	-
S	-	-	-	-	-	-	-	-	-	-	-
Cl	0.14	-	-	-	-	-	-	-	-	-	-
Total	100	100	100	100	100	100	100	100	100	100	100
H (ppm)	22	12	12	13	33	17	12	34	31	24	24
Sc	4.0	5.0	3.7	3.7	3.2	4.1	3.9	5.3	2.3	3.1	3.1
V	0.40	1.1	1.2	0.20	0.51	1.3	-	1.0	0.19	0.38	0.38
Cr	2.5	-	3.6	4.8	-	3.0	8.4	-	-	-	-
Co	0.90	0.92	0.65	0.67	0.44	1.5	4.25	24	30	0.56	0.56
Ni	-	1.2	-	0.53	-	1.2	-	2.1	1.6	0.67	0.67
Cu	61.5	80	35	6.3	3.3	42	57	62	8.3	8.4	8.4
As	7.2	6.2	5.6	6.7	16	4.9	4.6	14	18	9.2	9.2
Rb	354	347	289	340	457	320	335	399	446	396	396
Sr	8.8	5.7	21	5.4	9.7	20	5.2	7.4	7.2	10	10
Y	71	76	63	83	77	56	73	95	86	78	78
Zr	312	271	250	373	151	288	383	253	146	189	189
Nb	29	27	24	35	33	25	36	37	37	30	30
Mo	3.0	4.6	1.7	2.0	3.4	1.9	3.1	5.2	3.6	2.4	2.4
Ag	0.16	0.22	-	0.29	0.07	-	0.14	0.13	0.13	0.34	0.34
Sn	10	11	8.8	11	14	7.3	9	16	20	10	10
Sb	0.16	-	-	0.31	0.51	-	0.14	1.01	0.13	0.12	0.12
Cs	10	10	7.2	8.8	18	7.0	7.6	16	19	13	13
Ba	27	18	100	8.6	22	80	12	17	18	25	25
La	102	115	90	134	50	109	141	93	91	220	220
Ce	222	258	196	286	115	194	236	220	112	208	208
Pr	23	26	21	31	13	20	26	23	13	22	22
Nd	82	99	74	113	43	82	85	75	47	81	81
Sm	16	17	14	20	10	15	19	13	11	14	14
Eu	0.27	0.36	0.66	0.24	0.27	1.4	0.16	-	0.22	0.31	0.31
Gd	14	14	12	17	12	10	15	16	10	13	13
Tb	2.1	2.1	1.8	2.5	2.0	2.0	2.4	1.8	1.8	2.1	2.1
Dy	13	15	11	15	14	13	14	16	13	14	14
Ho	2.8	3.0	2.2	3.0	2.6	2.1	2.8	3.5	2.8	2.9	2.9
Er	7.8	8.5	5.9	8.3	9.0	7.0	8.6	10	10	8.0	8.0
Tm	1.1	1.1	0.94	1.3	1.3	0.8	1.1	1.3	1.2	1.1	1.1
Yb	7.3	7.8	5.7	8.8	11	6.5	8.1	13	11	9.0	9.0
Lu	1.0	0.90	1.0	1.1	1.1	0.9	0.9	1.2	1.4	1.1	1.1
Hf	12	10	8.0	11	6.6	10	13	9.3	6.8	7.2	7.2
Ta	2.8	2.7	2.2	3.0	4.3	2.2	3.4	5.0	4.5	3.2	3.2
W	1.8	2.4	1.5	2.9	3.5	1.7	1.9	2.4	3.8	3.3	3.3
Au	-	-	-	-	0.11	-	-	-	0.11	-	-
Pb	48	48	38	51	54	39	46	47	47	46	46
Bi	0.51	0.60	0.45	0.48	1.4	0.4	0.4	0.7	1.1	0.8	0.8
Th	38	40	34	42	46	35	38	62	51	44	44
U	11	12	8.7	12	19	9.2	10	23	21	14	14
U/Th	0.28	0.29	0.26	0.36	0.40	0.27	0.27	0.37	0.41	0.31	0.31

Figure 3.1. Continued 5

3.10. Summary of Contributions

Geochemical analysis (and the associated preparation), of whole rocks and melt inclusion microprobe work was completed by the primary author, with LA-ICP-MS analysis of melt inclusions conducted by the second and fourth authors. As the primary author, I completed multiple drafts of this paper with subsequent revisions completed predominantly by Dr. Jacob Hanley, with minor revisions undertaken by Dr. Jarda Dostal and Marcel Güillong. The primary author created all figures, with photographs in Fig. 2 (D, E, F, G, H) taken by Dr. Hanley. Editing of this manuscript is currently ongoing at the time of submission as the paper was recently accepted (May 27, 2010), and re-submitted (July 17, 2010).

CHAPTER 4: REVISED PETROGENIC HISTORY OF LATE PALEOZOIC RHYOLITES OF THE HARVEY FORMATION, NEW BRUNSWICK, CANADA

TARYN R. GRAY^{1*}, JAROSLAV DOSTAL¹, GREGORY J. SHELLNUT²

¹Department of Geology, Saint Mary's University, Halifax, Nova Scotia, B3H 3C3, Canada

²Academia Sinica, Institute of Earth Sciences, Nankang, Taipei, 11529, Taiwan

*corresponding author <Taryn.Gray@smu.ca>

4.1 Abstract

A suite of geochemical analyses of whole-rock samples were conducted to investigate the geochemical and petrogenic relationship between the Late Paleozoic Piskahegan and Harvey Groups of southern New Brunswick, Canada. ϵ_{Hf} and ϵ_{Nd} values revealed that Harvey formed from partial melting of juvenile crustal material and Gander basement rocks indicating the source material of Harvey is significantly older, and more heterogeneous than previously thought. Elevated fractionation during genesis resulted in strong negative Sr, and Ba anomalies consistent with feldspar fractionation, and a relatively flat REE pattern. Harvey also appeared to be highly enriched in uranium, which may have been aided by post-magmatic water circulation as revealed through $\delta^{18}\text{O}$ quartz isotopes and geochemical variation diagrams. Piskahegan in contrast formed through the melting of Avalon source rocks, and experienced less fractionation and post-magmatic alteration than Harvey. Through this study, the genetic history of Harvey has been revised, particularly the dissimilarity of the Harvey and Piskahegan Groups, despite being coeval in age and emplaced in the same environment.

4.2 Introduction

The Late Devonian Harvey Group is located within the Maritimes Basin, approximately 40km southeast of Fredericton, New Brunswick. This region of southern New Brunswick hosts a variety of distinct igneous intrusions (Dunning et al., 2002) resulting from the complex tectonic history of the region. While the exact age of the Harvey Group was previously unknown, it is believed to be synchronous to the nearby Piskahegan Group, which was deposited in 363.4 ± 1.8 Ma (Tucker et al., 1998), during the third major pulse of igneous activity within the Maritimes Basin (Dunning et al., 2002).

The Harvey Group was previously examined through mineralogy, stratigraphy and geochemistry (see Payette and Martin, 1986a,b), leading to the interpretation that the Harvey Group was composed of F-rich rhyolites, similar to topaz rhyolites (see Burt et al. 1982, Christiansen et al., 1983,1984, Naumov et al., 1984), despite the absence of the mineral topaz in any of the samples. Classifying the Harvey Group as F-rich rhyolites has become increasingly important in recent years with the identification of U mineralization in the region (McLeod and Johnson, 2007). Elevated concentrations of F within a melt have been shown to increase U concentration and heavy rare earth elements (HREE; Mineyev et al., 1963; Flynn and Burnham, 1978; Kerrich and Fryer, 1979; Taylor and Fryer, 1980; Webster et al., 1989). Given that a recent melt inclusion study conducted on the Harvey volcanics (see Gray et. al, 2010) failed to indicate elevated concentrations of F within the melt (~ 0.25 wt. %), an alternate mechanism must be responsible for the increased U concentration in this region.

It is apparent based on the current ambiguity regarding the petrogenesis and geochemistry within Harvey volcanics that an additional study is warranted to determine the origin of the Harvey Group. Through geochemical work, predominantly concerning the age, and composition of the source material, a stronger interpretation of the genetic history of the Harvey Group will be elucidated. This will aid in our overall understanding of how the Harvey Group is related to, if at all, the Piskahegan Group of southern New Brunswick, and topaz rhyolites. This study also aids in evaluating the economic potential of Harvey and enhances our current understanding of the Maritimes Basin genetic history.

4.3 Geologic Setting

The 12 km thick Maritimes Basin formed during the Mid-Devonian during the final formation phase of Pangea and would remain tectonically active until the early Permian (Gibling et al., 2009; Fig. 4.1). The Maritimes Basin experienced repeated subsidence throughout the Carboniferous, as well as basin inversions (with associated faulting) throughout the area. During the mid to late Devonian, the Western St. George Batholith formed, followed by two major basin extension phases during the Late Devonian- Early Mississippian. This was associated with continental sedimentation, although marine influence resulted in evaporite deposits in some areas (Gibling et al., 2009). The Harvey Group, as well as the Piskahegan Group formed during the third major pulse of igneous activity within the Maritimes (see Dunning et al., 2002), subsequent to the Acadian Orogeny.

The Harvey Group has been subdivided into three formations (Fm), York Mills, Cherry Hill and Harvey Mountain (Fig. 4.2; Kuan, 1970; Beaudin et al., 1980), all of which will be examined in this study. The uppermost Harvey Mountain Fm is overlain by conglomerate, sandstone and shale units within the Mississippian aged Bonaventure (Shin; Jutras et. al, 2007) Group, and the Pennsylvanian aged Cumberland (Pictou) Group. The Harvey Mountain Fm is a 75-100 m thick sequence composed of laminated rhyolites, pyroclastic breccia and ash-fall tuffs. The rhyolites are typically aphanatic, devitrified, and contain well-defined alteration characterized by grey-green spherulite (3-4mm) layers (Payette and Martin, 1986b). The predominant mineralogy is composed of albite, K-feldspar, quartz, with lithic fragments and fluorite within the groundmass. The Cherry Hill Fm contains most of the U-mineralization and is comprised of quartzfeldspar porphyry, with two poorly welded ash-flow sheets at the base, spanning 5-6 m and 100 m (Kuan, 1970; Beaudin et al., 1980). The volcanogenic sediments are devitrified, and contain lithic material (Beaudin et al., 1980), with mineralogy predominantly composed of K-feldspar, plagioclase, with rare quartz, zircons, broken spherulites and mafic inclusions (Payette and Martin, 1986b). The 60 m thick York Mills Fm contains mostly sedimentary rocks including red sandstones, conglomerates and shale, containing phenocrysts of quartz, feldspar and rhyolitic fragments (Payette and Martin, 1986b). There is however a volcanogenic component to the York Mills Fm, consisting of lithic tuffs intercalated by lapilli tuffs, and an overlying laminated rhyolite layer. The slightly welded to non-welded tuffs contain rare phenocrysts of feldspar in a devitrified groundmass; the rhyolite contains quartz, albite, and fluorite within cavities.

The Piskahegan Group represents one of only a few caldera sequences of the pre-Cenozoic preserving Exocaldera, Intracaldera and Latecaldera fill sequences (McCutcheon et al., 1997), the other located in Newfoundland (Coyle and Strong, 1987). The Mount Pleasant deposit is known to contain two distinct types of economic mineralization, W-Mo-Bi, and Sn-Cu-Zn-Pb, genetically related to various phases of the 361 Ma Mount Pleasant Granitic Suite (e.g. GRI, GRII, GRIII; see Kooiman et al., 1986; McCutcheon 1990; Sinclair and Kooiman, 1990). The extrusive samples analyzed within this study are located within the Mount Pleasant Caldera, inter dispersed between the intrusive Mount Pleasant Porphyry (340–30Ma; Kooiman *et al.* 1986) and the younger, McDougall Brook Granite. Both intrusive are believed to have formed from extreme fractionation of the same magmatic source, with the McDougall Brook Granite contaminated by wall rocks, while the Mount Pleasant Porphyry was significantly more fractionated during magmatic-hydrothermal evolution facilitating the enrichment of HFSE, especially Sn, W, Mo, and Bi (Yang et al., 2003).

The Intracaldera sequence (Scouller Mountain, Little Mount Pleasant, Seelys, McDougall Brook Fms) is composed mainly of rhyolite ash flow tuffs, andesites, and porphyritic microgranites towards the uppermost Fm. Two Fms from the Intracaldera sequence will be examined in this study for comparison to Harvey, the Little Mount Pleasant Fm, predominantly composed of flow banded rhyolite and volcanic tuffs and the Seelys Fm comprised of pumice bearing, lapilli tuffs (see McCutcheon et al., 1997 for further discussion). The Exocaldera sequence (Hoyt Station Basalt, Rothea, Carrow, The Bailey Rock) is located laterally to the Intracaldera sequence and considered the extrusive

equivalent of the Mount Pleasant Porphyry (McCutcheon et al., 1997). It contains basalts, rhyolite ash flow tuffs, andesite and alluvial redbeds. The Bailey Rock Fm will also be examined as it contains rhyolites. Both the Intracaldera and Exocaldera sequences are underlain by a disconformity and overlain by the Late Caldera Fill Sequence (Big Scott Mountain, Kleef and Mount Pleasant Porphyry), which is predominantly composed of rhyolite tuffs and lava flows, alluvial redbeds, basalt and porphyry.

Previous studies have indicated the economic potential of southern New Brunswick (see Pouliot et al., 1978; Yang et al., 2003; Sinclair et al., 2006), and of particular interest to this study; U mineralization has been identified within Harvey (Strong, 1980; McLeod and Johnson, 2007) as well as Piskahegan (Brack, 1982). Based on the presence of U, Harvey and Piskahegan can generally be classified as a volcanic- and caldera-related U deposits (Gandhi and Bell, 1996; IAEA, 2009). The mineralization in Harvey is largely structurally controlled by predominantly northwest bounded faulting (Fig. 4.1), and localized within felsic volcanics, and clastic sediments (Gandhi and Bell, 1996; IAEA, 2009). The U mineralization is hosted within the ignimbrites, and associated with clay alteration, silicification and hematization, grading up to 0.447% U_3O_8 over 0.6 m, and 0.24% U_3O_8 over 1.2 m (Capella, 2007), with concentrations up to 1500 ppm noted (N. Downey, pers. commun.). Piskahegan contains similar uranium concentrations, containing up to 1527 ppm in mineralized regions (Brack, 1982).

4.4 Methods

4.4.1. Sample Preparation and Field Work

During the summer 2008, 28 whole-rock samples were obtained from the Cherry Hill (n=18), Harvey Mountain (n=5), and York Mills (n=5) Fms of the Harvey Group, and 31 samples from the Bailey Rock (n=3), Little Mount Pleasant (n=10) and Seelys (n=18) Fms of the Piskahegan Group in order to complete petrographic and geochemical studies. A portion of each sample was chipped (1cm cubes) and powdered to prepare for further geochemical analysis, with the remainder sent to Vancouver Petrographics to obtain polished thin sections.

4.4.2. Major and Trace Element Analysis

Powdered whole-rock samples from Harvey (n=28), and Piskahegan (n=31) were sent to the University of Ottawa, G.G. Hatch Stable Isotope Laboratory, Ontario to determine loss of ignition (L.O.I) as well as the concentration of major elements and compounds using a Philips PW2400 X-Ray fluorescence spectrometer (XRF). Trace elements from Harvey (n=8) and Piskahegan (n=9) were analyzed by fusion using a Perkin Elmer Optima 3000 inductively coupled plasma mass spectrometer (ICP-MS) at Activation Laboratories, Ancaster, Ontario according to standard procedures (Hoffman, 1992).

4.4.3. $^{147}\text{Sm}/^{144}\text{Nd}$ Radiogenic Isotopes

Eight samples from Harvey (2, 11, 21, 28) and Piskahegan (35A, 56, 66, 81) were analyzed for Sm/Nd isotopic ratios using a Finnigan MAT 262V thermal ionization -mass spectrometer (TIMS) at Memorial University, Newfoundland. Samples chosen for analysis contained low Rb (<1075 ppm) and Sr (<950 ppm) concentrations, few inclusions and were relatively homogenous. Approximately 0.05-0.2g of powdered

sample was dissolved in concentrated HF and HNO₃ acids, and spiked with ¹⁵⁰Nd/¹⁴⁹Sm prior to acid digestion (five days). Once the sample evaporated, the remaining material was taken up into 2N HCl for two days, dried, and again taken up into 2N HCl. Samples were subsequently loaded into cationic exchange chromatography utilizing AG50W-X8 resin. After purification, the Sm and Nd fractions were isolated with a secondary column loaded with Eichrom© Ln resin and analyzed using a multicollector Finnigan Mat 262 mass spectrometer operated in static mode. All values were normalized to ¹⁴⁶Nd/¹⁴⁴Nd = 0.7219, calibrated to the JNdi-1 standard (¹⁴³Nd/¹⁴⁴Nd = 0.512115, Tanaka et al., 2000), with Nd values accurate to <0.002% and ¹⁴⁷Sm/¹⁴⁴Nd ratio accurate to <0.1%.

4.4.4. ²⁰⁶Pb/²³⁸U Geochronologic Dating

Zircon grains from sample 17 were concentrated by conventional magnetic and heavy liquid techniques and subsequently mounted to perform cathode luminescence and backscatter imaging. The U and Pb isotopic analyses were performed using laser ablation inductively coupled plasma mass spectrometry (LA-ICP-MS) at the Beijing SHRIMP Center, Institute of Geology, Chinese Academy of Geological Sciences. Standard analytical procedures were utilized for LA-ICP-MS (Chiu et al., 2009) with results calibrated to the GJ-1 zircon standard obtained from the Australian Research Council National Key Centre for Geochemical Evolution and Metallogeny of Continents, at Macquarie University, Sydney (Jackson et al., 2004; Elhlou et al., 2006), as well as secondary standards including the Harvard reference zircon 91500 (Wiedenbeck et al., 1995) and the Australian Mud Tank Carbonatite zircon. Final isotopic ratios were determined by GLITTER 4.0 (GEMOC) software and age corrected based on the

procedure established by Anderson (2002).

4.4.5. Hf zircon isotopes

In situ zircon Hf isotope analyses were carried out using a New Wave UP 213 laser-ablation microprobe, attached to a Nu Plasma multi-collector ICP-MS, coupled with a fixed detector array of 12 Faraday cups and 3 ion counters at the Institute of Earth Sciences, Academia Sinica in Taipei. Instrumental conditions, data acquisition, and analytical procedures were similar to Griffin et al. (2000). All results were calibrated to zircon standards, Mud Tank (Woodhead and Hergt, 2005; Griffin et al., 2006) and 91500 (Weidenbeck et al., 1995), with typical within run precision (2σ) of ± 0.000030 on the $^{176}\text{Hf}/^{177}\text{Hf}$ analysis.

4.4.6. $\delta^{18}\text{O}$ Quartz Isotopes

Six samples were analyzed at the Queen's University Stable Isotope and ICP-MS Lab for analysis of $\delta^{18}\text{O}$ in quartz using a conventional BrF_5 method of Clayton and Mayeda (1963) and run on a dual inlet Finnigan Mat 252 Isotope Ratio Mass Spectrometer. All values reported in standard delta notation relative to VSMOW, and were reproducible to 0.3‰.

4.5. Alteration and the Possible Effect on Chemical Composition

Whole-rock samples from the Harvey Group and to a minor extent the Piskahegan Group, show signs of post formation alteration. Petrographic characterization of the Harvey samples revealed significant oxidation of the samples, identified by red-brown staining of various minerals as well as the groundmass. Piskahegan displayed similar oxidation in various samples, but to a reduced degree. Examination of the geochemical

data yielded elevated L.O.I. values (>5 wt.%) in multiple samples from the Cherry Hill Fm (7, 9, 10, 12, 18) where alteration appears to be most substantial. Extensive alteration caused diminished SiO₂ concentrations in all samples, except 18. However, since sample 18 was completely dissimilar to all rhyolites analyzed, it was determined to be modified by alteration despite normal SiO₂ concentrations.

While alteration of this extent would usually be problematic, it is possible to elucidate which elements reflect the magmatic distribution of Harvey and Piskahegan by comparing whole-rock to melt inclusion data from Harvey and Piskahegan (Gray et al., 2010). According to Figure 3 of Gray et al. (2010), whole-rock values are depleted compared to melt inclusion values in all incompatible elements including large ion lithophile elements (LILE; e.g. Rb, Ce, Sr, Ba) and high field strength elements (HFSE; e.g. Zr, Hf, Th, U, Ta, REE). This implies any depletion exhibited within melt inclusions that is also preserved in whole-rock can be considered primary and not induced by alteration.

To avoid any ambiguity in the geochemical comparison between Piskahegan and Harvey, immobile elements (e.g. Ti, Nb, Ta, Zr, Hf, Y, Cr, and some REE) were predominantly used for comparison. This will insure secondary alteration did not manipulate geochemical trends and aid our understanding of which elements may have been influenced by alteration.

4.6. Results

4.6.1. Geochronology- $^{206}\text{Pb}/^{238}\text{U}$ ICP-MS

$^{206}\text{Pb}/^{238}\text{U}$ LA-ICP-MS geochronologic dating of zircons from sample 17 (Cherry Hill) revealed a bimodal distribution of ages centered on 361 ± 7 Ma (MSWD = 1.7) and 403 ± 11 Ma (MSWD = 2.1; Fig. 4.3, Table 4.1). Based on current understanding of igneous activity within the Maritimes basin (see Dunning et al., 2002), we interpret the volcanic rocks of the Harvey Group were emplaced in 361 Ma. This is consistent with the formation age of the Piskahegan deposit (363.4 ± 1.8 Ma; Tucker et al., 1998), and the stratigraphic history of the basin. Older, early Devonian aged (403 Ma) samples likely represent the age of the protolith, derived from a juvenile source, although some mixing may have occurred with older, Gander source rocks. This indicates the source material of the Harvey Group is much older than previously thought. The presence of similar aged plutons within Nova Scotia (e.g. 370 Ma South Mountain Batholith, Kontak and Martin, 1997) and New Brunswick (360 Ma Pleasant Ridge Pluton; Taylor, 1992) as well as Cobequid Highlands rhyolites of the Fountain Lake Group (362-368 Ma; Dunning et al., 2002), and Cape Breton rhyolites of Lowland Cove (365 Ma; Dunning et al., 2002) imply widespread volcanic activity occurred in the early Devonian.

4.6.2. Geochemistry- major element

Based on XRF data of whole-rock samples (concentrations un-normalized), the York Mills (81.19 ± 3.0 wt. %, $n=5$, 1σ), Harvey Mountain (79.33 ± 3.6 wt. %, $n=5$, 1σ), and Cherry Hill (75.63 ± 3.17 , $n=13$, 1σ) Fms are classified as high-silica rhyolites (Table 4.2; Fig. 4.4A). York Mills and Harvey Mountain are both significantly depleted in CaO, and slightly depleted in TiO_2 , Al_2O_3 compared to Cherry Hill, likely related to

accumulations of oxides, plagioclase feldspar and or mafic inclusions (Table 4.2). The large enrichment of CaO (8.06 wt. %) exhibited within Cherry Hill should be interpreted cautiously as sample 8 also contains anomalous values of Na₂O (6.81 wt. %) and SiO₂ (65.98 wt. %) compared to the average Cherry Hill samples (Na₂O = 3.34 ± 1.47 wt. %, CaO=1.21 ± 2.15 wt%, n=5, 1σ). Despite the absence of L.O.I. values for sample 8, it is assumed these uncharacteristic values are a result of alteration, given that mineralogy is not conclusive with a basaltic/andesitic rock. Only Cherry Hill contains any notable F concentration (0.20, ± 0.05 wt.%, n=4, 1σ), with Harvey Mountain (0.04 ± 0.01wt. %, n=3, 1σ) and York Mills (0.04 wt %, n=1) relatively barren.

Rhyolitic samples of the Piskahegan Group are uniform, and decreased in SiO₂ concentrations compared to Harvey yielding 75.90 ± 0.12 wt. % in Bailey Rock (n=2, 1σ), 74.80 ± 0.85 wt. % in Little Mount Pleasant (n=10, 1σ) and 75.54 ± 1.87 wt. % in the Seelys Fm (n=18, 1σ; Table 4.3). All other major elements exhibit homogenous concentrations between Fms, with Little Mount Pleasant slightly enriched in alkalis compared to Bailey Rock or Seelys. Overall Piskahegan is more enriched in Al₂O₃, Fe₂O₃, MgO, and TiO₂ compared to Harvey, while depleted in SiO₂.

Harker diagrams of major elements compared to SiO₂ revealed increases in SiO₂ correlate to a decrease in concentration of all compounds (TiO₂, MnO, CaO, Na₂O, MgO, K₂O, Fe₂O₃ and Al₂O₃), except K₂O in Harvey Mountain (Fig. 4.5). Negative Eu anomalies, associated with feldspar fractionation are exhibited within all three Fms, most notably the Harvey Mountain Fm. Previous mineralogical work by Payette and Martin (1986b) indicated the Harvey Mountain Fm contains significant feldspar accumulations,

with moderate quantities in Cherry Hill, and relatively rare phenocrysts in the York Mills Fm. Within the Piskahegan samples, only the Seelys Fm exhibited any change in major element concentrations with changing SiO₂, with Fe₂O₃ concentrations decreasing with increasing SiO₂. All other compounds remained constant, owing largely to the homogenous SiO₂ concentrations.

4.6.3. Geochemistry-trace element

Primitive mantle normalized diagrams indicate the Harvey Group is significantly depleted in Eu, Sr (not shown), and Ba, consistent with feldspar fractionation, as well as a negative Ti anomaly (Fig 4.6A). The magnitude of depletion exhibited in whole-rock is considerably smaller than the negative anomalies displayed in Cherry Hill and Harvey Mountain silicate melt inclusions (Gray et al., 2010). Given that the magnitude of depletion is less in whole-rock samples compared to melt inclusions, it is apparent that the depletion is magmatic and not related to any post-formation alterations. Whole-rocks are enriched in HFSE (Nb, Hf, REE, Th, U) except Ta. Piskahegan in contrast displays less significant depletions in Eu, Sr (not shown), and Ba, with a similar Ti anomaly to Harvey (Fig. 4.6C). Whole-rock samples from Piskahegan similarly displayed reduced depletion compared to melt inclusions (Gray et al., 2010). Whole-rock samples at Piskahegan are also enriched in HFSE, although to a lesser extent than Harvey.

A chondrite normalized REE diagram indicates a flat line REE pattern compared to Piskahegan, which is enriched in LREEs over HREEs (Fig. 4.6 B, D). Both Harvey and Piskahegan exhibit distinct Eu anomalies. This variation in chondrite normalized REE patterns is either related to a difference in the original magmatic source, or increased

fractionation at Harvey, as deciphered through melt inclusion analysis (Gray et al., 2010, 2010).

Harker diagrams revealed that the concentration of trace elements in Harvey were strongly influenced by the concentration of SiO₂ (Fig. 4.5). Increases in SiO₂ yielded a reduction in Y, Ce, Nb, and slightly Zr in all Fms. Concentration of Y was highly varied, especially within Cherry Hill despite similar SiO₂ concentration. This is expected due to the variable concentration of Y-bearing accessory mineral phases including zircon. Th concentrations remained unchanged except in York Mills, which exhibited a noticeable reduction in Th with increasing SiO₂. The concentration of trace elements was relatively unchanged with increasing SiO₂ in Piskahegan, however the Seelys Fm showed an increase in Th concentration.

U and Th concentrations of Harvey and Piskahegan were correlated to elucidate how post-magmatic processes, if any, may have influenced the U concentration at these sites since the absence of a positive correlation indicates post-magmatic remobilization of U (Dawood, 2004). No discernable trend within the Cherry Hill or York Mills Fms was documented, while Harvey Mountain has a slightly positive correlation (Fig. 4.7). Piskahegan in contrast exhibits a positive correlation between U and Th within the Seelys Fm, with neither Little Mount Pleasant, nor Bailey Rock illustrating an apparent trend. Figure 4.7 indicates that Harvey could have experienced post-magmatic remobilization of U, which may have influenced the higher U concentrations found within the Cherry Hill, and to a lesser extent the York Mills Fm compared to Piskahegan.

4.6.4. *Petrology- major and minor elements*

The geochemical work of this study support the earlier conclusions of Payette and Martin (1986b) regarding tectonic setting, and build on the interpretations concerning magmatic origin. Based on the Y versus Nb tectonic discrimination diagram of Pearce et al. (1984), and the elevated concentrations of K, Rb, Th and depletions in Ba and Sr, it is apparent the Harvey Group represents a within plate granite (WPG), consistent with similar aged Piskahegan Group (Fig. 4.4b). Due to insufficient geochemical evidence regarding the nature of the source material, it was previously assumed the genesis of the Harvey Group was similar to that of topaz rhyolites (Payette and Martin, 1986b). Burt et al., (1982) and Christiansen et al., (1983) hypothesized that the Spor Mountain topaz rhyolites formed from the emplacement of basaltic rich magma during basin extension. This enabled a sufficient heat source to initiate anatexis of crustal material, and explained the large volume of rhyolites exhibited at Harvey. Evidence for this hypothesis is exhibited by the peraluminous nature of the melt, and the presence of glassy inclusions (Payette and Martin, 1986b). Piskahegan volcanics are thought to have formed from similar processes either by extensive fractional crystallization of a basaltic magma (e.g. Musselwhite et al., 1989), or partial melting of lower crustal material subsequent to the intrusion of basaltic magma (Huppert & Sparks, 1988).

4.6.5. *ϵ_{Nd} isotopes*

Harvey rocks displayed a range in ϵ_{Nd} values from -4.6 to 0.64 (n=4), indicating a heterogeneous source material containing both juvenile (negative model ages) and older, Gander aged material (Table 4.4; Fig. 4.9). Consistent with earlier interpretations of

Payette and Martin (1986b), mafic and intermediate rocks likely provided the heat source to allow the partial melting of crustal material at Harvey. Sample NBO7-11, Cherry Hill exhibited a distinctly more negative ϵ_{Nd} value, than other Harvey samples. This could indicate a relative shift to older crustal source material, or a difference in geochemistry facilitated by coeval or subsequent intra-crustal processes such as hydrothermal activity or fractionation of REE bearing minerals. The later hypothesis is preferred since Harvey is highly fractionated, and sample 11 contains elevated concentrations of TiO_2 , Ba, Sr, V, Zr, with depletions in Pb, and Y.

The composition of Harvey is in stark contrast to that of Piskahegan, which displayed more uniform ϵ_{Nd} values (-0.11 to 0.86, n=4; Table 4.4). It is important to note however that only two of the samples examined were rhyolites (81, 66) with the other samples being granitic (35A) and basaltic (56). Despite the differing lithology, the values are still homogenous with a model age of approximately 1000 Ma indicating Piskahegan likely formed from Avalon source material. This provides further evidence that the variable geochemical signatures observed at Harvey and Piskahegan are not controlled by fractional crystallization, but rather they formed from entirely different magmatic sources, with Harvey originating from much older material than previously thought.

4.6.6. $\delta^{18}O$ Quartz

Three samples (16, 17, 30) from the Harvey Group and two samples from Piskahegan were analyzed for $\delta^{18}O$ quartz isotopes (Table 4.5). Due to low yield, samples 16 and 17 were excluded from interpretation as a result of possible contamination. Results yielded a $\delta^{18}O$ value of 14.7‰ for the York Mills Fm, while the Piskahegan samples ranged from

9.7‰ in the Little Mount Pleasant Fm to as high as 11.3‰ in the Bailey Rock Fm. The results exhibited at Harvey and Mount Pleasant are consistent with the $\delta^{18}\text{O}$ values of granitoids within the 550–537 Ma Brookville (+9 - +12.5‰; Samson et al., 2000), and Caledonia terranes (up to 14.7‰, n=7; Potter et al., 2008), southern New Brunswick, as well as the rhyolites of the 680 Ma Mira terrane (+9 – 10.9 ‰), Cape Breton (Potter et al., 2008). Recent studies of the Kidd Creek VMS deposit, located within the late Archean Abitibi subprovince within the Superior Province of Canada have also indicated elevated $\delta^{18}\text{O}_{\text{quartz}}$ (7.9-12‰) within similar fine grained rhyolites. Huston et al. (1996) attributed these values to be related to deep, S-type intrusion, which provided the heat for the anatexis of the crustal material, (forming the VMS deposit), while King et al. (1997) indicate the range in $\delta^{18}\text{O}_{\text{quartz}}$ imply a heterogeneous oxygen isotope exchange during hydrothermal activity. The second hypothesis is preferred based on a robust petrographic study, as well as analysis of $\delta^{18}\text{O}_{\text{zircons}}$ that were capable of determining the original magmatic ^{18}O signature. Therefore, the results of this study should be examined cautiously as $\delta^{18}\text{O}_{\text{quartz}}$ may not be as robust as previously thought, especially in low temperature hydrothermal systems.

4.6.7. ϵHf isotopes

The average value of ϵHf zircons in sample 17 was 6.6 +/- 1.4 (MSWD = 8.3; Table 4.6). When re-grouped by age, $\epsilon\text{Hf}(403 \text{ Ma})$ yielded an average value of 7.0 +/-1.7 (MSWD = 3.4), while $\epsilon\text{Hf}(361 \text{ Ma})$ equalled 6.3 +/- 2.6 (MSWD = 13). Depleted mantle (i.e. MORB) sources typically have ϵHf values ranging from 15 to 20 (Workman and

Hart, 2005), while crustal ϵ_{Hf} values are less than 2 (Rudnick and Fountain, 1995). Therefore, the source material of Cherry Hill is composed of both depleted mantle and juvenile crustal components, consistent with ϵ_{Nd} results. Since the ϵ_{Hf} values were relatively homogenous, the zircons, and by association whole rocks, formed from the same source. While the ϵ_{Hf} of zircons is relatively homogeneous, it is apparent based on ϵ_{Nd} values that the source material is clearly heterogeneous. This discrepancy is attributed to having analyzed a single sample from Cherry Hill, as neither York Mills nor Harvey Mountain contained suitable zircon yields to be analyzed.

4.7. Discussion

4.7.1. Harvey felsic volcanics comparison

While all three Fms within the Harvey Group displayed subtle variability, the Cherry Hill Fm was the most geochemically distinct. Cherry Hill contained consistently lower SiO_2 concentrations and was noticeably enriched in almost all elements; especially REE, alkalis, and Fe_2O_3 compared to Harvey Mountain and York Mills. Cherry Hill contains the greatest abundance of accessory minerals including zircon, which facilitated the elevated concentration of Y, and zircon served as a suitable host for U. Payette and Martin (1986b) also identified the presence of basaltic material within Cherry Hill groundmass, which could explain the distinct geochemistry of Cherry Hill compared to other Harvey Fms. It is difficult to ascertain exactly how the basaltic material influenced the geochemistry of the Cherry Hill Fm without being able to properly identify and quantify the mineral components of the basalt groundmass. Lastly, in addition to

mineralogical variability, Cherry Hill exhibited noticeable alteration in both geochemical and petrographic analysis and may have been influenced by post magmatic water circulation. The influence of alteration processes could have facilitated the increased concentration of trace elements compared to York Mills and Harvey Mountain.

4.7.2. Relationship to Piskahegan

The Harvey Group has previously been identified as coeval to the Piskahegan Group based on a similar stratigraphic history (see Kuan, 1970; van de Poll, 1972; Pajari, 1973; Gemmell, 1975; Beaudin et al. 1980; Ruitenberg and McCutcheon, 1985; Payette and Martin, 1986b) despite displaying distinct geochemical characteristics and subtle regional variability. $^{206}\text{Pb}/^{238}\text{U}$ LA-ICP-MS zircon dating supports that both Groups were derived during the same pulse of magmatic activity within the Maritimes Basin, and tectonic discrimination diagrams show that both Harvey and Piskahegan are WPG. These similarities are expected as the Maritimes basin underwent a significant phase of lithospheric extension subsequent to the Acadian Orogeny and provided an ideal setting for volcanic activity within the basin. However, despite similar timing and geologic setting, both formed from very different crustal material and experienced a varied genetic history.

The Piskahegan Group formed from the anatexis of subducted juvenile crustal material from the Avalon terrane based on the $^{87}\text{Sr}/^{86}\text{Sr}$ ratio of 0.713 (Kooiman et al., 1986), and positive ϵNd values (Table 4.4). The Harvey Group originated due to partial melting of juvenile crustal material and older, Gander aged, material based on ϵNd and ϵHf (Table 4.4, 4.6). The heat source required for the anatexis of the crustal material at both Harvey

and Piskahegan was likely facilitated by the emplacement of mafic and intermediate rocks during lithospheric thinning as previously hypothesized (Burt et al., 1982; Christiansen et al., 1983).

Trace and major element analyses of continental crust normalized melt inclusions hosted within quartz phenocrysts revealed that Harvey was significantly enriched in LREE and incompatible elements (Cs, B, U, and Th) compared to Piskahegan (Gray et al., 2010). A comparison of both chondrite and primitive mantle normalized whole-rock data (Fig. 4.6) also indicate that Piskahegan is enriched in HREE and depleted in LREE compared to Harvey which illustrates a relatively flat REE pattern implying variable geochemical source magma. Additional evidence is revealed in the highly fractionated signature of the Harvey Group compared to Piskahegan. Large negative Eu, Sr, and Ba anomalies are exhibited in both whole-rock and melt inclusions from Harvey, and a fractionation diagram of pre-eruptive melt comparing Cs content to U, Th, U/Th implied the degree of fractionation is 70 - 92% at Piskahegan, at least 95% at Harvey, and >99% in pre-eruptive Harvey (see Gray et al., 2010).

Lastly, the elevated ^{18}O values exhibited at Harvey contrasted to Piskahegan, as well as figure 4.7 reveal that Harvey was influenced by post-magmatic water circulation, which likely facilitated the elevated U mineralization at Harvey. The results of this study indicate that the differences between the Harvey and Piskahegan volcanics cannot be explained by alteration and increased fractionation at Harvey alone. It is evident when examining the ϵNd and ϵHf isotopes in conjunction with melt inclusion studies (Gray et al., 2010) that Harvey and Piskahegan evolved from distinct source material. Post-

formation alteration did however facilitate the variability within the Harvey Group itself, and complicate the determination of the relationship between Piskahegan and Harvey.

4.7.3. Similarity to Topaz Rich Rhyolites

Topaz rich rhyolites are generally high SiO_2 (>74 wt. %), Na_2O (>3.6 wt. %), enriched in F (>0.2 wt. %), high F/Cl ratio, low in TiO_2 (<0.2 wt. %), CaO (<0.9 wt. %), MgO (<0.2 wt. %), P_2O_5 , (~0.01 wt. %) and have flat REE pattern compared to typical rhyolites (Christiansen et al., 1983). High F/Cl ratio (>3) systems also tend to exhibit enrichment in Al, Na, Li, Rb, Cs, Ta, Th, and U, while Cl dominant systems show elevation in LREE, Na, Fe, Ti, Mn, Zn, Nb, and Zr (Flynn and Burnham, 1978; Kerrich and Fryer, 1979; Taylor and Fryer, 1980; Christiansen et al., 1986; Webster et al., 1989). Harvey rhyolites may appear to be geochemically similar to F-rich topaz rhyolites, however whole rocks have variable SiO_2 , Na_2O , and CaO, lower F (~0.1 wt. %) and TiO_2 , while melt inclusions contain equivalent SiO_2 , Na_2O , but lower CaO, TiO_2 , MgO, P_2O_5 , F (<0.25 wt. %) content (Gray et al., 2010), and variable F/Cl ratios (sample 18=1.28, n=11; sample 31=5.9, n=13). The low F content determined in this study, as well as the melt inclusion study of Gray et al. (2010) are in severe contrast to previously reported values of up to 1.97 wt. % in melt inclusions from Harvey (Payette and Martin, 1986a). This ambiguity can be explained though analytical error in the earlier study which may have had F-Fe peak overlaps during analysis. Alternatively, multiple inclusions analyzed contained solid phases, that if accidentally trapped, could artificially increase F concentration. Piskahegan whole-rocks have similar SiO_2 , TiO_2 lower Na_2O , CaO, F (~0.1 wt. %), while melt inclusions contain higher P_2O_5 , equivalent SiO_2 , and CaO, but lower Na_2O , TiO_2 , MgO,

and F (<0.25 wt. %) content (Gray et al., 2010), and variable F/Cl ratios (sample 39=3.45, n=12; sample 78=1.5, n=8). Therefore, based on new geochemical data, it is apparent Harvey, nr Piskahegan can be considered an F-rich topaz rhyolite.

4.8. Conclusions

The Harvey Group represents a distinct suite of volcanic rocks forming during a major phase of igneous activity subsequent to the Acadian Orogeny. Facilitated by lithospheric thinning, a pulse of basaltic rich magma provided the heat required for the anatexis of juvenile crustal material and Gander basement rock. Continued fractionation of the magma, and post-formation alteration processes created the unique REE, U-rich geochemistry of the Harvey volcanics. This is in contrast to the Piskahegan Group, which formed from the melting of younger, Avalon source rocks, and experienced significantly less fractionation and post-magmatic alteration than Harvey. Despite forming in the same tectonic environment, and displaying similar lithology and to some extent geochemistry, it is apparent that Harvey volcanics cannot be considered coeval to the Piskahegan Group. Similarly, Harvey volcanics in no way resemble F-rich rhyolites based on their distinct geochemistry. This illustrates that felsic volcanics, relatively barren of F, can still serve as an economic source of U in southern New Brunswick, and likely elsewhere.

4.9. Acknowledgements

Fieldwork costs were provided by a grant from the Geological Survey Branch of the New Brunswick Department of Natural Resources and Energy (JD). Major and trace element geochemical work was funded by the Natural Sciences and Engineering Research

Council of Canada (NSERC) Discovery Grant (JD), while remaining analysis were completed with the assistance of the Society of Economic Geologists Student Research Grant (TRG), and Mineralogical Association of Canada Travel and Research Grant (TRG).

4.10. Chapter 4 Appendix

All the figures and tables are located in a consecutive manner, in the general style required for manuscript submission to peer-reviewed journals.

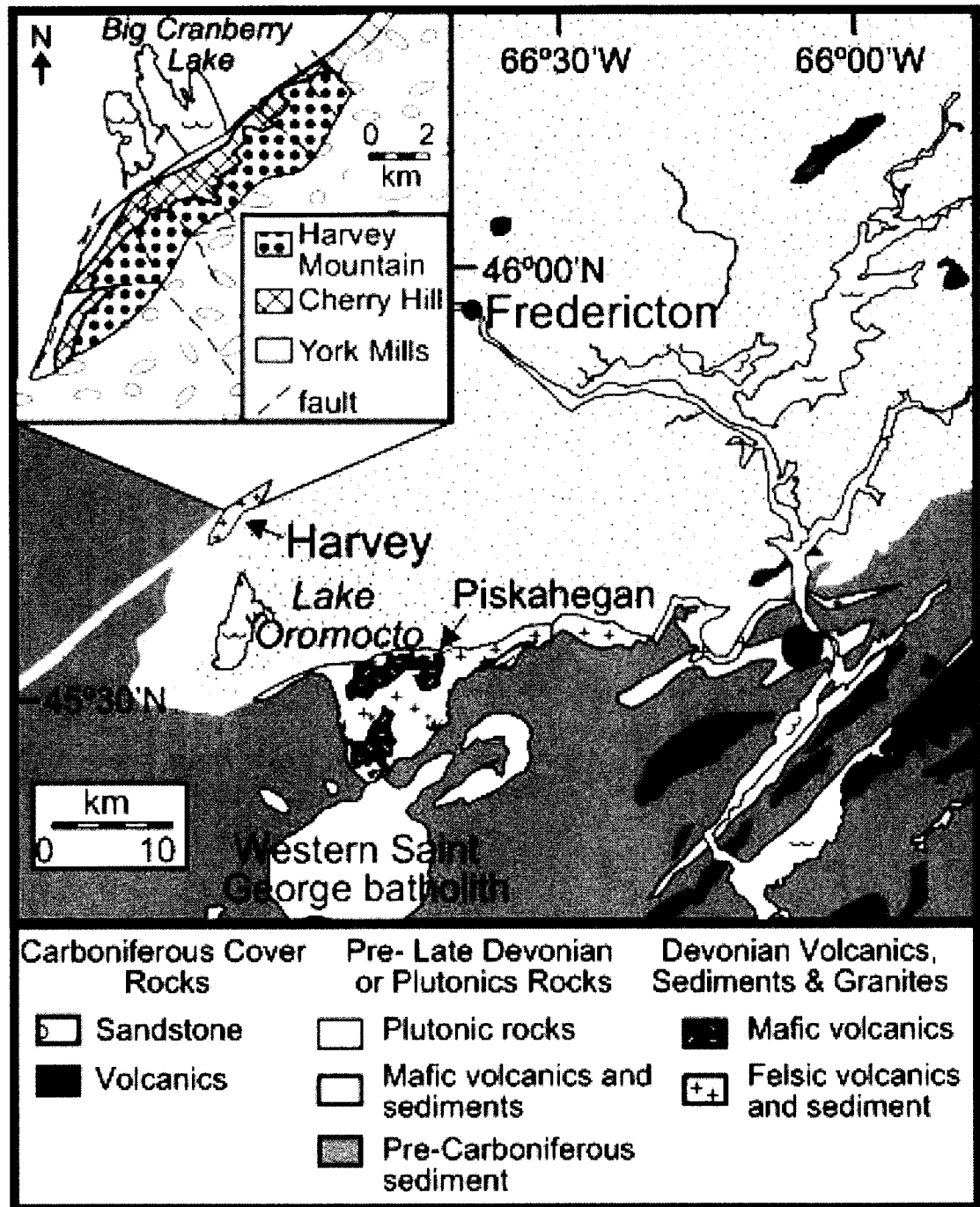


Figure 4.1. Map of study location. A. Geologic map of the Maritimes Basin, and B. Local surface geology of the Harvey Group (modified from Payette and Martin, 1986b).

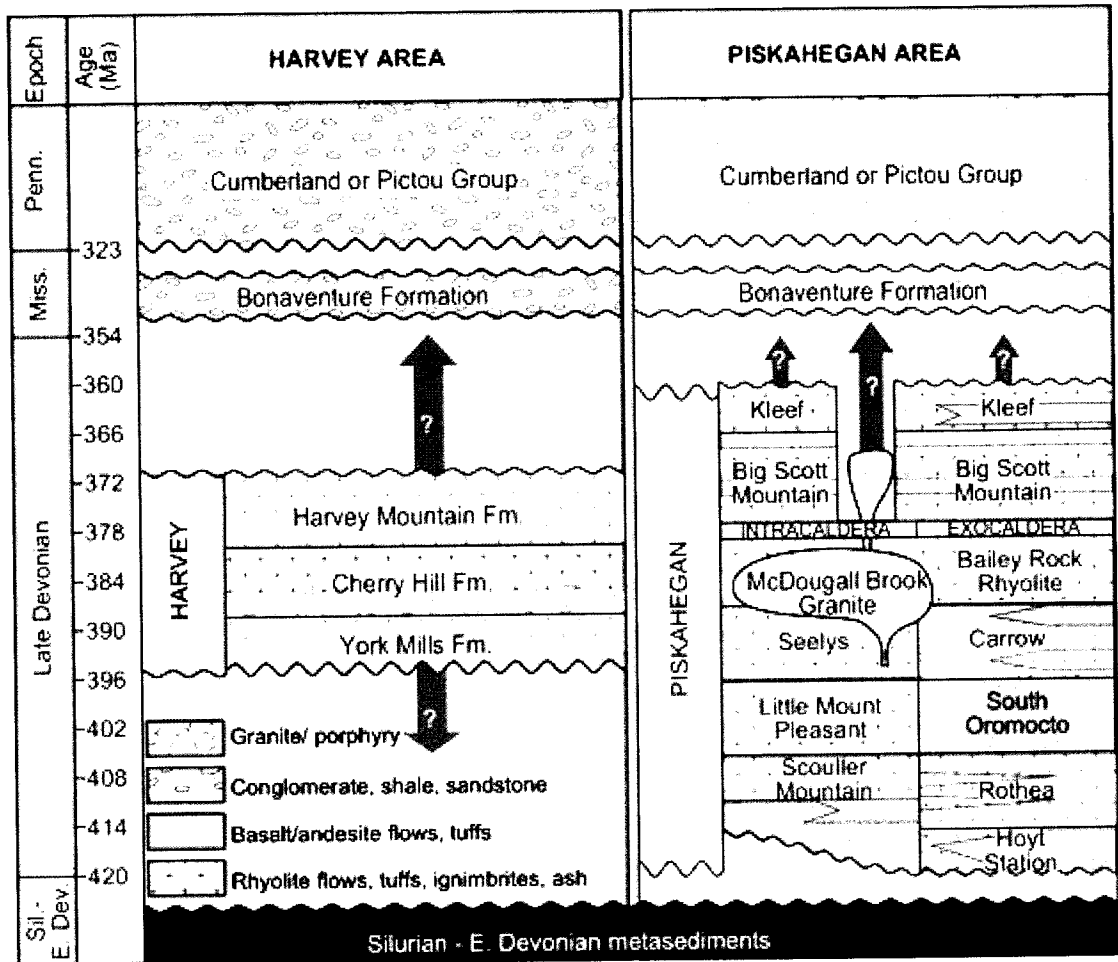


Figure 4.2. Simplified stratigraphic log of the Harvey Group and overlying sediments, modified from (Beaudin, 1980) compared to Piskahegan (modified from McCutcheon et al., 1997).

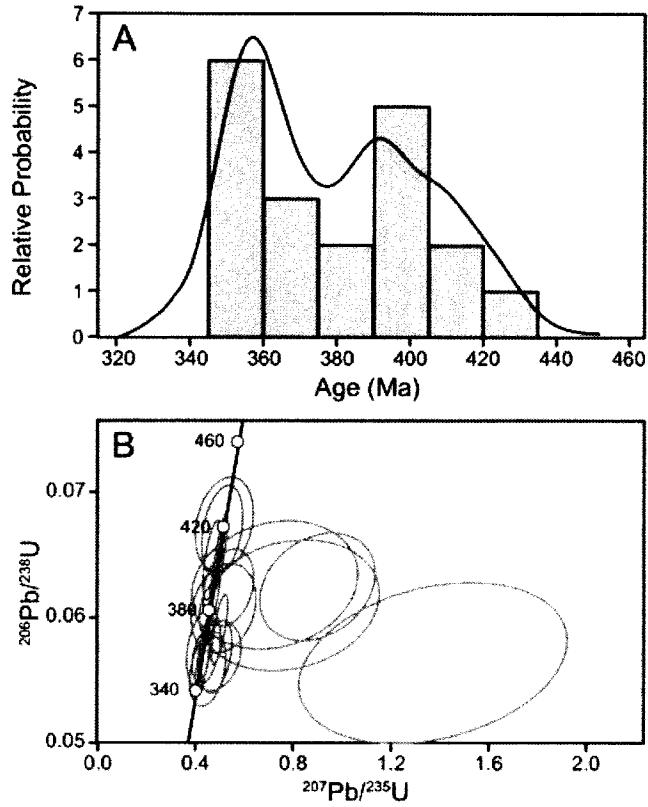


Figure 4.3. U/Pb zircon age diagrams. A. Age distribution, and B. Concordia plot of zircons from sample 17. Both indicate a bimodal age distribution of 361 Ma and 403 Ma.

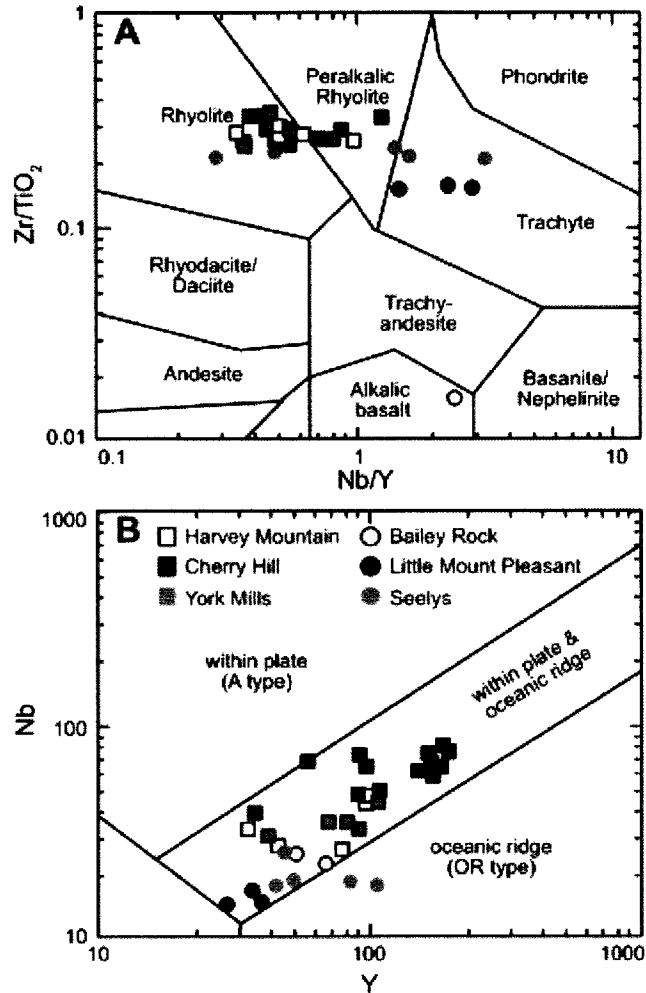


Figure 4.4. Discrimination diagrams of tectonic setting and rock type. (a) Nb/Y vs. Zr/TiO₂ of Fms of the Harvey Group, Cherry Hill (n=13), York Mills (n=5) and Harvey Mountain (n=5) compared to rhyolitic Fms of Piskahegan, Bailey Rock (n=2), Little Mount Pleasant (n=3) and Seelys (n=5) after Winchester and Floyd (1977), (b) Y vs. Nb, after Pearce et al., (1984). Only samples from Piskahegan analyzed for trace elements via ICP-MS were plotted.

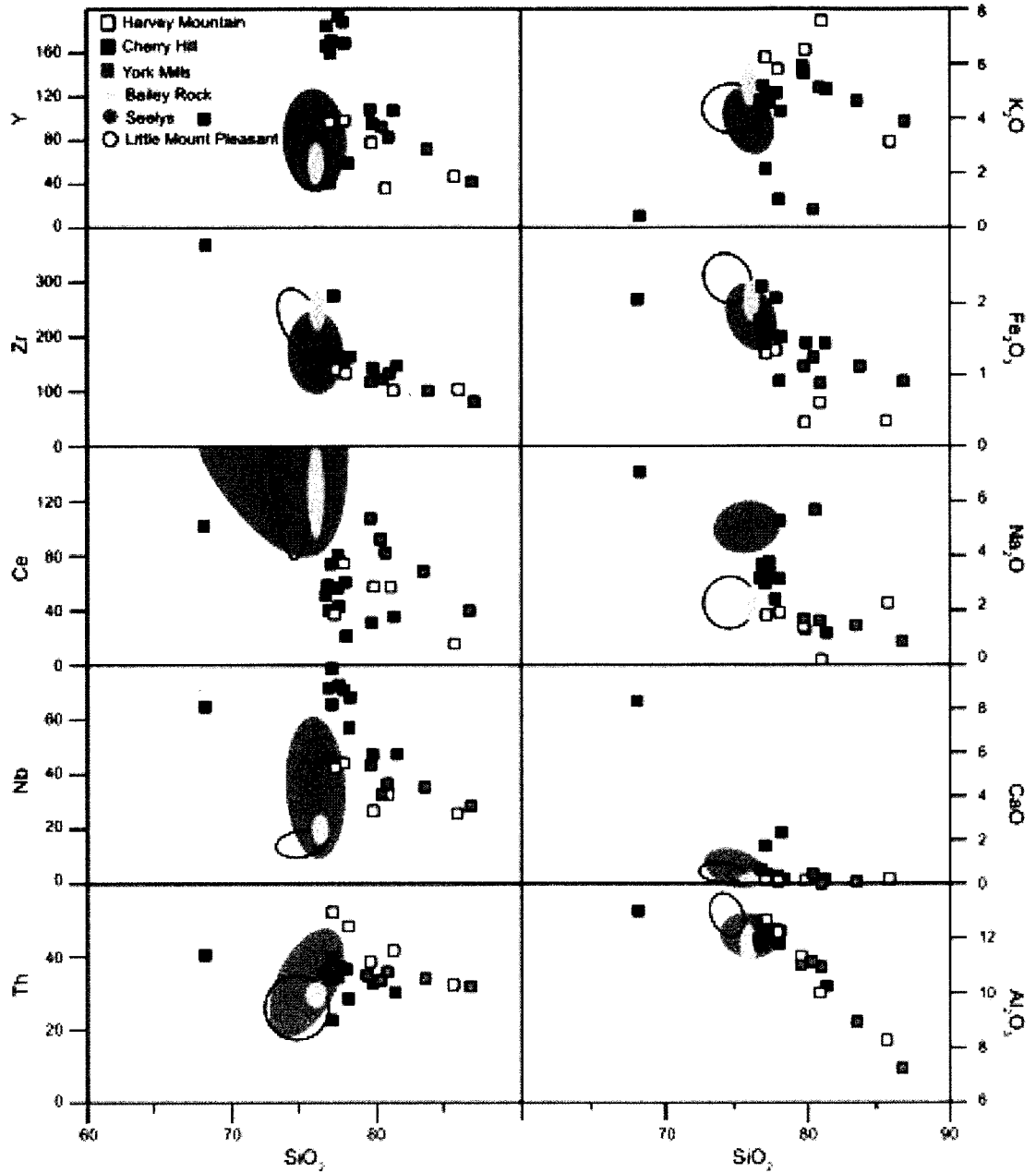


Figure 4.5. Harker diagram of major compounds and trace elements correlated to SiO_2 of the Harvey Group, Cherry Hill (n=13), York Mills (n=5), Harvey Mountain (n=5) compared to fields of Piskahegan, Bailey Rock (n=2), Seelys (n=5), Little Mount Pleasant (n=3). Only samples analyzed for ICP-MS were utilized to determine fields.

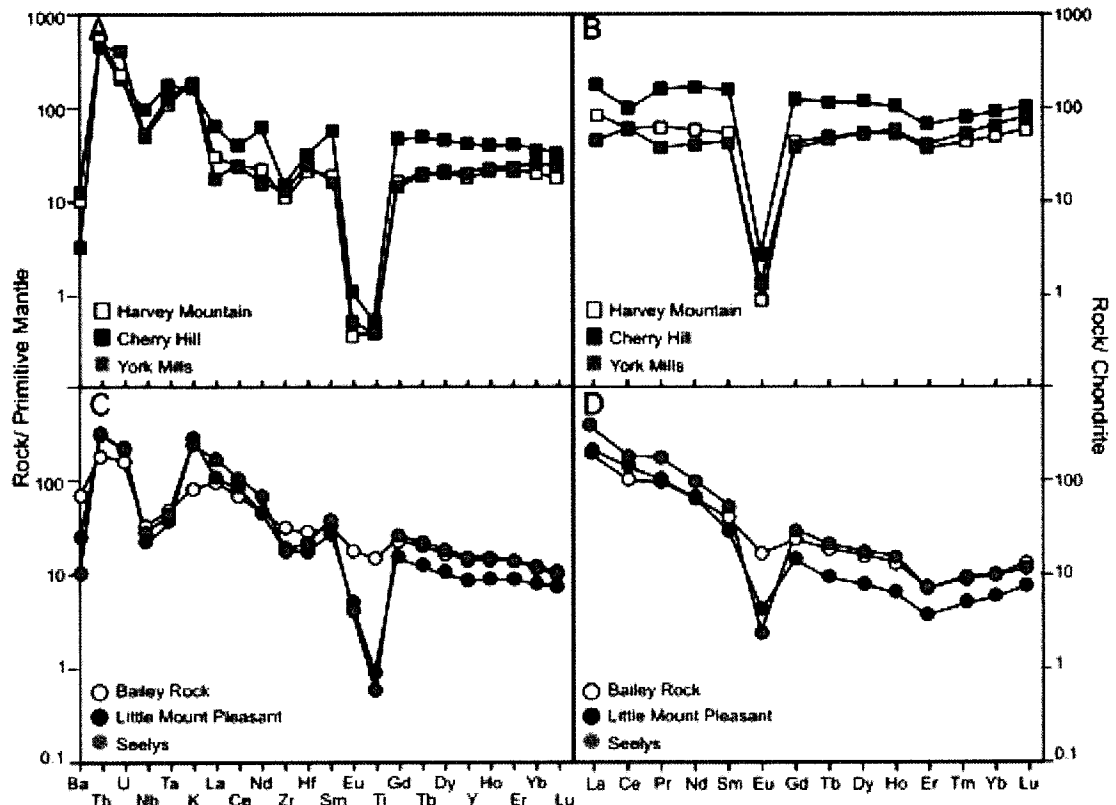


Figure 4.6. Normalized geochemical plots of Harvey and Piskahegan. A. Primitive mantle plot of Harvey (Cherry Hill, n=3; Harvey Mountain, n=3; York Mills, n=1), B. Chondrite normalized plot of Harvey, C. Primitive mantle plot of Piskahegan rhyolites (Bailey Rock, n=2; Little Mount Pleasant, n=3; Seelys, n=5), D. Chondrite normalized plot of Piskahegan. Primitive mantle and chondrite normalized values after Sun and McDonough (1989).

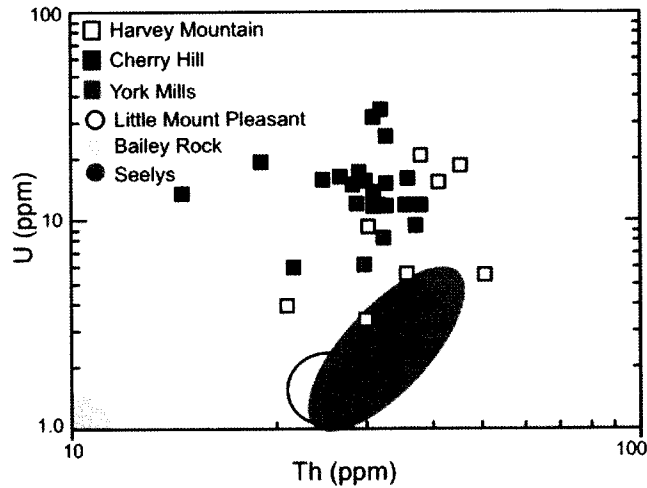


Figure 4.7. Bivariate plot of U vs. Th in Harvey Fms Cherry Hill (n=22), York Mills (n=6) and Harvey Mountain (n=8), compared to Piskahegan fields (Bailey Rock, n=2; Little Mount Pleasant, n=3; Seelys, n=5) of samples analyzed for trace elements via ICP-MS.

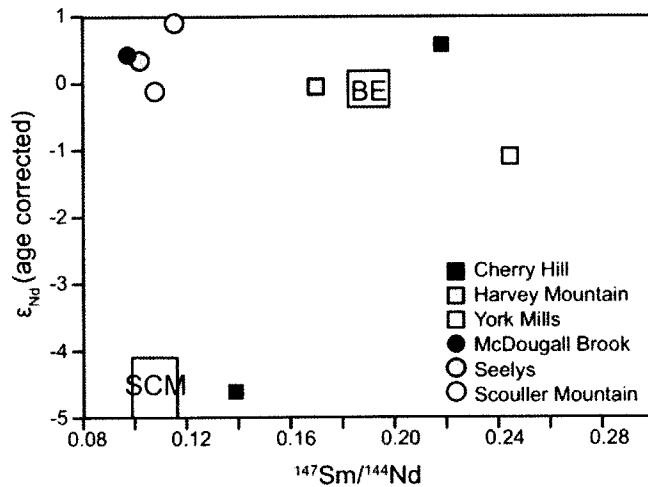


Figure 4.8. ϵ_{Nd} (age corrected) vs. $^{147}Sm/^{144}Nd$ plot. Mantle and subduction components interpreted to generate the rocks from Harvey and Piskahegan (fields after Swinden et al.,

1990). Abbreviations used in diagram: BE – Bulk Earth, SCM – Subducted Crustal Material

Analysis Number	Corrected Atomic Ratios						Apparent Age (Ma)					
	$^{206}\text{Pb}/^{238}\text{U}$		$^{207}\text{Pb}/^{235}\text{U}$		$^{207}\text{Pb}/^{206}\text{Pb}$		$^{206}\text{Pb}/^{238}\text{U}$		$^{207}\text{Pb}/^{235}\text{U}$		$^{207}\text{Pb}/^{206}\text{Pb}$	
	Value	1σ	Value	1σ	Value	1σ	Value	1σ	Value	1σ	Value	1σ
1	0.0404	0.0011	0.2699	0.056	0.04846	0.00907	255	7	243	45	122	315
2	0.0625	0.0017	0.9048	0.0964	0.10493	0.00864	391	11	654	51	1713	148
3	0.0412	0.0014	0.4382	0.0971	0.07718	0.01479	260	9	369	69	1126	398
4	0.067	0.0015	0.5139	0.0342	0.05567	0.00274	418	9	421	23	439	106
5	0.0577	0.0012	0.4386	0.0286	0.05515	0.0027	361	8	369	20	418	106
6	0.0565	0.0026	1.3792	0.2246	0.17694	0.02124	355	16	880	96	2624	198
7	0.0646	0.0013	0.4737	0.0156	0.05317	0.00092	404	8	394	11	336	38
8	0.0567	0.0011	0.4349	0.0121	0.05566	0.00075	355	7	367	9	439	29
9	0.0577	0.0011	0.4484	0.0121	0.05634	0.00072	362	7	376	8	466	27
10	0.0556	0.0014	0.4175	0.0503	0.05449	0.00547	349	8	354	36	391	218
11	0.057	0.0012	0.493	0.0256	0.06274	0.00222	357	7	407	17	699	73
12	0.0675	0.0015	0.5221	0.0487	0.05612	0.00423	421	9	427	33	457	163
13	0.0627	0.0021	0.7291	0.1392	0.08435	0.01361	392	13	556	82	1301	319
14	0.056	0.0012	0.456	0.0303	0.05905	0.00294	351	7	381	21	569	105
15	0.0611	0.0021	0.7891	0.1506	0.09372	0.015	382	13	591	85	1503	308
16	0.0518	0.001	0.388	0.0089	0.05434	0.00056	325	6	333	7	385	22
17	0.0608	0.0014	0.5199	0.0543	0.06199	0.00529	381	9	425	36	674	179
18	0.0653	0.0012	0.507	0.0119	0.05631	0.00059	408	7	416	8	465	22
19	0.0628	0.0012	0.4878	0.0116	0.05639	0.0006	392	7	403	8	468	23
20	0.0592	0.0011	0.505	0.0135	0.06191	0.00078	371	7	415	9	671	26
21	0.0625	0.0012	0.54	0.0422	0.0627	0.00411	391	8	438	28	698	140
22	0.0571	0.0011	0.4916	0.0411	0.06249	0.00447	358	7	406	28	691	153

Table 4.1. U-Pb SHRIMP dating of zircons, sample 17.

	Cherry Hill (n=18)																			
	1 2**	3	4	5 6**	7*	8	9*	10*	11**	12*	14	15**	16	17	18*	20				
SiO ₂ (wt. %)*	76.53	76.11	76.45	75.84	75.71	76.03	62.63	65.98	48.74	44.66	74.32	47.77	75.88	76.46	77.12	76.67	76.07	80.11		
TiO ₂	0.08	0.07	0.08	0.08	0.08	0.08	0.24	0.23	0.11	0.15	0.58	0.12	0.10	0.11	0.08	0.09	0.09	0.09		
Al ₂ O ₃	12.05	12.45	12.24	12.09	11.96	12.02	16.16	12.73	12.81	11.57	11.46	10.13	11.54	11.98	12.13	10.74	10.36	10.23		
Fe ₂ O ₃	1.64	1.43	1.54	1.54	1.71	1.55	2.11	1.96	4.09	4.60	2.15	4.46	0.89	1.97	1.51	1.34	1.35	1.38		
MnO	0.01	0.02	0.02	0.02	0.02	0.02	0.21	0.30	0.31	0.84	0.11	0.34	0.02	0.02	0.01	0.02	0.02	0.01		
MgO	0.08	0.09	0.10	0.09	0.08	0.08	0.33	0.21	4.29	4.80	0.99	5.09	0.27	0.20	0.18	0.25	0.23	0.24		
CaO	0.32	0.45	0.18	0.64	0.83	0.58	4.72	8.06	10.00	12.30	1.67	12.07	2.22	0.32	0.26	0.08	1.15	0.08		
Na ₂ O	3.68	3.53	3.24	3.09	3.53	3.49	8.07	6.81	7.13	6.42	2.98	5.76	5.19	2.32	3.12	1.28	1.21	1.18		
K ₂ O	4.55	4.62	4.82	5.25	4.69	4.93	0.86	0.42	0.31	0.27	2.13	0.12	1.01	4.92	4.29	5.56	5.12	5.06		
P ₂ O ₅	0.01	0.02	0.01	0.01	0.01	0.01	0.08	0.07	0.04	0.04	0.11	0.04	0.02	0.02	0.01	0.01	0.02	0.02		
F		0.23				0.24					0.13			0.18						
LOI	0.70	0.80			1.10	0.70	5.40		14.40	17.00	3.70	17.20	2.80	1.20	1.30	1.20	7.40	1.70		
Total	99.09	98.91	98.81	98.79	98.77	98.93	95.59	96.93	87.98	85.82	96.63	86.06	97.27	98.46	98.81	96.16	95.76	98.50		
Cr(ppm)*	16		9.0	19	12		30	23	17	22	70	22	18		15	15	10	18		
Ni	6.0		3.0		4.0		13	10	25	14		27			3.0	2.0		5.0		
Co			1.0				6.0	8.0	18	17	6.0	15		1.0	5.0			3.0		
V	6.0		9.0		16		24	17	24	27	54	35	11		10	8.0	9.0	6.0		
Pb	55	33	54	67	67	45	56	58	47	52	17	68	274	34	49	63	135	54		
Zn	97	110	105	99	110	100	95	160	276	524	90	408	58	100	104	95	87	106		
Sn		18				12					5.0				19					
W		3.3				5.7					6.6				8.2					
Sb		6.6				7.2					4.5				6.4					
Rb	449	461	495	530	473	490	78	39	37	25	168	17	143	503	451	487	442	435		
Cs		9.8				8.7					8.6			13						
Ba	32	10	35	44	29	10	280	273	66	60	184	88	98	44	18	47	31	23		
Sr	30	22	26	33	39	26	248	291	314	328	101	339	109	24	56	37	42	34		
Tl		4.2				4.3					1.1				4.3					
Ga	21	28	25	26	28	25	13	10	6.0	9.0	15	5.0	21	27	29	23	24	22		
Ta		6.61				6.59					2.21			6.20						
Nb	72.0	59.7	71.0	71.0	79.0	65.4	59.0	65.0	58.0	74.0	39.0	67.0	57.0	62.7	68.0	47.0	47.0	48.0		
Hf		8.10				8.40					8.30			8.40						
Zr	157	148	142	158	161	161	347	372	202	201	294	173	152	158	157	135	142	142		
Y	194	148	91.0	163	184	164	125	98.0	82.0	95.0	38.0	102	168	183	60.0	93.0	133	107		
Th	34.0	37.0	36.0	39.0	35.0	41.7	41.0	40.0	35.0	25.0	15.7	34.0	36.0	38.6	28.0	32.0	31.0	30.0		
U	12.0	3.32	12.0	16.0	12.0	4.00	12.0	10.0	34.0	6.00	13.3	31.0	26.0	4.60	16.0	17.0	15.0	16.0		
La	72.0	28.4	34.0	44.0	47.0	29.4	38.0	90.0	78.0	46.0	32.9	42.0	40.0	76.3	9.00	26.0	40.0	29.0		
Ce	59.0	67.1	45.0	42.0	51.0	67.5	123.0	102.0	94.0	75.0	80.0	119.0	61.0	56.0	21.0	32.0	64.0	36.0		
Pr		10.1				10.6					7.56			24.1						
Nd	85.0	50.2	39.0	41.0	32.0	55.3	49.0	35.0	39.0	29.0	29.0	47.0	37.0	122.0	6.0	6.0	45.0	17.0		
Sm		15.8				17.5					6.93			37.5						
Eu		0.062				0.072					0.933			0.322						
Gd		17.4				19.2					6.12			39.5						
Th		3.74				4.09					1.09			6.52						
Dy		25.3				28.0					6.79			37.0						
Ho		5.23				5.74					1.37			6.97						
Er		15.4				16.9					4.09			18.9						
Tm		2.28				2.48					0.62			2.59						
Yb		14.3				15.6					3.95			15.5						
Lu		1.97				2.14					0.58			2.08						

Table 4.2. Harvey whole-rock major and trace element data. * Major compounds and elements were analyzed via XRF, ** trace element data was obtained through ICP-MS. #Sample excluded from interpretations due to high LOI value. - indicates no data available

	Harvey Mountain (n=5)					York Mills (n=5)				
	21**	22	23**	25**	31	26	27	28**	29	30
SiO ₂ (wt. %)*	78.81	76.75	75.81	84.94	80.32	78.44	85.81	79.61	82.54	79.55
TiO ₂	0.07	0.08	0.07	0.05	0.06	0.07	0.05	0.06	0.06	0.08
Al ₂ O ₃	11.22	12.12	12.60	8.26	10.00	10.98	7.17	10.83	8.91	11.06
Fe ₂ O ₃	0.31	1.29	1.21	0.34	0.58	1.06	0.87	0.85	1.06	1.18
MnO	0.01	0.02	0.02	0.01	0.01	0.01	0.02	0.02	0.01	0.01
MgO	0.11	0.44	0.48	0.16	0.23	0.24	0.16	0.21	0.19	0.17
CaO	0.08	0.18	0.18	0.10	0.05	0.12	0.13	0.08	0.09	0.47
Na ₂ O	1.53	1.78	1.70	2.16	0.20	1.53	0.83	1.54	1.27	5.56
K ₂ O	6.49	5.80	6.19	3.14	7.65	5.92	3.88	5.17	4.70	0.71
P ₂ O ₅	0.07	0.01	0.01	0.01	0.02	0.01	0.02	0.01	0.01	0.02
F	0.05		0.05	0.03				0.04		
LOI	0.90	1.70	1.50	0.80	1.00	1.20	1.10	1.40	1.10	0.60
Total	98.86	98.59	98.41	99.23	99.24	98.50	99.02	98.50	98.93	98.95
Cr(ppm)*		11			14	12	20		18	17
Ni		6.0			2.0		4.0		1.0	
Co		1.0								3.0
V		7.0			9.0	14	11	9.0	6.0	20
Pb	36	61	38	9.0	24	28	29	18	24	30
Zn		54	60		29	63	44	80	36	24
Sn	13		13	4.0				14		
W	1.5		5.7	1.7				5.0		
Sb	6.4		6.6	3.4				4.4		
Rb	479	610	671	295	655	503	309	446	395	50
Cs	8.4		22	7.3				74		
Ba	153	48	24	10	49	84	85	79	94	213
Sr	430	61	53	41	28	115	91	114	94	490
Tl	4.7		4.8	1.6				2.3		
Ga	12	24	25	10	14	21	14	23	16	9.0
Ta	3.85		5.53	3.12				4.72		
Nb	25.9	45.0	43.0	26.2	33.0	44.0	30.0	36.0	35.0	32.0
Hf	5.60		6.90	4.50				6.50		
Zr	117	128	133	88.0	100	116	77.0	130	94.0	121
Y	80.9	96.0	96.0	47.3	36.0	107	41.0	82.4	69.0	92.0
Th	38.3	48.0	52.5	32.5	41.0	35.0	32.0	35.6	34.0	33.0
U	5.23	18.0	5.37	3.24	20.0	12.0	12.0	8.23	14.0	6.00
La	40.3	38.0	17.5	6.06	3.00	4.00	41.0	11.6		49.0
Ce	58.6	77.0	37.4	18.1	61.0	9.00	29.0	39.7	33.0	89.0
Pr	9.65		5.13	2.36				3.54		
Nd	39.8	30.0	25.2	13.2	15.0	16.0	14.0	18.8	21.0	34.0
Sm	10.4		7.58	4.63				6.26		
Eu	0.068		0.052	0.029				0.074		
Gd	11.2		9.00	5.47				7.59		
Tb	2.18		2.20	1.40				1.85		
Dy	14.6		16.1	9.93				13.8		
Ho	3.02		3.61	2.16				3.15		
Er	9.34		11.0	6.57				9.96		
Tm	1.36		1.66	0.97				1.56		
Yb	8.19		10.9	6.07				10.7		
Lu	1.16		1.55	0.82				1.60		

Table 4.2. Continued.

	Bailey Rock Rhyolite (n=3)					Little Mount Pleasant (n=10)							
	39	73	78	42	43	97	98**	99	100**	104	105	106**	107
SiO ₂ (wt. %)	-	75.81	75.96	74.27	75.96	75.50	75.35	75.38	75.15	73.35	74.67	73.56	74.77
TiO ₂	-	0.22	0.23	0.28	0.16	0.22	0.21	0.23	0.23	0.30	0.25	0.29	0.26
Al ₂ O ₃	-	13.32	11.81	13.16	11.80	12.20	12.35	12.28	12.50	13.04	12.50	13.15	12.61
Fe ₂ O ₃	-	2.13	1.81	1.83	1.75	1.58	1.43	1.62	1.46	1.65	1.74	1.85	1.69
MnO	-	0.03	0.02	0.03	0.04	0.04	0.03	0.03	0.03	0.03	0.03	0.04	0.03
MgO	-	0.38	0.13	0.38	0.23	0.32	0.28	0.29	0.25	0.25	0.32	0.35	0.33
CaO	-	0.15	0.14	0.17	0.55	0.17	0.51	0.33	0.44	0.57	0.42	0.52	0.41
Na ₂ O	-	1.90	2.51	1.54	2.23	2.14	2.80	2.79	3.01	2.65	2.35	1.84	2.34
K ₂ O	-	5.49	5.50	6.07	5.29	6.18	5.49	5.44	5.40	6.23	5.87	6.31	5.88
P ₂ O ₅	-	0.05	0.05	0.05	0.03	0.04	0.04	0.04	0.04	0.06	0.05	0.06	0.05
F	-						0.06		0.03			0.03	
LOI	-	2.20	1.00	1.00	0.90	0.80	0.80	1.30	0.80	1.10	1.50	1.20	1.60
Total	-	99.66	99.18	98.77	98.94	99.18	99.35	99.72	99.33	99.23	99.70	99.71	99.07
Cr(ppm)	-	17	10	14	24	32		18		16	20	20	10
Ni	-				6.0	14		35		7.0	18		8.0
Co	3.0	3.0	5.0	1.0	3.0	4.0		3.0	1.0	6.0		1.0	6.0
V	15	9.0	23	11	8.0		6	9	8	16	12	12	13
Pb	27	21	18	23	21	30	17	35	24	32	28	12	33
Zn	60	39	19	32	48	33	40	41	50	34	23	30	43
Sn	5.0						4.0		4.0			3.0	
W	0.60						2.2		0.60			1.9	
Sb	5.6						2.2		3.3			2.0	
Rb	228	100	177	244	195	349	251	219	219	222	243	296	229
Cs	2.0						5.9		7.0			7.2	
Ba	499	477	382	379	130	169	132	185	182	444	305	445	334
Se	67	128	328	41	30	56	63	30	61	81	68	58	66
Tl	2.0						2.6		2.3			3.3	
Ga	18	13	17	16	16	15	19	16	19	15	17	19	16
Ta	1.95						1.57		1.38			1.29	
Nb	21.80	17.00	22.00	14.00	18.00	17.00	16.20	15.00	14.40	14.00	15.00	14.40	16.00
Hf	9.30						5.50		5.30			6.60	
Zr	357	220	267	251	196	178	198	191	201	262	209	260	228
Y	67.7	41.0	33.0	15.0	79.0	37.0	36.7	39.0	39.5	30.0	43.0	29.4	35.0
Th	26.0	31.0	31.0	28.0	28.0	28.0	25.2	31.0	22.9	25.0	25.0	19.5	28.0
U	5.86	12.0	4.00	11.0	12.0	14.0	5.40	12.0	3.99	12.0	13.0	4.93	11.0
La	106	57.0	19.0	43.0	197	115	82.7	97.0	80.4	71.0	105	75.5	93.0
Ce	156	83.0	158.0	78.0	235	181	162	164	150	132	173	144	166
Pr	22.3						18.0		18.5			15.7	
Nd	77.8	29.0	32.0	27.0	124	90.0	58.9	65.0	61.8	49.0	76.0	52.6	63.0
Sm	15.9						11.2		11.2			9.8	
Eu	1.95						0.706		0.925			1.39	
Gd	14.2						8.71		9.15			7.50	
Tb	2.56						1.27		1.36			1.07	
Dy	13.4						6.95		7.60			5.78	
Ho	2.59						1.34		1.46			1.11	
Er	7.47						3.91		4.23			3.30	
Tm	1.07						0.578		0.617			0.504	
Yb	6.57						3.61		3.85			3.27	
Lu	0.925						0.542		0.557			0.478	

Table 4.3. Piskahegan whole-rock major and trace element data. * Major compounds and elements were analyzed via XRF, ** trace element data was obtained through ICP-MS. - indicates no data available

Sechys (n=18)																
	44**	46	48	49	50	51	52**	80	81**	82	83	84	86**	87	89	90
SiO ₂ (wt. %)	77.30	77.01	75.44	76.44	75.98	76.26	76.10	75.55	74.67	75.69	74.65	75.01	75.64	76.11	75.71	68.70
TiO ₂	0.11	0.12	0.16	0.15	0.10	0.10	0.15	0.18	0.18	0.19	0.17	0.17	0.17	0.12	0.09	0.86
Al ₂ O ₃	11.79	11.85	12.21	11.86	12.28	12.30	11.90	11.79	11.93	11.66	11.63	11.58	11.91	12.10	11.63	13.01
Fe ₂ O ₃	1.23	1.44	1.85	1.51	1.18	1.33	1.56	1.64	1.75	1.74	1.79	1.68	1.81	1.31	1.32	4.60
MnO	0.03	0.03	0.05	0.03	0.03	0.03	0.04	0.04	0.04	0.04	0.05	0.04	0.04	0.02	0.07	0.09
MgO	0.15	0.16	0.28	0.20	0.13	0.12	0.19	0.35	0.34	0.30	0.31	0.31	0.21	0.21	0.37	1.26
CaO	0.20	0.14	0.54	0.30	0.22	0.22	0.43	0.58	0.97	0.74	1.23	1.12	0.35	0.22	0.91	1.95
Na ₂ O	2.72	2.37	2.73	2.81	3.31	3.57	3.06	1.92	2.39	2.19	2.23	2.27	2.62	3.02	2.91	2.58
K ₂ O	4.84	5.37	5.10	5.28	5.03	4.73	5.12	5.61	5.46	5.03	5.40	5.31	5.40	4.97	4.77	4.03
P ₂ O ₅	0.02	0.02	0.03	0.02	0.02	0.02	0.02	0.03	0.03	0.03	0.03	0.03	0.02	0.02	0.02	0.30
F							0.06		0.04				0.03			
LOI	0.20	0.60	1.20	1.20	1.20	1.20	-	1.60	1.80	1.60	2.10	1.60	0.90	1.50	1.60	1.90
Total	*98.59	*99.11	*99.58	*99.80	*99.48	*99.88	98.64	*99.30	99.60	*99.21	*99.59	*99.12	99.09	*99.60	*99.39	*99.27
Cr(ppm)		21	19	15	13	18		14	20	17	25	21	30	9	24	24
Ni		1.0	3.0	1.0	-	7.0				1.0	8.0				6.0	7.0
Co		3.0	3.0		1.0	1.0	1.0	3.0	1.0		5.0			1.0		13
V		11	10	8.0	10	11	5.0	3	6	12	10	9		6	5	69
Pb	16	33	26	41	38	40	23	33	16	32	35	33	13	21	17	13
Zn	40	33	56	46	37	31	80	49	40	49	45	43	60	49	46	68
Sn	7.0						4.0		3.0				3.0			
W	1.1						0.60		0.60				1.2			
Sb	3.2						3.1		2.9				4.1			
Rb	287	284	247	202	368	357	200	198	192	182	189	186	194	248	262	165
Cs	7.6						5.5		7.3				5.8			
Ba	39	30	97	38	41	35	50	104	108	110	112	108	36	54	94	1181
Se	19	29	28	24	24	21	22.0	52	48	56	55	53	31	25	52	184
Tl	2.3						1.8		1.3				2.0			
Ga	16	18	16	18	18	19	20	17	20	17	16	16	21	17	10	13
Ta	2.52						1.59		1.36				1.36			
Nb	24.50	26.00	26.00	17.00	35.00	39.00	18.10	16.00	16.70	16.00	16.00	18.00	17.30	28.00	59.00	16.00
Hf	5.30						6.60		6.50				6.10			
Zr	137	143	192	182	127	133	211	205	230	188	186	191	210	138	111	392
Y	47.0	69.0	80.0	42.0	73.0	58.0	50.8	51.0	44.1	39.0	42.0	40.0	104.0	56.0	123.0	45.0
Th	38.3	39.0	36.0	34.0	45.0	43.0	26.7	29.0	21.4	29.0	30.0	29.0	22.8	42.0	42.0	23.0
U	6.43	17.0	15.0	15.0	23.0	17.0	4.04	10.0	3.85	9.00	12.0	11.0	3.69	16.0	19.0	12.0
La	52.6	93.0	131	75.0	47.0	33.0	89.9	126	82.3	105	87.0	108	277	89.0	25.0	53.0
Ce	117	151	185	176	102	97.0	172	169	159	180	140	170	266	89.0	26.0	124
Pr	13.2						19.8		18.0				51.8			
Nd	49.0	74.0	84.0	61.0	41.0	39.0	65.8	77.0	60.5		53.0	60.0	164	72.0	25.0	61.0
Sm	11.0						13.0		11.6				29.4			
Eu	0.223						0.37		0.67				1.30			
Gd	9.29						10.9		9.66				27.0			
Tb	1.61						1.72		1.50				3.6			
Dy	9.50						9.93		8.37				17.3			
Ho	1.85						1.95		1.60				3.01			
Er	5.50						5.75		4.67				7.97			
Tm	0.806						0.84		0.679				1.07			
Yb	5.15						5.20		4.30				6.03			
Lu	0.737						0.726		0.629				0.806			

Table 4.3. Continued.

	Unit	Sample Name	Nd (ppm)	Sm (ppm)	¹⁴⁷ Sm/ ¹⁴⁴ Nd	¹⁴³ Nd/ ¹⁴⁴ Nd*	2σ	Epsilon (0)**	T De Paolo	TDM2*	Epsilon (380)
Harvey	Cherry Hill	NB07-11	28.02	6.44	0.138800	0.512266	4	-7.26	1575.00	1796.47	-4.60
	Cherry Hill	NB07-2	39.80	14.39	0.218500	0.512722	4	1.64	-	-	0.64
	Harvey Mountain	NB07-21	34.20	9.62	0.170100	0.512575	4	-1.23	1625.00	2007.92	-0.01
	York Mills	NB07-26	13.97	5.65	0.244400	0.512697	7	1.15	-	-	-1.04
	McDougall Brook	NB07-35A	65.50	10.62	0.098000	0.512429	5	-4.06	817.00	950.71	0.46
Piskahegan	Seefys	NB07-81	67.41	11.44	0.102600	0.512437	5	-3.92	838.00	979.03	0.41
	Scouller Mountain	NB07-56	38.97	7.48	0.116000	0.512492	5	-2.85	866.00	1027.40	0.86
	Scouller Mountain	NB07-66	90.59	16.23	0.106300	0.512424	5	-4.17	900.00	1050.60	-0.11

Table 4.4. Results of the Sm–Nd isotope analyses of whole–rock samples from Harvey and Piskahegan. * ¹⁴³Nd/¹⁴⁴Nd corrected from the deviation from JNdi-1 with mean value obtained from the Memorial University TIMS Lab of ¹⁴³/¹⁴⁴ (0.51237, n=112, 0.000019). **εNd values were calculated based on the present day chondrite uniform reservoir (CHUR; ¹⁴⁷Sm/¹⁴⁴Nd = 0.1967 and ¹⁴³Nd/¹⁴⁴Nd = 0.512638), and age equations were modeled using the De Paolo mantle model, and the known decay constant (6.54x10⁻¹² years; Steiger and Jäger, 1977). ^TDM2 calculated using a linear evolution for a mantle separated from the CHUR at 4.55Ga and having a present day Epsilon value of +10.

	Unit	Sample	Host Rock	Yield	δ18O (VSMOW)
Harvey	Cherry Hill	NB07-16	rhyolite	13.1	10.4
		NB07-17	quartz-feldspar porphyry	14.9	11.9
	York Mills	NB07-30	rhyolite	15.7	14.7
Piskahegan	Big Scott Mountain	NB07-33A	quartz-feldspar porphyry	16.2	13.5
	Bailey Rock	NB07-73	rhyolite	15.6	11.3
	Little Mount Pleasant	NB07-106 (1)	rhyolite	16.3	9.7

Table 4.5. δ¹⁸O of quartz within whole–rock samples from Harvey and Piskahegan. Pure quartz should yield 16.7 ± 0.3, samples 16 and 17 were excluded from interpretation due to low yield.

Analysis Number	$^{176}\text{Hf}/^{177}\text{Hf}$	$^{176}\text{Lu}/^{177}\text{Hf}$	$^{176}\text{Yb}/^{177}\text{Hf}$	U/Pb Age	Hf _c	$\varepsilon\text{Hf}(T)^*$	T(DM) ₁	T(DM) ₂	Hf Chur (t)	Hf DM (t)
4	0.282785	0.00059	0.02502	403	0.282781	9.5	0.66	0.79	0.282513	0.282951
5	0.282665	0.00384	0.21257	361	0.282639	3.5	0.90	1.14	0.282540	0.282983
7	0.282693	0.00051	0.02322	403	0.282689	6.2	0.783	1.00	0.282513	0.282951
8	0.282629	0.00137	0.00698	361	0.282620	2.8	0.89	1.19	0.282540	0.282983
10	0.282762	0.00185	0.08355	361	0.282749	7.4	0.71	0.89	0.282540	0.282983
11	0.282664	0.00240	0.12648	361	0.282648	3.8	0.87	1.12	0.282540	0.282983
12	0.282745	0.00194	0.10121	403	0.282730	7.7	0.74	0.91	0.282513	0.282951
15	0.282673	0.00150	0.00788	361	0.282663	4.4	0.83	1.09	0.282540	0.282983
17	0.282829	0.00158	0.07463	361	0.282818	9.9	0.61	0.74	0.282540	0.282983
18	0.282682	0.00111	0.06408	403	0.282674	5.7	0.81	1.04	0.282513	0.282951
19	0.282661	0.00199	0.08856	403	0.282646	4.7	0.861	1.10	0.282513	0.282951
20	0.282824	0.00146	0.08476	361	0.282814	9.7	0.61	0.75	0.282540	0.282983
21	0.282744	0.00123	0.06907	403	0.282735	7.9	0.725	0.90	0.282513	0.282951
22	0.282641	0.00323	0.18784	361	0.282619	2.8	0.92	1.19	0.282540	0.282983

Table 4.6. Lu-Hf isotopic analysis of zircons, sample 17. * $\varepsilon\text{Hf}(T)$ values were calculated using chondritic ratios of $^{176}\text{Hf}/^{177}\text{Hf}$ (0.282772) and $^{176}\text{Lu}/^{177}\text{Hf}$ (0.0332) as derived by Blichert-Toft and Albarede (1997). All isobaric interferences of ^{176}Lu and ^{176}Yb on ^{176}Hf were corrected, and the recommended $^{176}\text{Lu}/^{175}\text{Lu}$ and $^{176}\text{Yb}/^{172}\text{Yb}$ ratios of 0.02669 (De BiÈvre and Taylor, 1993) and 0.5865 were used for the data reproduction.

4.11. Summary of Contributions

This study involved a variety of geochemical analyses, of which the facilities were not available at Saint Marys. As a result, preparation for all geochemical analyses were completed by the primary author, and funded largely through grants provided to TRG, and JD. LA-ICP-MS and Hf analyses of zircon were completed by Greg Shellnut at the University of Taiwan. All figures within this manuscript were created by the primary author. While the manuscript was improved through conversations with the co-authors, the manuscript was written in its entirety by the primary author. Revisions of this manuscript are ongoing at time of submission as it is still being prepared for publication submission.

CHAPTER 5: GEOCHEMISTRY OF LATE PALEOZOIC PERALKALINE FELSIC VOLCANIC ROCKS, CENTRAL NEW BRUNSWICK: URANIUM POTENTIAL

Accepted to Atlantic Geology, June 28, 2010

Taryn R. Gray^{1*}, Jaroslav Dostal¹, Malcolm M. McLeod², Duncan Keppie³

¹Department of Geology, Saint Mary's University, Halifax, Nova Scotia, B3H 3C3, Canada <Taryn.Gray@smu.ca>

²New Brunswick Department of Natural Resources and Energy, Geological Surveys Branch, P.O. Box 5040, Sussex New Brunswick E4E 5L2, Canada

³Instituto de Geología, Universidad Nacional Autónoma de México, 04510, México

*corresponding author

5.1. Abstract

Felsic volcanic rocks from the 335 Ma Cumberland Hill Formation of southern New Brunswick, Canada correspond to peralkaline rhyolites and trachytes. These rocks, which underwent extensive fractional crystallization from an alkali basaltic magma, have high concentrations of incompatible trace elements including uranium (up to ca. 20 ppm). Mafic parent magma was derived from either decompression mantle melting occurring during rifting, or a mantle plume, with the latter hypothesis preferred. Cumberland Hill peralkaline rhyolites may represent an economic source of uranium based on the elevated uranium concentrations and high degree of similarity with volcanic rocks of the Streltsovka caldera (Transbaikalia, Russia), one of the largest, hydrothermal, uranium deposits in the world.

5.2. Introduction

Igneous rocks are sparsely distributed throughout the Middle Devonian-Permian Maritimes Basin, and they appear to decrease in volume through time from: (i) Middle to Late Devonian tholeiites, minor alkali basalt, bimodal gabbro and A-type to evolved I-

type granite; (ii) Lower Carboniferous bimodal igneous rocks, and most sparsely, (iii) Upper Carboniferous bimodal igneous rocks (Fyffe and Barr, 1986; McCutcheon, 1990). The felsic igneous rocks of the Cumberland Hill Formation (Fm), the topic of this paper, were considered part of the Late Westphalian Pictou Group, and consequently associated with the latter phase of magmatism based on stratigraphic relationships (Fyffe and Barr, 1986). However, recent mapping indicated these volcanic rocks lie within the Viséan to early Namurian Mabou Group, and therefore associated with the middle phase (St. Peter, 1997; New Brunswick Department of Natural Resources, 2010). A mid-Viséan U-Pb zircon date of 335 ± 2 Ma age substantiates this interpretation (St. Peter, 2002). The Cumberland Hill Fm now appears to have approximately the same age as several, alkalic mafic formations in New Brunswick (e.g. the Hardwood Ridge, Royal Road and Queenstown basalts), and the tholeiitic-alkalic mafic rocks of the Cap aux Diabes Fm in the Magdalen Islands (Barr et al., 1985; Fyffe and Barr, 1986; La Fleche et al., 1998; New Brunswick Department of Natural Resources, 2010).

The mafic rocks of the Magdalen Islands have continental within-plate characteristics (Barr et al. 1985), and HIMU-OIB Pb-isotopic signatures that have been related either to a mantle plume (Pe-Piper and Piper, 1998) or to decompression melting below a pull-apart rift (LaFleche et al., 1998). The plume origin is consistent with the model proposed by Murphy et al. (1999) and Keppie and Krogh (1999) wherein the magmatism and deformation front migrated northwards from southern Nova Scotia at 380-370 Ma through northern Nova Scotia at 365-355 Ma to the Magdalen Islands in 335 Ma. The plume model is also consistent with the presence of a high-density lens beneath the

Maritimes Basin (Marillier and Verhoef, 1989), which may represent the beheaded portion of the plume. In this paper, we present whole-rock major and trace element analyses for the volcanic rocks of the Cumberland Hill Fm, and although we recognize that the data cannot distinguish between the various tectonic models, they can be of economic value as such rocks can be related to potential uranium mineralization (Dahlkamp, 1993; Plant et al., 1999; Cuney, 2009; Nash, 2010).

5.3. Geological Setting

Late Devonian to Early Permian rocks of New Brunswick comprise the western portion of the Maritimes Basin of the Atlantic Canada region, in which a successor basin developed during the waning stages and subsequent to the Middle Devonian Acadian Orogeny (e.g. St. Peter and Johnson, 2009, Fig. 5.1a). In New Brunswick, these rocks occur within deep depositional centers or subbasins, or on shallowly buried or partially exposed basement uplifts and platforms.

The volcanic rocks of the Cumberland Hill Fm crop out as several inliers over 20 km² and are unconformably overlain by the Upper Carboniferous Pictou Group on the New Brunswick Platform (Fig. 5.1b). The outcrops are likely related to a single volcanic centre partially hidden beneath Pictou Group (or Mabou Group) rocks, since the area incorporating the inliers clearly defines a circular area of high magnetic response on recent aeromagnetic maps (Thomas and Kiss, 2005).

Fyffe and Barr (1986) examined some of the felsic volcanic rocks in the vicinity of Cumberland Hill including lava flows and tuffs in a rhyolitic formation and underlying trachytic formation. Subsequently, St. Peter (1997) delineated the distribution of these

formations in more detail, depicting the trachytes as mostly underlying, but in part interdigitating with the rhyolites. There is also one massive intrusive porphyry plug with several smaller dikes/pipes, interpreted by Thomas and Kiss (2005) as volcanic feeder dikes based on their bulls eye positive magnetic anomalies (50-375 nT) within the magnetically anomalous area. The exact thickness of these formations is unknown as they are poorly exposed, however, both trachytic and rhyolitic formations are believed to be tens of meters thick.

The rhyolites are generally aphanitic to porphyric laminated flows and tuffs with feldspar phenocrysts and microphenocrysts (0.1- 4 mm in length) set in quartzfeldspathic groundmass. They contain green clinopyroxene as rare phenocrysts as well as Fe-Ti oxide accessories. The more altered trachytes contain aligned and extensively altered feldspar phenocrysts (0.1 - 2 mm), rare Fe-Ti oxides and altered clinopyroxene phenocrysts set in a fine-grained feldspar-rich groundmass or devitrified glass matrix.

5.4. Geochemistry

Major and trace elements of 15 whole-rock samples from the Cumberland Hill Fm (Table 5.1) were determined using a Perkin Elmer Optima 3000 inductively coupled plasma mass spectrometer (ICP-MS) in the Activation Laboratories in Ancaster, Ontario. Prior to analysis, samples were digested by fusion to ensure the complete dissolution of accessory minerals. Full analytical and technical parameters utilized can be found in Activation Labs on-line manual.

According to the $(\text{Na}_2\text{O}+\text{K}_2\text{O})$ vs SiO_2 classification of LeMaitre et al. (1989; Fig. 5.2) and the Zr/TiO_2 vs SiO_2 diagram (Fig. 5.3) of Winchester and Floyd (1977), the rocks can

be subdivided into two groups, trachytes and peralkaline rhyolites, analogous to comendite/pantellerite fields according to Winchester and Floyd (1977). Most rocks are peralkaline with a high agpaitic index ($AI = \text{mole (Na+K)/Al}$; Shand, 1951) and acmite in their norms. Considering loss of ignition (L.O.I) free analyses (Table 5.1), the trachytes on average ($n=7, 1\sigma$) have moderate SiO_2 (65 ± 2.48 wt. %) accompanied by high total alkalis (9.5 ± 1.81 wt. %), low CaO (2.5 ± 1.21 wt. %), high $\text{FeO}_{\text{tot}}/\text{MgO}$ (ca. 25) and elevated concentrations of high field strength elements (HFSE; e.g. 947 ± 334 ppm Zr, 85 ± 29 ppm Nb). The average rhyolitic rocks ($n=8, 1\sigma$) have higher SiO_2 (75 ± 0.66 wt. %), equivalent total alkali concentrations (9.0 ± 0.29 wt. %, very low CaO (0.23 ± 0.08 wt. %), high $\text{FeO}_{\text{tot}}/\text{MgO}$ (ca. 140) and high HFSE (e.g. 2369 ± 138 ppm Zr, 251 ± 36 ppm Nb). The $\text{Al}_2\text{O}_3/(\text{CaO}+\text{Na}_2\text{O}+\text{K}_2\text{O})$ ratios (mole) of both trachytes and rhyolites are <1 , typical of peralkaline rocks.

Major and trace elements in volcanic rocks of the Cumberland Hill Fm vary largely due to the degree of fractionation exhibited within trachytes and rhyolites. In order to determine the fractionation trends, Nb was utilized as a differentiation index (see White et al., 2006; Fig. 5.4). With increasing concentration of Nb, the trachytes displayed a positive correlation to Al_2O_3 , and a negative correlation to TiO_2 ; rhyolites in contrast have relatively constant Al_2O_3 (Fig. 5.4a), and TiO_2 (Fig. 5.4b). The reduction in TiO_2 can most likely be attributed to crystallization of Fe-Ti oxides. Trace elements also displayed distinct fractionation trends when compared to Nb in both trachytes and rhyolites. Trachyte samples showed marked decreases in Ba with increasing Nb (Fig. 5.4c), reflecting the crystallization of feldspars, as well as an increase in incompatible trace

elements including Zr, La, and Ga (Fig. 5.4d, e, f). However, the abundances of these trace elements in the rhyolites remained virtually unchanged with increasing Nb. The contrast in the fractional crystallization between trachytes and rhyolites is highlighted by a CaO-K₂O-Na₂O ternary diagram (Fig. 5.5), which illustrates trachytes move away from the CaO apex, while rhyolite variation is parallel to the K₂O-Na₂O join. This is most readily explained by the crystallization of Ca-bearing plagioclase and clinopyroxene in trachytes, and alkali feldspar crystallization in rhyolites.

The chondrite-normalized rare earth element (REE) patterns (Fig. 5.6a) are strongly enriched in light REE (LREE) and have fractionated heavy REE (HREE). The rhyolites have higher contents of LREE with (La)_n values of ca. 440-510 compared to the trachytes with (La)_n ca. 270-430, while the trachytes have higher (La/Yb)_n ratios (ca. 8-11) than rhyolites (ca. 4-6). A similar relationship is observed for (La/Sm)_n which in the trachytes is ca. 2.6-3.4 and in the rhyolites is ca. 2.2-2.6. The shape of the REE patterns of trachytes does not change significantly, although the absolute abundances are escalating with the increasing degree of differentiation. Such a variation, together with the presence of a small but distinct negative Eu anomaly is consistent with low-pressure fractional crystallization of common rock forming minerals including feldspars. The REE patterns of the rhyolites are characterized by a pronounced negative Eu anomaly although the shape of the patterns and the absolute abundances of the rhyolites vary in a narrow range. Primitive mantle-normalized trace element patterns of both rock types (Fig. 5.6b) are fairly similar. Both are highly fractionated and peak at Th-Nb, however rhyolites display a strong, negative Ba, Sr, and moderately negative Eu anomalies, while the trachytes

contain only slightly negative anomalies of these elements. This implies that the rhyolites underwent a more extensive fractionation of feldspars compared with the trachytes.

The abundances of U and Th in the felsic rocks of the Cumberland Hill Fm are high and variable (Table 5.1). Rhyolites display significantly higher contents of U (14 ± 4.0 ppm, $n=8$, 1σ), and Th (33 ± 3.1 ppm, $n=8$, 1σ) compared to trachytes (U = 2.4 ± 2.4 ppm, $n=7$, 1σ ; Th = 12 ± 1.4 ppm, $n=7$, 1σ). As a result, the rhyolites also have a higher U/Th ratio (0.44 ± 0.13 , $n=8$, 1σ) than trachytes (0.32 ± 0.09 , $n=7$, 1σ), which is comparable to the whole-rock or melt inclusion data from peralkaline rhyolites of various U districts in the world (Cuney and Kyser, 2009). The concentration of both Th and U are notably higher in Cumberland rhyolites than exhibited in the Devonian-Carboniferous rhyolites of Nova Scotia where Th and U are averaging 18.3 and 4.6 ppm, respectively (Dostal et al., 1983a) although the Nova Scotia rhyolites also have within-plate characteristics (Dostal et al., 1983b).

In contrast to typical igneous rocks (see Heier et al., 1965), there is no coherence of radioactive trace elements with K since both the trachytes and rhyolites have similar concentrations of K. In addition, the lack of correlation of radioactive trace elements with Zr and Y suggests that primary accessory minerals such as zircon are not the principal host of these elements (Dupuy and Dostal, 1983). These minerals are modally insignificant in the rocks. Therefore, it is more plausible that U and Th are primarily hosted as groundmass as suggested by their correlation with Ba and Sr.

5.5. Petrogenesis

Overall the geochemical and mineralogical similarities of the spatially and temporally associated trachytes and rhyolites imply they are genetically related. However, discontinuous and/or contrasting variation trends and significant differences in incompatible trace element ratios indicate the rhyolites were not derived from the trachytes via continuous fractional crystallization, although fractional crystallization may be responsible for the variations within the individual suites. The evolution of trachytes involved crystallization of feldspars, clinopyroxene and Fe-Ti oxides, while the fractionation of rhyolites was dominated by crystallization of alkali feldspar.

An alternative model to continuous fractional crystallization for the origin of the rhyolites is assimilation-fractional crystallization. However, the low and overlapping Th/Ta ratio of the trachytes and rhyolites (Fig. 5.7a), a sensitive indicator of crustal contamination (Gorton and Schandl, 2000), demonstrates that assimilation-fractional crystallization and crustal contamination processes cannot solely account for derivation of the rhyolites from the trachytes. This is also supported by Nd isotope data of Pe-Piper and Piper (1998), who reported an ϵ_{Nd} value of ca. 3.3 from the Cumberland Hill rhyolite. Although the Th/La ratio, another sensitive indicator of upper crustal contamination, is relatively high in the rhyolites (ca. 0.15-0.3), it suggests limited crustal contamination occurred.

K/Rb ratios in trachytes are much higher than in rhyolites (Fig. 5.8a,b), which suggest the evolution of the rhyolites may have been affected by fluids (Dostal and Chatterjee, 1995). Again, this mechanism cannot explain the origin of the rhyolites, but rather

indicates that fluids played an important role during the evolution of these rocks and perhaps even led to the mobilization of U (Cuney and Kyser, 2009; Nash, 2010) in the rhyolites (Fig. 5.8b).

A comparison with similar rocks (e.g. Peccerillo et al., 2003) suggests the Cumberland Hill trachytes and rhyolites could represent various stages of fractional crystallization within an evolving alkali basaltic magma. Considering the Y-Nb-Ce diagram of Eby (1992), it is apparent the rocks plot within the mantle derived source rock field (Fig. 5.7b) and are similar to A-type granites (Fig. 5.7c). The absence of a negative Ta-Nb anomaly suggests the parent magmas were not derived from subcontinental lithospheric mantle, but more plausibly originated from asthenospheric mantle. The rhyolites were also influenced partially by crustal contamination as indicated by the high Th/La ratio.

LaFleche et al (1998) and Pe-Piper and Piper (1998) described alkali basaltic rocks of comparable age from other parts of the Maritimes basin. The presence of alkali gabbroic rocks and lamprophyre dikes of a similar age (Johnson 2008) in the area suggests that the felsic rocks of Cumberland Hill Fm could be derived from such a parent by fractional crystallization. In fact, peralkaline felsic volcanic complexes are typically associated with a shallow-seated alkaline intrusions ranging in compositions from gabbros to highly fractionated granitic rocks. Although there is insufficient geochemical data available on the mafic alkali rocks in the vicinity of the Cumberland Hill Fm, the chemical analyses of alkali basaltic rocks reported by LaFleche et al. (1998) from the Magdalen Islands indicate that similar basalts could have been a parent for the trachytes and rhyolites. Trachytes of similar compositions have been documented to evolve from alkali basalts by

extensive fractional crystallization (Peccerillo et al., 2003) and peralkaline rhyolites could have evolved from such magma by further fractional crystallization in the magma chamber. A likely scenario for the Cumberland Hill felsic rocks is that they are the products of fractional crystallization of alkali basaltic magma, and that the trachytes and rhyolites represent separate magma pulses with the latter being younger having undergone more extensive fractionation prior to emplacement.

5.6. Economic Potential

Silica-oversaturated peralkaline felsic volcanic rocks, particularly rhyolites, are frequently enriched in U and represent a potential source of uranium for volcanic-related hydrothermal U deposits, such as the late Jurassic Streltsovka caldera located in Transbaikalia, Russia near the Chinese-Mongolian border (Ischukova, 1997; Chabiron et al., 2001, 2003; Cuney and Kyser, 2009; Nash, 2010). Uranium mineralization within Streltsovka is generally isolated within the sandstones, conglomerates and rhyolitic tuffs of the caldera, commonly isolated in subvertical veins and stockworks grading up to 0.6% U_3O_8 in large stockworks, and as high as 1.0% U_3O_8 in veins (Chabiron et al., 2003). Sediment-hosted U deposits may also occur in siliciclastic sedimentary basins, such as the Jurassic Tim Mersoï basin in Niger, grading up to 0.11% U_3O_8 in organic material entombed in sandstone (Forbes et al., 1984; Forbes, 1989; Plant et al., 1999; Pagel et al., 2005; IAEA, 2009).

The crystallization of U-bearing accessory minerals in highly polymerized peralkaline melts is typically suppressed (Cuney, 2009; Cuney and Kyser, 2009) leading to progressive enrichment of U in residual melts during fractional crystallization and

entrapment of U in the glassy groundmass. Subsequently U can be leached during the alteration or devitrification of the glass (Nash, 2010). Cuney (2009) and Cuney and Kyser (2009) inferred that ignimbritic tuffs, in which U is hosted in the glass, are the most favourable type of volcanic rock; such rhyolitic pyroclastic rocks are abundant in the Cumberland Hill Fm.

The rhyolites of the Cumberland Hill Fm have relatively high abundances of U compared to associated trachytes and may be a source of U mineralization. The U concentrations in these rhyolites are elevated compared to similar felsic and mafic Late Tournaisian–Early Viséan deposits of the Maritimes Basin (Magdalen Islands, 0.4-1.9 ppm; Central New Brunswick, 0.8-1.9 ppm; Cobequid Highland dykes, 0.2 ppm; Pe-Piper and Piper, 1998) and Nova Scotia Devonian-Carboniferous basalts (0.5-0.8 ppm; Dupuy and Dostal, 1983) and rhyolites (~4.6 ppm; Dostal et al., 1983a,b). The abundances of U in the rhyolites are comparable to the U concentrations of the peralkaline rhyolites of the Streltsovka caldera (Fig. 5.6b), the largest, volcanic-related, U ore field in the world (Cuney, 2009). Despite similar U concentration, it is important to consider where U is hosted in rhyolites. When U is hosted in zircon or other resistant accessory minerals it cannot be readily remobilized. Based on current geochemical work, it appears U is present within the glassy groundmass of the Cumberland Hill rhyolites and can therefore be released and redeposited and thus could be a source of U.

5.7. Conclusions

Although the geochemistry of the felsic rocks of the Cumberland Hill Fm is consistent with both the plume and decompression melting models, other factors such as NNE-

migration of the magmatism and deformation front are more consistent with the plume model (Keppie and Krogh, 1999; Murphy et al., 1999). The high potential for U mineralization related to the rhyolitic rocks of the Cumberland Hill Fm, and equivalent exposed or buried formations on the New Brunswick Platform is perhaps the most important aspect of this study as it furthers the economic viability of the region.

5.8 Acknowledgements

A grant from the Geological Survey Branch of the New Brunswick Department of Natural Resources and Energy (JD) graciously provided fieldwork expenses. Analytical work was predominantly funded by the Natural Sciences and Engineering Research Council of Canada (NSERC) Discovery Grant (JD), and in part by the Society of Economic Geologists Student Research Grant (TRG).

5.9. Chapter 5 Appendix

All the figures and table are located in a consecutive manner, in the general style required for manuscript submission to peer-reviewed journals.

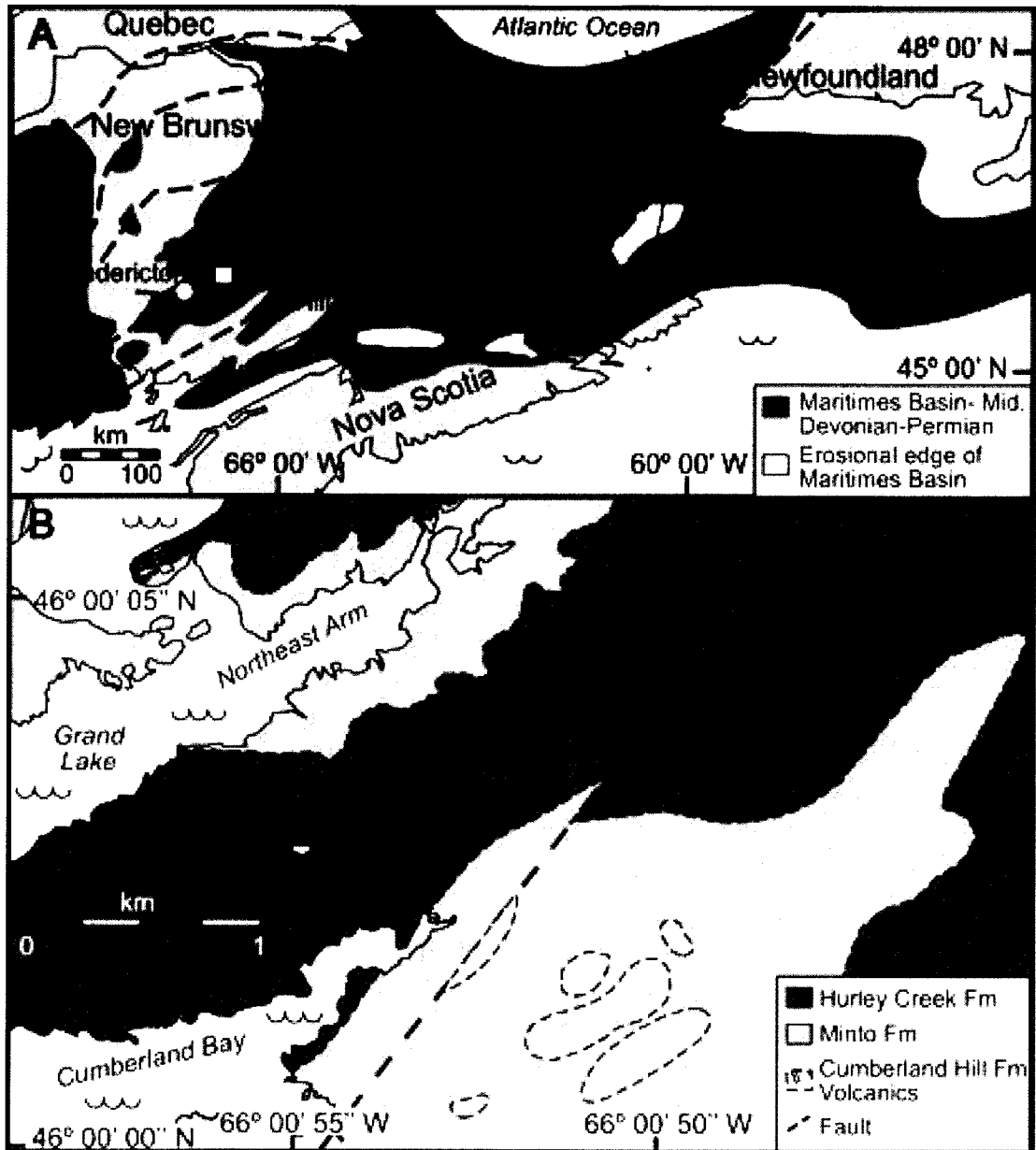


Figure. 5.1. Map of Study Area. a) Map of Atlantic Canada depicting the Maritimes Basin and its present erosional edge (adapted from Roliff 1962; Williams 1974; Bradley 1982; and Fyffe and Barr 1986). Major faults are indicated as dashed lines, study area is indicated with a box, (b) Geological map of the Cumberland Hill area, southern New

Brunswick (adapted from Smith, 2007). Minto Fm represents grey to red medium grained sandstone with red mudstone with conglomerate and traces of coal, while the Minto Fm-Hurley Creek Member is characterized by reddish brown coarse grained sandstone and conglomerate interbedded with fine grain mudstones. The Cumberland Hill Fm volcanic rocks contain rhyolitic and trachytic lavas and volcanoclastic rocks and minor feldspar porphyry and red-brown lithic sandstone.

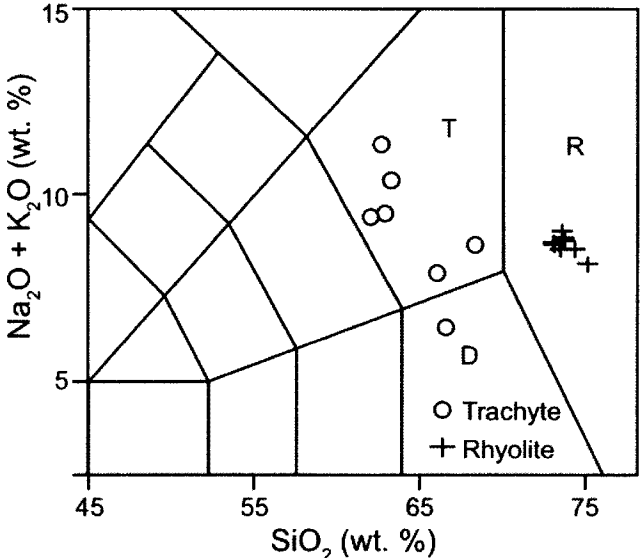


Figure 5.2. (Na₂O+K₂O) versus SiO₂ (wt. %) diagram of Le Maitre et al. 1989 for the volcanic rocks of the Cumberland Hill Fm. Abbreviations: D – dacite; T – trachyte; R – rhyolite.

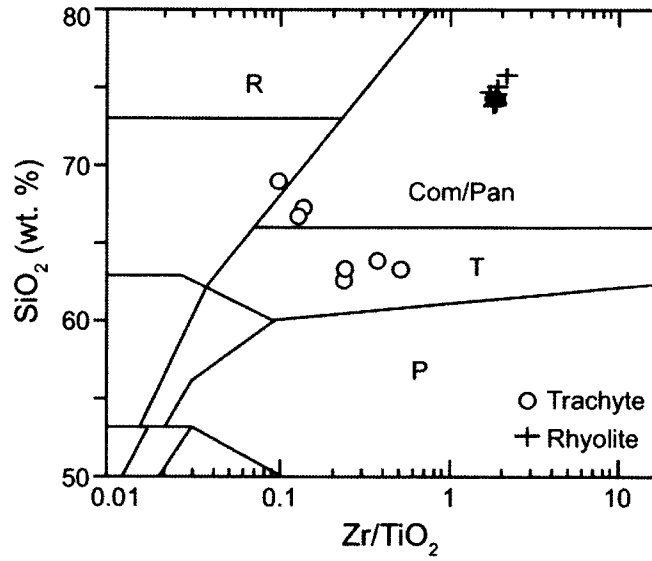


Figure 5.3. Zr/TiO₂ versus SiO₂ diagram of Winchester and Floyd (1977) for the felsic volcanic rocks of the Cumberland Hill Fm. Abbreviations: Com/Pan – comendite/pantellerite; T – trachyte; R – rhyolite; P – phonolite

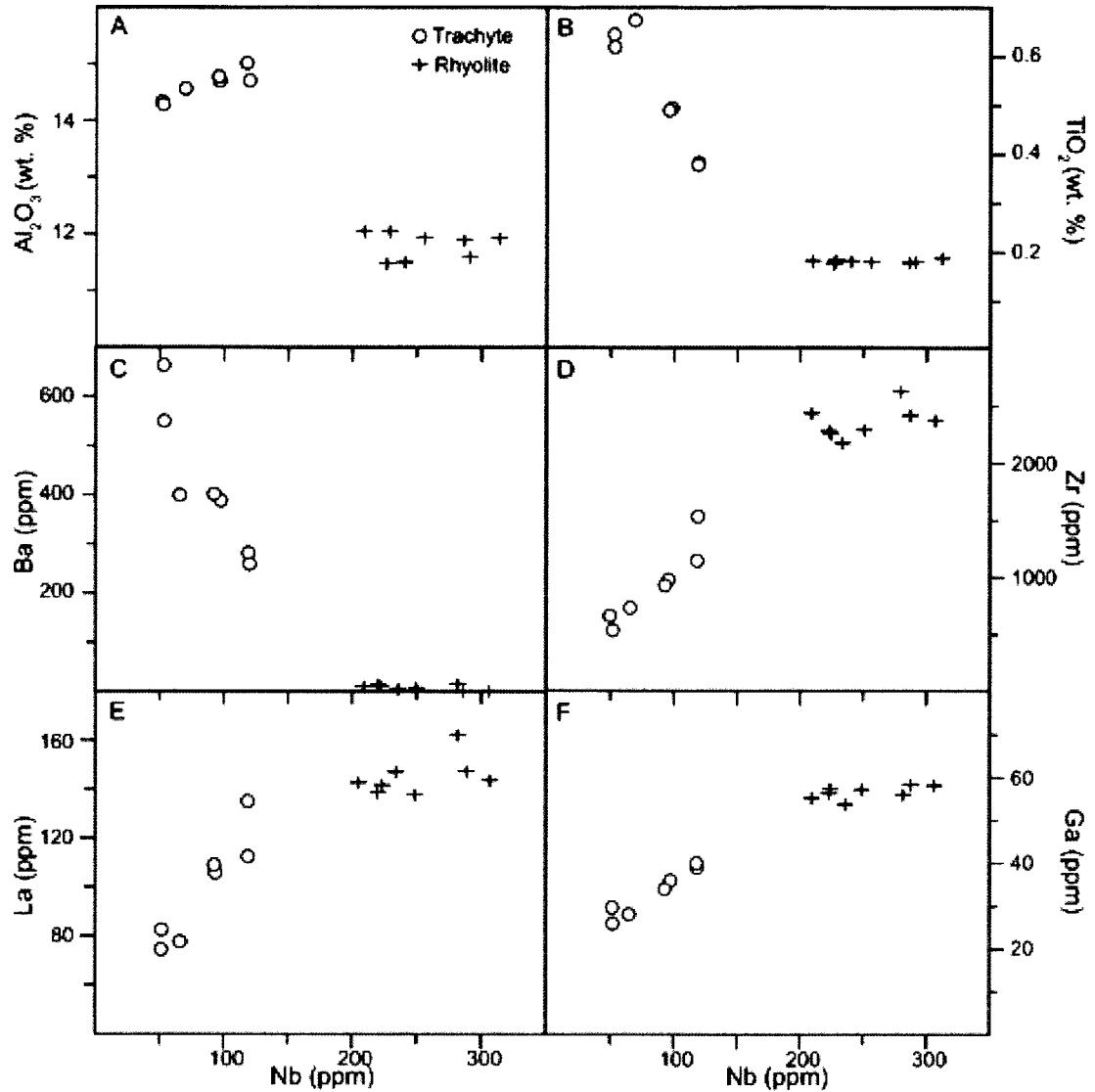


Figure 5.4. Fractionation diagram using Nb as a tracer. Nb (ppm) versus (a) Al₂O₃ (wt. %), (b) TiO₂ (wt. %), (c) Ba (ppm), (d) Zr (ppm), (e) La (ppm), and (f) Ga (ppm) diagrams for felsic volcanic rocks from the Cumberland Hill Fm.

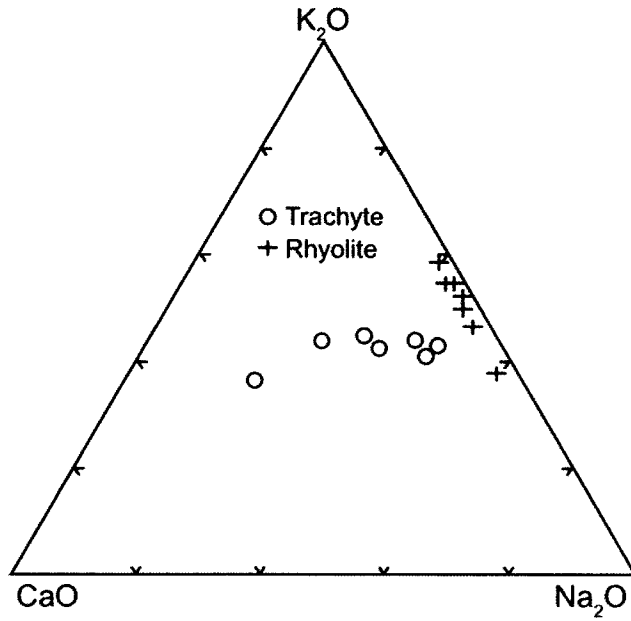


Figure 5.5. CaO-K₂O-Na₂O ternary diagram. Volcanic rocks of the Cumberland Hill Fm show fractionation of Ca-plagioclase and clinopyroxene in trachytes, while only alkali feldspar played a role in rhyolites.

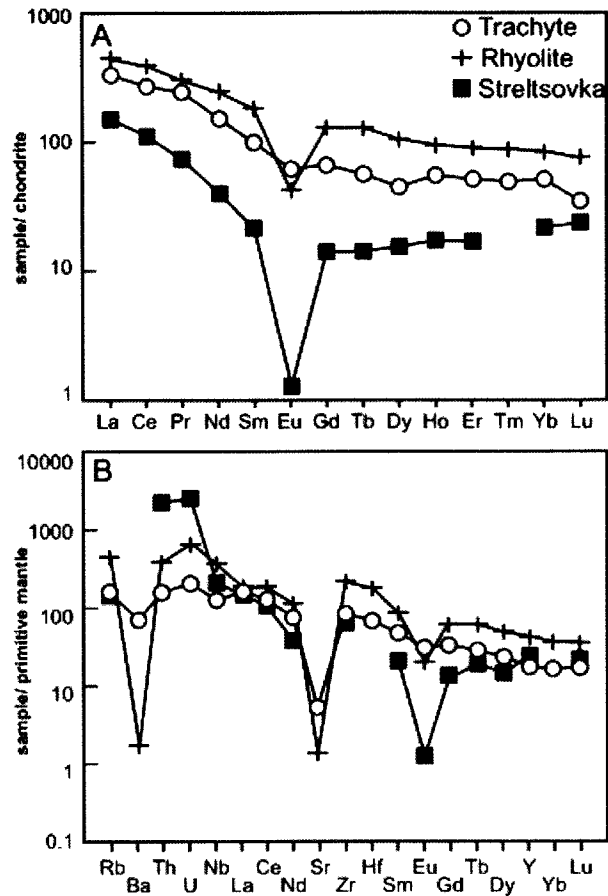


Figure 5.6. Normalization diagrams. (a) Chondrite-normalized REE patterns of the average of trachytes (n=7) and rhyolites (n=8) from the Cumberland Hill Fm. and rhyolite from Streltsovka (n=1; Chabiron et al. 2003); (b) Primitive mantle-normalized multi-element plots of the average of trachytes (n=7) and rhyolites (n=8) from the Cumberland Hill Fm. and rhyolite from Streltsovka (n=1; Chabiron et al. 2003). Normalizing values are after Sun and McDonough (1989).

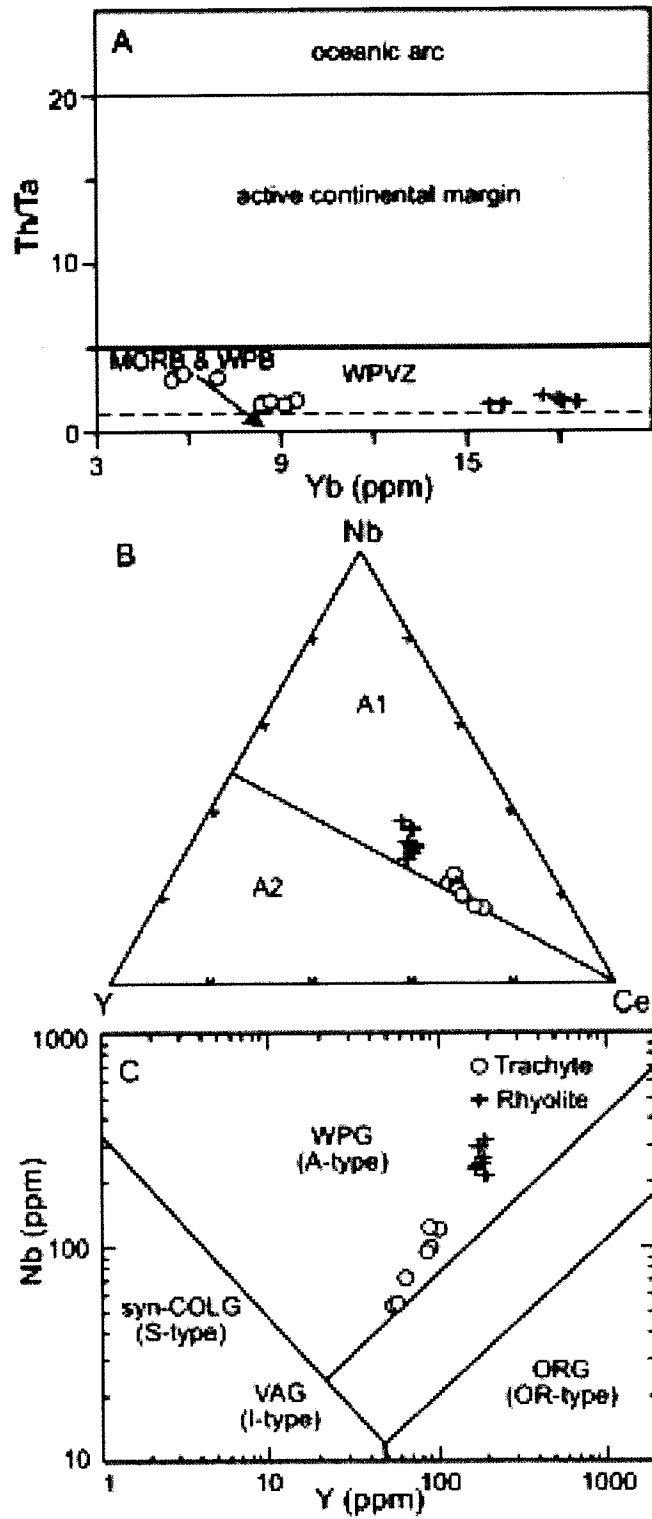


Figure 5.7. Discrimination diagrams for felsic volcanic rocks from the Cumberland Hill Fm. (a) Diagram Yb (ppm) versus Th/Ta diagram of Gorton and Schandl (2000); WPVZ = within plate volcanic zones; MORB = mid-ocean ridge basalts; WPB = within plate basalts, (b) Plot of Y–Nb–Ce (A1 granites with element ratios similar to the mantle, whereas A2 are granites originated from continental crust or arcs), dividing line between groups is from Eby (1992), (c) Y (ppm) versus Nb (ppm). Field boundaries are from Pearce et al. (1984) as modified by Christiansen and Keith (1996); VAG-volcanic arc granite; WPG- within plate granite; ORG- ocean ridge granite; syn-COLG – syncollisional granite.

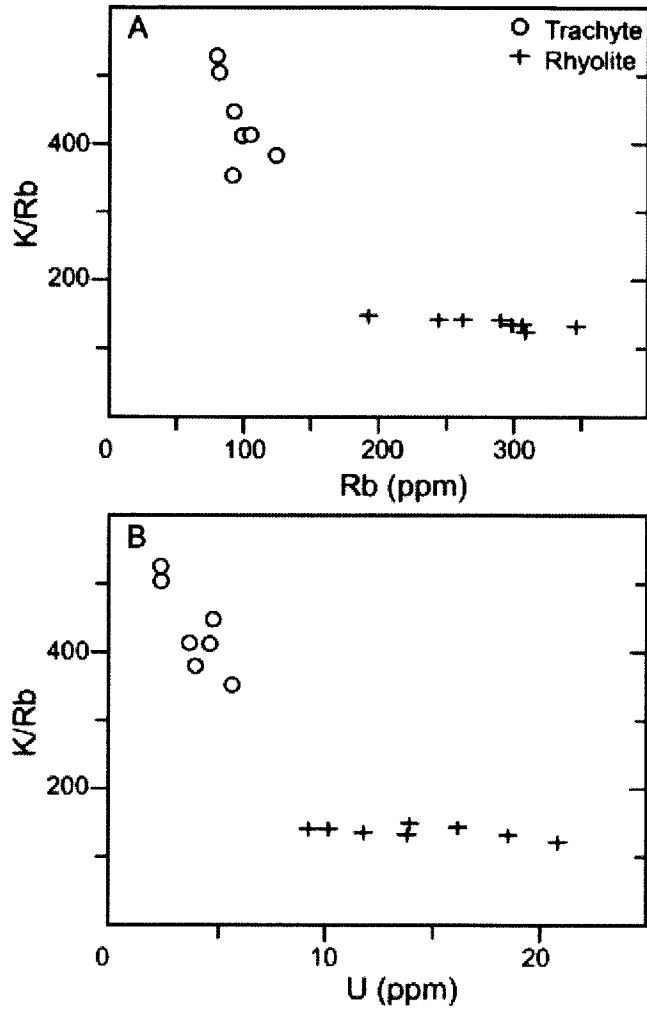


Figure 5.8. Remobilization and fractionation diagrams. K/Rb versus (a) Rb (ppm) and (b) U (ppm) in the felsic volcanic rocks of the Cumberland Hill Fm.

	Trachyte							Rhyolite							
	1-202	1-203	1-206	1-207	1-01	1-12	1-14	2-01	2-8A	2-8B	2-09	2-10	2-11	2-12	2-13
SiO ₂ (wt. %)	62	60	67	64	64	62	62	74	73	73	73	72	72	72	74
TiO ₂	0.48	0.47	0.63	0.37	0.60	0.63	0.38	0.17	0.17	0.17	0.17	0.17	0.17	0.18	0.18
Al ₂ O ₃	14	14	14	15	14	14	14	12	11	11	11	12	12	12	12
Fe ₂ O ₃ (T)	9.3	8.8	4.1	7.8	6.1	5.1	7.8	3.4	4.2	4.1	4.1	4.4	4.2	4.4	3.4
MnO	0.18	0.25	0.11	0.22	0.19	0.17	0.22	0.04	0.10	0.10	0.12	0.10	0.10	0.09	0.03
MgO	0.13	0.37	0.20	0.08	0.37	0.29	0.07	0.02	0.02	-	0.02	0.02	0.05	0.02	0.03
CaO	1.5	2.4	2.3	1.7	3.1	4.5	1.4	0.11	0.15	0.15	0.22	0.31	0.26	0.23	0.34
Na ₂ O	4.8	4.4	3.7	5.8	3.0	2.2	6.2	3.7	3.9	4.2	3.7	3.8	4.3	4.5	5.3
K ₂ O	4.9	5.0	5.0	5.2	4.9	3.9	5.7	4.6	5.0	4.8	5.6	5.0	4.5	4.2	3.5
P ₂ O ₅	0.14	0.13	0.23	0.09	0.17	0.19	0.08	-	0.01	-	0.01	-	-	-	-
LOI	1.8	2.5	2.8	0.66	4.0	6.3	0.62	1.0	1.3	1.2	2.0	1.8	2.1	1.0	1.4
Total	99	98	100	100	100	99	99	99	99	100	100	99	99	99	100
Pb (ppm)	26	13	18	21	9	16	90	15	62	21	37	28	82	24	17
Zn	250	150	110	210	90.0	60.0	210	390	280	300	360	300	300	310	290
W	1.6	1.4	1.8	1.4	1.1	3.5	0.7	3.2	6.6	8.2	2.9	3.5	3.4	23	9.4
Rb	81	79	92	104	98	91	124	308	290	299	347	306	262	244	192
Cs	0.6	0.20	1.3	0.70	1.7	1.7	0.70	1.9	1.7	1.9	1.9	2.1	1.5	1.7	1.1
Ba	384	403	552	259	664	398	280	15	4.0	-	12	6.0	9.0	-	9.0
Sr	107	281	100	42	93	96	39	25	16	17	37	39	38	21	28
Ga	36	34	26	40	30	28	39	56	54	58	57	57	56	58	55
Ta	6.7	6.7	3.7	8.1	3.7	4.3	8.3	15	18	19	18	18	18	19	19
Nb	96	93	52	118	51	66	118	281	235	287	222	249	223	306	208
Hf	22	22	12	25	14	16	31	57	51	56	53	50	52	55	55
Zr	991	944	557	1150	679	755	1550	2640	2190	2420	2290	2300	2280	2380	2450
Y	87	83	52	101	54	62	89	177	179	175	179	184	162	187	191
Th	12	11	11	12	13	14	15	30	31	31	39	33	29	33	35
U	2.4	2.4	4.8	3.7	4.7	5.8	4.0	21	9.3	12	19	14	16	10	14
La	114	116	93	139	86	88	120	164	150	151	144	142	146	148	146
Ce	239	243	195	286	183	189	259	337	331	334	330	327	315	319	322
Pr	26	26	21	31	22	22	31	39	39	40	38	38	38	39	39
Nd	93	95	70	110	87	89	122	152	155	155	147	147	151	152	152
Sm	21	21	15	24	17	18	25	36	37	37	35	36	36	36	36
Eu	5.3	5.4	3.6	5.4	3.4	3.6	4.9	3.1	3.2	3.2	3.1	3.1	3.2	3.1	3.2
Gd	19	20	13	22	14	15	22	33	35	36	35	35	35	36	36
Tb	3.1	3.0	2.0	3.5	2.1	2.3	3.4	6.1	6.0	6.1	6.1	6.1	6.0	6.3	6.4
Dy	17	17	11	20	11	13	18	33	35	34	35	35	33	36	36
Ho	3.2	3.1	2.0	3.7	2.2	2.5	3.6	6.6	6.7	6.7	7.2	7.0	6.2	7.1	7.2
Er	8.9	8.6	5.6	10.0	5.9	6.8	9.7	18	18	18	20	19	17	19	20
Tm	1.3	1.2	0.81	1.4	0.88	1.0	1.5	2.9	2.6	2.6	3.0	2.9	2.6	3.0	3.0
Yb	8.4	8.0	5.3	9.1	5.6	6.5	9.4	18	18	16	17	18	16	18	18
Lu	1.3	1.3	0.80	1.4	0.89	1.0	1.5	2.5	2.7	2.2	2.4	2.6	2.3	2.6	2.6

Table 5.1. Major and trace element concentrations of Cumberland Hill trachytes and rhyolites. All values were obtained through ICP-MS, - symbol indicates value below detection limits.

5.10. Summary of Contributions

This study involved the analysis of major and trace elements using XRF and ICP-MS, equipment unavailable at Saint Marys. Rocks were sliced and chipped in preparation for

geochemical analysis (TRG) and funded through grants (TRG, JD). All figures within this manuscript were created by the primary author, aided by helpful suggestions of Malcolm McLeod (Fig. 1). The original draft of this manuscript was completed during an independent study, under the direction of Dr. Dostal. Subsequently, the co-authors made large improvements to the original manuscript. Dr. Dostal and Dr. Keppie offered further insight into the mantle plume theory and aided the petrologic discussion. Additionally, the regional geology and lithology sections were enhanced by Malcolm McLeod. Final revisions of the manuscript were completed by the primary author. Revisions of this manuscript are currently complete as the submission is still in review with *Atlantic Geology*.

CHAPTER 6: CONCLUSIONS

To answer the original research question that initiated this thesis, it is clear that Harvey and Piskahegan did not evolved from the same magmatic source, despite being similar in age. While both are within plate granites, the Harvey Group formed by partial melting of juvenile crustal material and Gander aged basement rock. Continued fractionation of the magma, and post-formation alteration created the unique REE, U-rich geochemistry of the Harvey volcanics. The Piskahegan Group, formed from the melting of younger, Avalon source rocks, and experienced significantly less fractionation and post-magmatic alteration than Harvey.

Both deposits show very distinct trace and major element geochemical signatures as studied via melt inclusions and whole rock. Harvey was enriched in LREE and Cs, B, U, and Th compared to Piskahegan. Harvey was also highly fractionated, at least 95%, while Piskahegan was only fractionated 70 - 92% as elucidated though the analysis of the Cs content within melt inclusions. Increased fractionation, coupled with post-magmatic water circulation, likely facilitated the elevated U mineralization at Harvey compared to Piskahegan.

6.1. Addressing the Central Research Questions

The first research question was: *“What was the original geochemical composition of the Harvey formation and how did it evolve?”*

The original geochemical composition of the Harvey calc-alkaline rhyolites was deduced through melt inclusion analysis. Rock from the Harvey Group are classified as

high silica, peralkaline rhyolites with limited concentrations of fluorine. Normalized abundance diagrams indicated that silicate melt inclusions are slightly enriched in most incompatible trace elements and significantly depleted in Ba, Sr, and Eu compared to whole rock, with a slight enrichment of HREE relative to LREE. As identified above, Harvey was also quite fractionated with large negative anomaly's in Ba, Eu, and Sr, indicative of feldspar fractionation.

Whole-rocks are depleted in MgO and TiO₂, likely related to accumulations of oxides, plagioclase feldspar and or mafic inclusions. Whole-rocks are enriched in HFSE (Nb, Hf, REE, Th, U) except Ta. Harvey remains enriched in HREE compared to LREE according to continental crust normalized diagrams, however both chondrite and primitive mantle normalized diagrams indicate a flat REE pattern. Mineralogical investigations revealed that Harvey rocks are quite altered, and geochemistry indicates that remobilization has occurred.

While the magmatic geochemistry offered insight into the element concentrations of the melt, radiogenic and oxygen isotopes were required to elucidate the nature of the source material. Slightly positive ϵ_{Nd} values indicated partial melting of juvenile crustal material and Gander basement rock. Continued fractionation of the magma, and post-formation alteration processed created the unique REE, U-rich geochemistry of the Harvey volcanics. The formation of Harvey was facilitated by lithospheric thinning, during which a pulse of basaltic rich magma may have provided the heat required. This result was supported by Hf isotopes which indicated a source composed of both depleted mantle (i.e. MORB) and crustal material.

The second research question was: *“How does the geochemistry of the Cumberland Hill Formation compare to other deposits within southern New Brunswick and what impact does this have on our current understanding of the geological history of the Maritimes?”*

The rocks of the Cumberland Hill Fm can be subdivided into two groups, trachytes and peralkaline rhyolites. Both have lower SiO₂, equivalent alkalies, and lower Cao compared to Harvey or Piskahegan rhyolites. Major and trace element concentrations vary significantly in the trachytes and rhyolites of Cumberland Hill due to the high degree of fractionation exhibited within rhyolites. The chondrite-normalized REE patterns indicated Cumberland Hill volcanics are strongly enriched in LREE and have fractionated HREE, with rhyolites more enriched in LREE overall. The abundances of U and Th in the felsic rocks of the Cumberland Hill Fm are low compared to Harvey or Piskahegan, although all three formations exhibit concentrations notably higher than exhibited in the Devonian-Carboniferous rhyolites of Nova Scotia.

The Cumberland Hill trachytes and rhyolites likely represent various stages of fractional crystallization that coincided with an evolving alkali basaltic magma. The parent magma was probably derived from asthenospheric mantle that was influenced partially by crustal contamination. Alternatively, it has been hypothesized that trachytes and rhyolites from the Magdalen Islands, with similar geochemical composition were derived through fractionation of alkali basaltic. However, without further geochemical

work ascertain the nature of the source material, the nature of the petrogenesis within this deposit is still largely speculative.

Igneous rocks are sparsely scattered throughout the Maritimes Basin, and seem to decrease in volume throughout the Devonian to Permian. The Cumberland Hill Fm formed at approximately the same times as many alkalic mafic formations in New Brunswick (e.g. the Hardwood Ridge, Royal Road and Queenstown basalts), and the tholeiitic-alkalic mafic rocks of the Cap aux Diables Fm in the Magdalen Islands, all of which have within plate characteristics. Interestingly, the mafic rocks of the Magdalen Islands have an HIMU-OIB Pb-isotopic signatures that suggests origin related to either a mantle plume or decompression melting. The location of the Cumberland Hill Fm supports the hypothesis that a mantle plume migrated northwards from southern Nova Scotia at 380-370 Ma, through northern Nova Scotia at 365-355 Ma, and finally reaching the Magdalen Islands in 335 Ma.

The third research question was *“What economic potential lies within the U deposits of Southern New Brunswick?”*

Based on this body of research, it is evident the province of New Brunswick is host to a variety of deposits with considerable economic potential, not only in previously explored commodities such as gold, molybdenum, and tin, but also uranium. The abundances of U and Th in the felsic rocks of the Cumberland Hill Fm are low compared to Harvey or Piskahegan. However, both Harvey and Piskahegan contain significantly larger concentrations of U and Th than other rhyolite deposits in Nova Scotia (ex. Fisset

Brook, McAras Brook, Upper Byers Brook, Middle Diamond Brook, Horton Group, Murphy Brook, Fountain Lake Group).

While it is clear none of these deposits are co-magmatic, the presence of such elevated concentrations of uranium, and REE imply that either the mantle, or crust in this region contains anomalously high concentrations of these elements. Therefore, similar deposits may exist in this region, although it is unclear at present time where they may be located. Additional melt inclusion and radiogenic isotope work could help constrain the nature of the source material and aid in locating additional economic deposits within southern New Brunswick, or possibly within Europe, Nova Scotia, and Newfoundland considering the tectonic history of the Maritimes Basin.

6.2. Environmental Implications

The rocks analyzed within this study all contained U within a devitrified groundmass, and therefore over time, U could have been eroded from these source rocks. Erosion is facilitated by water, which is capable of transporting U^{6+} within oxidized waters, that once reduced, precipitates U^{4+} (i.e. pitchblende, uraninite). How far U is transported is entirely dependant on the climate of the region (i.e. precipitation), nature of host rocks (i.e. permeability) and how long before reducing conditions are met. Given the extremely large half life of U (4.5×10^9 years), it is possible for U to travel large distances, becoming hosted in multiple different sources over time. As a result, a significant portion of the U previously isolated within Carboniferous volcanics is currently localized in conglomerates and red-bed type deposits, particularly in reduced traps including roll-fronts, coal-rich shales, bogs and even tree trunks. This implies that despite the push to

cease exploration for U due to health concerns, dangerous concentrations may already be present throughout New Brunswick (i.e. shallow wells). Figure 6.2.1. illustrates the occurrence of U mineralization within New Brunswick. The previously discussed Harvey and Piskahegan Groups, located south of Fredericton are characterized as stratabound volcanics, and are relatively rare considering U distribution within the province. Given that the most significant accumulations of U mineralization exist near the provinces most populated cities (Fredericton, Moncton and Saint Johns), the large concentrations of U identified within Piskahegan, Harvey and Cumberland Hill should be considered cautiously, as they represent significant volumes of U that could be remobilized to surrounding regions.

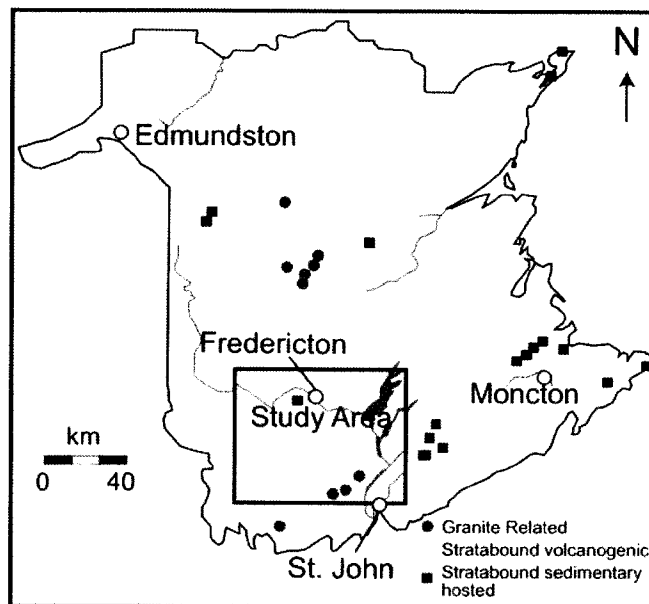


Figure 6.2.1. Map of New Brunswick uranium occurrences (modified from New Brunswick Natural Resources, 2010). Note that symbols may represent more than one U deposit within that area.

CHAPTER 7: REFERENCES

- Anderson, A.T., 1973, The before-eruption water content of some high-alumina magmas: *Bulletin of Volcanology*, v. 37, p. 530–552.
- Audétat, A., Pettke, T., 2003, The magmatic-hydrothermal evolution of two barren granites: A melt and fluid inclusion study of the Rito del Medio and Cañada Pinabete plutons in northern New Mexico (USA): *Geochimica et Cosmochimica Acta*, v. 67, p. 97–121.
- Bacon, C.R., 1989, Crystallization of accessory phases in magmas by local saturation adjacent to phenocrysts: *Geochimica Cosmochimica Acta*, v. 53, p. 1055–1066.
- Bacon, C.R., Newman, S., Stolper, E., 1992, Water, CO₂, Cl, and F in melt inclusions in phenocrysts from three Holocene explosive eruptions, Crater Lake, Oregon: *American Mineralogist*, v. 77, p. 1021–1030.
- Baker, D.A., 2008, The fidelity of melt inclusions as records of melt composition: *Contributions to Mineralogy and Petrology*, v. 156, p. 377–395.
- Bali, E., Audétat, A., Keppler, H., 2009. Mobility of U and Th in subduction zones- a synthetic fluid inclusion study: *Geodynamics Research Center-Bayerisches Geoinstitut Workshop on Deep Earth Mineralogy, Bayreuth, 17–19 June 2009.*
- Barr, S.M., Brisebois, D., and MacDonald, A.S., 1985, Carboniferous volcanic rocks of the Magdalen Islands, Gulf of St. Lawrence: *Canadian Journal of Earth Sciences*, v. 22, p. 1679–1688.
- Beaudin, J., LeGallais, C., and Schimann, K., 1980, Rapport final des travaux de la campagne 1979. Groupe de claims Manners Sutton. Project 24-147, comte York, Nouveau-Brunswick, volume 1, Seru Nucleaire du Canada, Montreal.
- Blichert-Toft, J., and Albarede, F., 1997, Lu-Hf isotope geochemistry of chondrites and the evolution of the mantle-crust system: *Earth and Planetary Science Letters*, v. 148, p. 243–258.
- Brack, W., 1982, Assessment report Juvenile Mountain (Duck Lake) New Brunswick: Uranerz Exploration and Mining LTD. Report 472895, p. 86.
- Bradley, D.C., 1982, Subsidence in the late Paleozoic Basins in the eastern Appalachians: *Tectonics*, v.1, p. 107–123.

Brown, H., Harrison, Silver, L.T., 1956, The possibilities of obtaining long-range supplies of uranium, thorium and other substances from igneous rocks, *in* Page, L.R., Stocking, H.E., and Smith, H.B., compilers, Contributions to the geology of uranium and thorium: U.S. Geological Survey Professional Paper 300, p. 85–89.

Burt, D.M., Sheridan, M.F., Bikun, J.V., and Christiansen, E.H., 1982, Topaz rhyolites-distribution, origin and significance for exploration: *Economic Geology*, v. 77, p. 1818–1836.

Capella Resources Ltd., 2007, Harvey Project: Harvey Project Assay Highlights (<http://www.capellaresources.com/s/HarveyProject.asp>).

Chabiron, A., Alyoshin, A.P., Cuney, M., Deloule, E., Golubev, V.N., Velitchkin, V.I., and Poty, B., 2001, Geochemistry of the rhyolitic magmas from the Streltsovka caldera (Transbaikalia, Russia): a melt inclusion study: *Chemical Geology*, v. 175, p. 273–290.

Chabiron, A., Cuney, M., and Poty, B., 2003, Possible uranium sources for the largest uranium district associated with volcanism: the Streltsovka caldera (Transbaikalia, Russia): *Mineralium Deposita*, v. 38, p. 127–140.

Chen, Z., and Fang, Z., 1985, Main characteristics and genesis of Phanerozoic vein-type uranium deposits, *in* Uranium Deposits in Volcanic Rocks, Proceedings of a Technical Committee Meeting, El Paso, Texas, April 1984, International Atomic Energy Agency, p. 69–82.

Chiu, H.Y., Chung, S.L., Wu, F.Y., Liu, D., Liang, Y.H., Lin, I.J., Iizuka, Y., Xie, L.W., Wang, Y., and Chu, M.F., 2009, Zircon U–Pb and Hf isotopic constraints from eastern Transhimalayan batholiths on the precollisional magmatic and tectonic evolution in southern Tibet: *Tectonophysics*, v. 477, p. 3–19.

Christiansen, E.H., Bikun, J.V., Sheridan, M.F., and Wilson, R.T., 1983, The petrogenesis of topaz rhyolites from the Western United States: *Contributions of Mineralogy, Petrology*, v. 83, p. 16–30.

Christiansen, E.H., Bikun, J.V., Sheridan, M.F., and Burt, D.M., 1984, Geochemical evolution of topaz rhyolites from the Thomas Range and Spor Mountain, Utah: *American Mineralogist*, v. 69, p. 223–236.

Christiansen, E.H., and Keith, J.D., 1996, Trace-element systematics in silicic magmas: a metallogenic perspective, *in* Wyman, D.A., ed., Trace Element Geochemistry of Volcanic Rocks. *Edited by* Geological Association of Canada, Short Course Notes, v.12. p. 115–151.

- Clayton, R.N., and Mayeda, T.K., 1963, The use of bromine pentafluoride in the extraction of oxygen from oxides and silicates for isotopic analysis: *Geochimica et Cosmochimica Acta*, v. 27, p. 43–52.
- Cormier, C.F.M., Barr, S.M., and Dunning, G.R., 1995, Geological setting and petrochemistry of early Middle Devonian volcanic and gabbroic rocks in the Guysborough area, Nova Scotia: *Atlantic Geology*, v. 31, p. 153–166.
- Cullers, R.L., and Graf, J.L., 1984, Rare earth elements in igneous rocks of the continental crust: intermediate to silicic rocks – ore petrogenesis: *Rare Earth Element Geochemistry*, London, Elsevier, p. 275–316.
- Cuney, M., 2009, The extreme diversity of uranium deposits: *Mineralium Deposita*, v. 44, p. 3–9.
- Cuney, M., and Kyser, K. (*Editors*), 2009, Recent and not-so-recent developments in uranium deposits and implications for exploration: *Mineralogical Association of Canada, Short Course Series*, v. 39, 257 p.
- Dahlkamp, F.J., 1993, *Uranium ore deposits*, Springer-Verlag, Heidelberg, 460 p.
- Davidson, J.P., Morgan, D.J., Charlier, B.L.A., Harlou, R., and Hora, J.M., 2007, Microsampling and isotopic analysis of igneous rocks: Implications for the study of magmatic systems: *Annual Review of Earth and Planetary Sciences*, v. 35, p. 273–311.
- Dawood, Y.H., Abd El-Naby, H.H., and Sharafeldin, A.A., 2004, Influence of the alteration processes on the origin of uranium and europium anomalies in trachyte, central Eastern Desert, Egypt: *Journal of Geological Exploration*, v. 88, p. 15–27.
- Dostal, J., and Chatterjee, A.K., 1995, Origin of topaz-bearing and related peraluminous granites of late Devonian Davis Lake pluton, Nova Scotia, Canada: *Chemical Geology*, v. 123, p. 67–88.
- Dostal, J., Dupuy, C., and Keppie, J.D., 1983a, Uranium and thorium in Paleozoic rhyolites of Nova Scotia: *Canadian Journal of Earth Sciences*, v. 20, p. 266–274.
- Dostal, J., Keppie, J.D., and Dupuy, C., 1983b, Petrology and geochemistry of Devonian-Carboniferous volcanic rocks in Nova Scotia: *Maritime Sediments and Atlantic Geology*, v. 19, p. 59–71.
- Douce, A.E.P., 1999, What do experiments tell us about the relative contributions of crust and mantle to the origin of granitic magmas?: *Geological Society, London, Special Publications*, v. 168, p. 55–75.

Dunning, G.R., Barr, S.M., Giles, P.S., McGregor, D.G., Pe-Piper, G., and Piper, D.J.W., 2002, Chronology of Devonian to early Carboniferous rifting and igneous activity in southern Magdalen Basin based on U–Pb (zircon) dating: *Canadian Journal of Earth Sciences*, v. 39, p. 1219–1237.

Dupuy, C., and Dostal, J., 1983, Uranium and thorium in Paleozoic basalts of Nova Scotia: *Bulletin of Volcanology*, v. 46, p. 125–133.

Eby, G.N., 1992, Chemical subdivision of the A-type granitoids: petrogenetic and tectonic implications: *Geology*, v. 20, p. 640–644.

Elhlou, S., Belousova, E., Griffin, W.L., Pearson, N.J., and O'Reilly, S.Y., 2006, Trace element and isotopic composition of GJ-red zircon standard by laser ablation: *Geochimica Cosmochimica Acta*, v. 70, Supplement 1, p. A158.

Finch, W., Feng, S., Zuyi, C., and McCammon, R.B., 1993, Descriptive models of major uranium deposits in China: *Natural Resources Research*, v. 2, p. 39–48.

Flynn, R.T., and Burnham, C.W., 1978, An experimental determination of rare earth partition coefficients between a chloride-containing vapor phase and silicate melts: *Geochimica Cosmochimica Acta*, v. 42, p. 679–684.

Forbes, P., 1989, Roles des structures sedimentaires et tectoniques, du volcanisme alcalin regional et des fluids diagenetiques hydrothermaux pour la Fm des mineralizations a U-Zr-Zn-V-Mo d'Akouta (Niger): *Geol. Geochim. Uranium Mem. Nancy.*, v. 17, 376 p.

Forbes, P., Pagel, M., Pacquet, A., Chantret, F., and Oumarou, J., 1984, Volcanic components in the Akouta uranium deposit (Niger): *Comptes Rendus de l' Academie des Sciences Serie II*, v. 298, p. 647–650.

Fyffe, L.R., and Barr, S.M., 1986, Petrochemistry and tectonic significance of Carboniferous volcanic rocks in New Brunswick: *Canadian Journal of Earth Sciences*, v. 23, p. 1243–1256.

Gandhi, S.S., and Bell, R.T., 1996, Volcanic-associated uranium, *in* Eckstrand, O.R., Sinclair, W.D., and Thorpe, R.I., eds., *Geology of Canadian Mineral Deposit Types: Geological Survey of Canada*, v. 8, p. 269–276.

Gemmel, D.E., 1975, Carboniferous volcanic and sedimentary rocks of the Mount Pleasant Caldera and Hoyt Appendage: Unpublished M.Sc. thesis, Fredericton, Canada, The University of New Brunswick, 110 p.

- Gibling, M.R., Culshaw, N., Rygel, M.C, and Pasucci, V., 2009, The Maritimes Basin of Atlantic Canada: Basin creation and destruction in the collision zone of Pangea: *Sedimentary Basins of the World*, v. 5, p. 211–238.
- Goodell, P.C., 1981. Geology of the Peña Blanca uranium deposits, Chihuahua, Mexico, *in* Goodell, P.C., and Waters, A.C., eds., *Uranium in Volcanic and Volcaniclastic Rocks: American Association of Petroleum Geologists, Studies in Geology*, v. 13, p. 275–291.
- Goodell, P.C., Trentham, R.C., 1980, Experimental leaching of uranium from tuffaceous rocks. Department Of Energy; Department of Geological Sciences, University of Texas, El Paso, Subcontract 78-164-E, p. 113.
- Gorton, M.P., and Schandl, E.S., 2000, From continents to island arcs: a geochemical index of tectonic setting for arc-related and within-plate felsic to intermediate volcanic rocks: *Canadian Mineralogist*, v. 38, p. 1065–1073.
- Gray, T.R., Hanley, J.J., Dostal, J., and Guillong, M., in press, 2010. Magmatic enrichment of uranium, thorium and rare earth elements in late Paleozoic rhyolites of southern New Brunswick, Canada: evidence from silicate melt inclusions: *Economic Geology*.
- Griffin, W.L., Pearson, N.J., Belousova, E., Jackson, S.E., van Achterberg, E., O'Reilly, S.Y., and Shee, S.R., 2000, The Hf isotope composition of cratonic mantle: LAM-MC-ICPMS analysis of zircon megacrysts in kimberlites: *Geochimica et Cosmochimica Acta*, v. 64, p. 133–147.
- Griffin, W.L., Pearson, N.J., Belousova, E.A., and Saeed, A., 2006, Comment: Hf-isotope heterogeneity in zircon 91500: *Chemical Geology*, v. 233, p. 358–363.
- Guillong, M.M., Maier, D.L., Allan, M.M., Heinrich, C.A., and Yardley, B.W.D., 2008, Appendix A6: SILLS: a MATLAB based program for the reduction of laser ablation ICPMS data of homogeneous materials and inclusions. In: Sylvester P (ed) *Laser Ablation ICP-MS in the Earth Sciences: Current Practices and Outstanding Issues*. Mineralogical Association of Canada Short Course Series, v. 40, 328-333.
- Günther, D., Frischknecht, R., Heinrich, C.A., and Kahlert, H J., 1997, Capabilities of an Argon Fluoride 193 nm excimer laser for laser ablation inductively coupled plasma mass spectrometry microanalysis of geological materials: *Journal of Analytical Atomic Spectrometry*, v. 12, p. 939–944.
- Halter W.E., Pettke T., Heinrich C.A., and Rothen-Rutishauser B., 2002, Major to trace element analysis of melt inclusions by laser ablation ICP-MS: Methods of quantification: *Chemical Geology*, v. 183, p. 63–86.

- Harrison, T.M., Watson, E.B., 1984, The behavior of apatite during crustal anatexis: equilibrium and kinetic considerations: *Geochimica Cosmochimica Acta*, v. 48, p. 1467–1477
- Heier, K.S., Compston, W., and McDougall, I., 1965, Thorium and uranium concentrations, and the isotopic composition of strontium in the differentiated Tasmanian dolerites: *Geochimica et Cosmochimica Acta*, v.29, p. 643–659.
- Heinrich, C.A., Pettke, T., Halter, W.E., Aigner-Torres, M., Audétat, A., Günther, D., Hattendorf, B., Bleiner, D., Guillong, M., and Horn, I., 2003, Quantitative multi-element analysis of minerals, fluid and melt inclusions by laser-ablation inductively-coupled-plasma mass spectrometry: *Geochimica et Cosmochimica Acta*, v. 67, p. 3473–3497.
- Hildreth, E.W., 1979, The Bishop Tuff: evidence for the origin of compositional zonation in silicic magma chambers: *Geological Society of America Special Paper*, v. 180, p. 43–75.
- Hoffman, E.L., 1992, Instrumental Neutron Activation in Geoanalysis. *Journal of Geochemical Exploration*: v. 44, p. 297–319.
- Huppert, H.E., and Sparks, R.S.J., 1988, The generation of granitic magmas by intrusion of basalt into continental crust: *Journal of Petrology*, v. 29, p. 599–624.
- International Atomic Energy Agency, 2009, World Distribution of Uranium Deposits (UDEPO) with Uranium Deposit Classification: Vienna, Austria, p. 1–126.
- Jackson, S.E., Pearson, N.J., Griffin, W.L., and Belousova, E.A., 2004, The application of laser ablation-inductively coupled plasma–mass spectrometry to in situ U–Pb zircon geochronology: *Chemical Geology*, v. 211, p. 47–69.
- Johnson, S.C., and Gardiner, W.W., 2003, Conceptual models and potential gold environments in Carboniferous rocks of New Brunswick. *in* Carroll, B.M.D. (ed), Abstracts 2003: 28th annual Review of Activities, New Brunswick Department of Natural Resources, Minerals, Policy and Planning Division, Information Circular 2003-1, 23 p.
- Johnson, S.C., 2008, Bedrock geology of Pre-Carboniferous basement inliers in the Coal Creek, Canaan River, and Thorne Brook areas, southeastern New Brunswick Platform. *in* Merlini, S.A.S. (ed), Abstracts 2008: Exploration Mining and Petroleum New Brunswick, New Brunswick Department of Natural Resources, Minerals, Policy and Planning Division, Information Circular 2008-1, 39 p.

Keppie, J.D., and Krogh, T.E., 1999, U-Pb geochronology of Devonian granites in the Meguma Terrane of Nova Scotia, Canada: evidence for hotspot melting of a Neoproterozoic source: *Journal of Geology*, v. 107, p. 555–568.

Keppler, H., and Wyllie, P.J., 1990, Role of fluids in transport and fractionation of uranium and thorium in magmatic processes: *Nature*, v. 348, p. 531–533.

Kerrick, R., and Fryer, B.J., 1979, Archean precious-metal hydrothermal systems, Dome mine, Abitibi greenstone belt II. REE and oxygen isotope relations: *Canadian Journal of Earth Science*, v. 16, p. 440–458.

Kooiman, G.J.A., Mcleod, M.J, and Sinclair, W.D., 1986., Porphyry tungsten-molybdenum ore bodies, polymetallic veins and replacement bodies, and tin-bearing zones in the Fire Tower Zone, Mount Pleasant, New Brunswick: *Economic Geology*, v. 81, p. 1356–73.

Kuan, S., 1970, The geology of the Carboniferous volcanic rocks of New Brunswick: Unpublished M.Sc. thesis, Fredericton, Canada, The University of New Brunswick, 147 p.

Larsen, E.S. Jr., and Phair, G., 1954, The distribution of uranium and thorium in igneous rocks, *in* Faul, H. ed., *Nuclear Geology*, New York, John Wiley and Sons, p. 75–89.

Larsen, E.S., Jr., 1961, Distribution of uranium in rocks and minerals of Mesozoic batholiths in western United States: *U.S. Geological Survey Bulletin 1070-C*, p. 63–103.

LaFleche, M.R., Camire, G., and Jenner, G.A., 1998, Geochemistry of post-Acadian, Carboniferous continental intraplate basalts from the Maritimes Basin, Magdalen Islands, Quebec, Canada: *Chemical Geology*, v. 148, p. 115–136.

Le Maitre, R.W., Bateman, P., Dudek, A., Keller, J., Lameyre, J., Le Bas, M.J., Sabine, P.A., Schmid, R., Sorensen, H., Streckeisen, A., Wooley, A.R., and Zanettin, B., 1989, *A Classification of Igneous Rocks and Glossary of Terms*, Blackwell, Oxford, 193 p.

Locardi, 1985, Uranium in acidic volcanic environments, *in* *Uranium Deposits in Volcanic Rocks*, Proceedings of a Technical Committee Meeting, El Paso, Texas, April 1984, International Atomic Energy Agency, p. 17–27.

London, D., Hervig, R.L., and Morgan, G.B., 1988, Melt-vapor solubilities and elemental partitioning in peraluminous granite-pegmatite systems: experimental results with Macusani glass at 200 MPa: *Contributions to Mineralogy and Petrology*, v.99, p. 360–373.

Longerich, H.P., Jackson, S.E., and Günther, D., 1996, Laser ablation inductively coupled

plasma mass spectrometric transient signal data acquisition and analyte concentration calculation: *Journal of Analytical Atomic Spectrometry*, v. 11, p. 899–904.

Longstaffe, F.J., Smith, T.E., and Muehlenbachs, K., 1980, Oxygen isotope evidence for the genesis of Upper Paleozoic granitoids from southwestern Nova Scotia. *Canadian Journal of Earth Sciences*, v. 17, p. 132–141.

Lowenstern, J.B., 2003, Melt inclusions come of age: volatiles, volcanoes, and Sorby's Legacy, in De Vivo, B., and Bodnar, R.J., eds., *Melt Inclusions in Volcanic Systems: Methods, Applications and Problems. Developments in Volcanology*: Amsterdam, Elsevier Press, v. 5, p. 1–21.

Lu, F., Anderson, A.T., and Davis, A.M., 1995. Diffusional gradients at the crystal/melt interface and their effect on the composition of melt inclusions: *Journal of Geology*, v. 103, p. 591–597.

Mahood, G.A., and Hildreth, E.W., 1983, Large partition coefficients for trace elements in high-silica rhyolites: *Geochimica et Cosmochimica Acta*, v. 47, p. 11-30.

Marillier, F., and Verhoef, J., 1989, Crustal thickness under the Gulf of St. Lawrence, northern Appalachians, from gravity and deep seismic data: *Canadian Journal of Earth Sciences*, v. 26, p. 1517–1532.

McCutcheon, S.R., 1990, The Late Devonian Mount Pleasant Caldera complex stratigraphy, mineralogy, geochemistry and geological setting of a Sn-W deposit in southwestern New Brunswick, Unpublished Ph.D. thesis, Dalhousie University, Halifax, Nova Scotia, 609 p.

McCutcheon, S.R., Anderson, H.E., and Robinson, P.T., 1997, Stratigraphy and eruptive history of the Late Devonian Mount Pleasant Caldera Complex, *Canadian Appalachians: Geological Magazine*, v. 134, p. 17–36.

McLeod, M., and Johnson, S., 2007, Exploration activity and setting of uranium in New Brunswick: Québec Exploration, Chateau Frontenac, 26–29 November 2007 (http://www.quebecexploration.qc.ca/2007/pdf/session_05/S5-08_mcleod.pdf).

McNamara, H.C., 1978, West Mill Settlement, Rio Tinto Canadian Exploration Ltd, Open-File Report 470336.

Mineyev, D.A., 1963, Geochemical Differentiation of the rare earths: *Geokhimiya*, v. 12, p. 1082–1100.

Mironov, Y.B., Filonenko, Y.D., Solov'ev, N.S., Petrov, V.A., Golovin, V.A., and

- Strel'tsov, V.A., 1993, Lead-zinc, uranium and fluorite deposits in the Dornot volcano-tectonic structure (East Mongolia): *Geological Ore Deposits*, v. 35, p. 31–43.
- Murphy, J.B., van Staal, C.R., and Keppie, J.D., 1999, Middle to Late Paleozoic Acadian Orogeny in the northern Appalachians: a Laramide-style plume-modified orogeny?: *Geology*, v.27, p. 653–656.
- Musselwhite, D.S., DePaelo, D.J., and McCurry, M., 1989, The evolution of a silicic magma system: isotopic and chemical evidence from the Woods Mountain volcanic center, eastern California: *Contributions to Mineralogy and Petrology*, v. 101, p.19–29.
- Nash, J. T., 2010, *Volcanogenic Uranium Deposits: Geology, Geochemical Processes, and Criteria for Resource Assessment*: US Geological Survey, Open-File Report 2010–1001, p. 99.
- Naumov, V.B., Kovalenko, V.I., Clocchiatti, R., and Solovova, I.P., 1984, Crystallization parameters and phase compositions for melt inclusions in ongorhyolite quartz: *Geochemistry International*, v. 4, p. 19–32.
- Neuerburg, C.J., 1956, Uranium in igneous rocks of the United States, *in* Page, L.R., Stocking, H.E., and Smith, H.B., compilers, *Contributions to the geology of uranium and thorium*: U.S. Geological Survey Professional Paper 300, 55–64.
- New Brunswick Department of Natural Resources, 2010, *New Brunswick Bedrock Lexicon*, <http://dnre-mrne.gnb.ca/Lexicon> (accessed April 2010).
- Pagel, M., Cavellec, S., Forbes, P., Gerbaud, O., Vergely, P., and Wagani, I., 2005, Uranium deposits in the Arlit area (Niger). *in* Bierlein, M.P., and Mao, J. (eds), *Mineral deposit research, Meeting the global challenge*, Proceedings of the 8th SGA Meeting in Beijing, China, p. 303–305.
- Pajari, G.E., 1973, The Harvey volcanic area, *in* Rast, N., ed., *Geology of New Brunswick, Field Guide to Excursions*, New England Intercollegiate Geological Conference, p. 119–123.
- Payette, C., and Martin, R.F., 1986a, The Harvey volcanic suite in New Brunswick. I. Inclusions of magma in quartz phenocrysts: *Canadian Mineralogist*, v. 24, p. 557–570.
- Payette, C., and Martin, R.F., 1986b, The Harvey volcanic suite in New Brunswick. II. Postmagmatic adjustments in the mineralogy and bulk composition of high fluorine rhyolite: *Canadian Mineralogist*, v. 24, p. 571–584.

Pearce, J.A., Harris, N.B.W., and Tindle, A.G. 1984, Trace element discrimination diagrams for tectonic interpretation of granitic rocks: *Journal of Petrology*, v. 25, 956–983.

Peccerillo, A., Barberio, M.R., Yirgu, G., Ayalew, D., Barbieri, M., and Wu, T.W., 2003, Relationships between mafic and peralkaline silicic magmatism in continental rift settings: a petrological, geochemical, and isotopic study of the Gedemsa Volcano, central Ethiopian Rift: *Journal of Petrology*, v. 44, p. 2003–2032.

Peiffert, C., Nguyen Trung, C., and Cuney, M., 1994, Uranium in granitic magmas. Part II: experimental determination of uranium solubility and fluid–melt partition coefficients in the UO_2 –haplogranite– H_2O –halides system at 720–770°C, 200 MPa: *Geochimica Cosmochimica Acta*, v. 60, p. 1515–1529.

Pe-Piper, G., and Piper, D.J.W., 1998, Geochemical evolution of Devonian-Carboniferous igneous rocks of the Magdalen basin, Eastern Canada: Pb- and Nd-isotope evidence for mantle and lower crustal sources: *Canadian Journal of Earth Science*, v. 35, p. 201–221.

Pettke, T., Halter, W.E., Webster, J.D., Algner-Torres, M., and Heinrich, C.A., 2004, Accurate quantification of melt inclusion chemistry by LA-ICPMS: a comparison with EMP and SIMS and advantages and possible limitations of these methods: *Lithos*, v. 78, p. 333–361.

Pichavant, M., 1981, An experimental study of the effect of boron on a water saturated haplogranite at 1 Kbar vapour pressure: *Contributions to Mineralogy and Petrology*, v. 76, p. 430–439.

Plant, J., Simpson, P.R., Smith, B., and Windley, B.F., 1999, Uranium ore deposits: products of the radioactive earth, *in* Burns, P.C., and Finch, R. (eds), *Uranium–Mineralogy, geochemistry, and the environment*: Mineralogical Society of America, *Reviews in Mineralogy*, v. 38, p. 255–320.

Potter, J., Longstaffe, F.J., and Barr, S.M., 2008, Regional ^{18}O -depletion of Neoproterozoic igneous rocks from Avalonia, Cape Breton Island and southern New Brunswick, Canada: *Geological Society of America Bulletin*, v. 120, p. 347–367.

Pouliot, G., Barondeau, B., Suave, P., and Davis, M., 1978, Distribution of alteration minerals and metals in the fire tower zone at Brunswick Tin Mines LTD., Mount Pleasant area, New Brunswick: *Canadian Mineralogist*, v. 16, p. 223–237.

Preto, V.A., 1978, Setting and genesis of uranium mineralization at Rexpar: *The Canadian Institute of Mining and Metallurgy Bulletin*, v. 71, p. 82–88.

- Roliff, W.A., 1962. The Maritime Carboniferous basin of eastern Canada, Geological Association of Canada, Proceedings 14, p. 21–41.
- Rudnick, R.L., and Fountain, D.M. 1995, Reviews of Geophysics.: v. 33, p. 267–309.
- Rudnick, R.L. and Gao, S., 2004, Composition of the Continental Crust, *in* Holland, H.D. and Turekian, K.K., eds., Treatise on Geochemistry: Amsterdam, Elsevier, v. 3, p. 1–64.
- Ruitenbergh, A.A., McCutcheon, S.R., Venugopal, D.V., and Pierce, G.A., 1977, Mineralization related to Post-Acadian tectonism in southern New Brunswick: Geoscience Canada, v. 4, p. 13–22.
- Rytuba, J.J., and Glazman, R.K., 1979, Relation of mercury, uranium and lithium deposits of the McDermitt caldera complex, Nevada-Oregon, *in* Papers on mineral deposits of western North America: Nevada Bureau of Mines and Geology, report 33, p. 109–118.
- Samson, S.D., Barr, S.M., and White, C.E., 2000, Nd isotopic characteristics of terranes within the Avalon Zone, southern New Brunswick: Canadian Journal of Earth Sciences, v. 37, p. 1039–1052.
- Schiano, P., 2003, Primitive mantle magmas recorded as silicate melt inclusions in igneous minerals: Earth Science Reviews, v. 63, p. 121–144.
- Shand, S.J., 1951, Eruptive rocks; their genesis, composition, classification, and their relation to ore-deposits, 4th edition, John Wiley and Sons, New York, 488 p.
- Sinclair, W.D., and Kooiman, G.J.A., 1990. The Mount Pleasant tungsten-molybdenum and tin deposits. *In* Boyle, D.R. (ed.), Mineral deposits of New Brunswick and Nova Scotia, 8th IAGOD Symposium field trip guidebook, Geological Survey of Canada, Open File 2157, p. 78–87.
- Sinclair, W.D., Kooiman, G.J.A., Martin, D.A., and Kjarsgaard, I.M., 2006, Geology, geochemistry and mineralogy of indium resources at Mount Pleasant, New Brunswick, Canada, Ore Geology Reviews. v. 28, p. 123-145.
- Smith, E.A. (compiler), 2007, Bedrock geology of the Chipman Area (NTS 21 I/04). Sunbury and Queens Counties, New Brunswick: Department of Natural Resources: Mineral, Policy and Planning Division., Plate 2007-50, Scale 1:50 000.
- Sommer, M.A., 1977, Volatiles H₂O, CO₂ and CO in silicate melt inclusions in quartz phenocrysts from the rhyolitic Bandelier air-fall and ash-flow tuff, New Mexico: Journal of Geology, v. 85, p. 423–432.

Stix, J., Gorton, M.P., 1990, Variations in trace-element partition-coefficients in sanidine in the Cerro Toledo rhyolite, Jemez Mountains, New-Mexico - Effects of Composition, Temperature, and Volatiles: *Geochimica et Cosmochimica Acta*, v. 54, p. 2697–2708.

St. Peter, C. J., 1997, Bedrock geology of Chipman – Canaan River map area (parts of NTS 21 I/04 and 21 H/13), Sunbury, Queens and Kings counties, New Brunswick. New Brunswick Department of Natural Resources and Energy, Mineral Resources, Plate 97-34, Scale 1:20,000.

St. Peter, C.J., 2002 (unpublished), Bedrock Nomenclature of New Brunswick: Cumberland Hill Formation (Mabou Group). *in* New Brunswick Natural Resources., <http://dnre-mrne.gnb.ca/Lexicon> (accessed April 2010).

St. Peter C.J., and Johnson S.C., 2009, Stratigraphy and structural history of the late Paleozoic Maritimes Basin in southeastern New Brunswick, Canada: New Brunswick Department of Natural Resources; Minerals, Policy and Planning Division, Memoir 3, 348 p.

Streck, M.J., Grunder, A.L., 1997, Compositional gradients and gaps in high-silica rhyolites of the Rattlesnake Tuff, Oregon: *Journal of Petrology*, v. 38, p. 133–163.

Strong, D.F., 1980, Granitoid rocks and associated mineral deposits of eastern Canada and western Europe. *in* The Continental Crust and its Mineral Deposits: Geological Association of Canada, Special Paper, v. 20, 741–769.

Sun, S.S., and McDonough, W.F., 1989, Chemical and isotopic systematics of oceanic basalts: implications for mantle composition and processes, *in* Saunders, A.D., and Norry, M.J., Magmatism in the Ocean Basins: Geological Society London, Special Publication v. 42, p. 313–345.

Swinden, S., Jenner, G.A., Fryer, B.J., Hertogen, J., and Roddick, J.C., 1990., Petrogenesis and paleotectonic history of the Wild Bight Group, an Ordovician rifted island arc in central Newfoundland: *Contributions to Mineralogy and Petrology*, v. 105, p. 219–241.

Tanaka, T., Togashi, S., Kamioka, H., Amakawa, H., Kagami, H., Hamamoto, T., Yuhara, M., Orihashi, Y., Yoneda, S., Shimizu, H., Kunimaru, T., Takahashi, K., Yanagi, T., Nakano, T., Fujimaki, H., Shinjo, R., Asahara, Y., Tanimizu, M., and Dragusanu, C., 2000, JNdi-1: a Neodymium isotopic reference in consistency with La Jolla Neodymium: *Chemical Geology*, v. 168, p. 279–281.

Taylor, R.P., and Fryer, B.J., 1980, Multiple-stage hydrothermal alteration in porphyry copper systems in northern Turkey: the temporal interplay of potassic, propylitic and

phyllitic fluids: *Canadian Journal of Earth Science*, v. 17, p. 901–926.

Taylor, H.P. and Jr., Epstein, S., 1962, Relationship between O^{18}/O^{16} ratios in coexisting minerals of igneous and meta morphic rocks: Part 1: Principles and experimental Results: *Geological Society of America Bulletin*, v. 73, p. 461–480.

Taylor, H.P. Jr., and Sheppard, S.M.F., 1986, Igneous rocks: I. Processes of isotopic fractionation and isotope systematics. *Reviews in Mineralogy and Geochemistry*. v. 16, p. 227–271.

Taylor, R.P., and Fryer, B.J.. 1980, Multiple-stage hydrothermal alteration in porphyry copper systems in northern Turkey: the temporal interplay of potassic, propylitic and phyllitic fluids: *Canadian Journal of Earth Science*, v. 17, p. 901–926.

Taylor, R.P., Strong, D.F., and Fryer, B.J., 1981, Volatile control of contrasting trace element distributions in peralkaline granite and volcanic rocks: *Contributions to Mineralogy and Petrology*, v. 77, p. 267–271.

Thomas, M.D., and Kiss, F., 2005, Geological interpretation of the 2004 Marri town aeromagnetic survey, Southeastern New Brunswick, Geological Survey of Canada, Open File 4953, New Brunswick Department of Natural Resources, Minerals, Policy and Planning Division, Plate 2005-21D, Scale 1:125 000.

Treuil, M., 1985, A global geochemical model of uranium distribution and concentration in volcanic rock series, *in* Uranium Deposits in Volcanic Rocks, Proceedings of a Technical Committee Meeting, El Paso, Texas, April 1984, International Atomic Energy Agency, p. 53–68.

Tucker, R.D., Bradley, D.C., Ver Straeten, C.A., Harris, A.G., Ebert, J.R., and McCutcheon, S.R., 1998, New U-Pb zircon ages and the duration and division of Devonian time: *Earth and Planetary Science Letters*, v. 158, p. 175–186.

Van de Poll, H.W., 1972, Stratigraphy and economic geology of the Carboniferous basins in the Maritimes provinces: *International Geology Congress 24th*, Guidebook Excursion, A60.

Webster, J.D., Holloway, J.R., and Hervig, R.L., 1989, Partitioning of lithophile trace elements between H_2O and $H_2O + CO_2$ fluids and topaz rhyolite melt: *Economic Geology*. v. 84, p. 116–134.

Webster, J.D., Congdon, R.D., and Lyons, P.C., 1995, Determining pre-eruptive compositions of late Paleozoic magma from kaolinized volcanic ashes: analysis of glass

- inclusions in quartz microphenocrysts from Tonsteins: *Geochimica Cosmochimica Acta*, v. 59, p. 711–720.
- White, A.J.R., and Chappell, B.W., 1977, Ultrametamorphism and granite genesis: *Tectonophysics*, v. 43, p. 7–22.
- White, J.C., Benker, S.C., Ren, M., Urbanczyk, K.M., and Corrick, D.W., 2006, Petrogenesis and tectonic setting of the peralkaline Pine Canyon caldera, Trans-Pecos Texas, USA: *Lithos*, v.91, p. 74–94.
- Whitfield, J.M., Rogers, J.J.W., Adams, J.A.S., 1959, The relationship between the petrology and the thorium and uranium contents of some granitic rocks: *Geochimica Cosmochimica Acta*: v.17, p. 248–271.
- Wiedenbeck, M., Allé, P., Corfu, F., Griffin, W.L., Meier, M., Oberli, F., Von Quadt, A., Roddick, J.C., and Spiegel, W., 1995, Three natural zircon standards for U–Th–Pb, Lu–Hf, trace element and REE analyses: *Geostandards Newsletter*, v. 19, p. 1–23.
- Williams, E.P., 1974, Geology and petroleum possibilities in and around Gulf of St. Lawrence: *American Association of Petroleum Geologists, Bulletin* 58, v.6, p. 1137–1155.
- Winchester, J.A., and Floyd, P.A., 1977, Geochemical discrimination of different magma series and their differentiation products using immobile elements: *Chemical Geology*, v.20, p. 325–343.
- Woodhead, J.D., and Hergt, J.M., 2005, A Preliminary Appraisal of Seven Natural Zircon Reference Materials for In Situ Hf Isotope Determination: *Geostandards and Geoanalytical Research*, v. 29, p. 183–195.
- Workman, R.K., and Hart, S.R., 2005, Major and trace element composition of the depleted MORB mantle (DMM): *Earth and Planetary Science Letters*, v. 231, p. 53–72.
- Yang, X., Lentz, D.R., and McCutcheon, S.R., 2003, Petrochemical evolution of subvolcanic granitoid intrusions within the Late Devonian Mount Pleasant Caldera, southwestern New Brunswick, Canada: comparison of Au versus Sn–W–Mo–polymetallic mineralization systems: *Atlantic Geology*, v. 39, p. 97–121.
- Zajacz, Z., Halter, W.E., Pettke, T., and Guillong, M., 2008, Determination of fluid/melt partition coefficients by LA-ICPMS analysis of co-existing fluid and silicate melt inclusions: Controls on element partitioning: *Geochimica Cosmochimica Acta*, v. 72, p. 2169–2197.

CHAPTER 8: APPENDIX

Additional figures and tables not submitted for publication can be found in section below with all figures and table therein following similar format to the general style of peer-reviewed journals.

8.1. Additional Figures

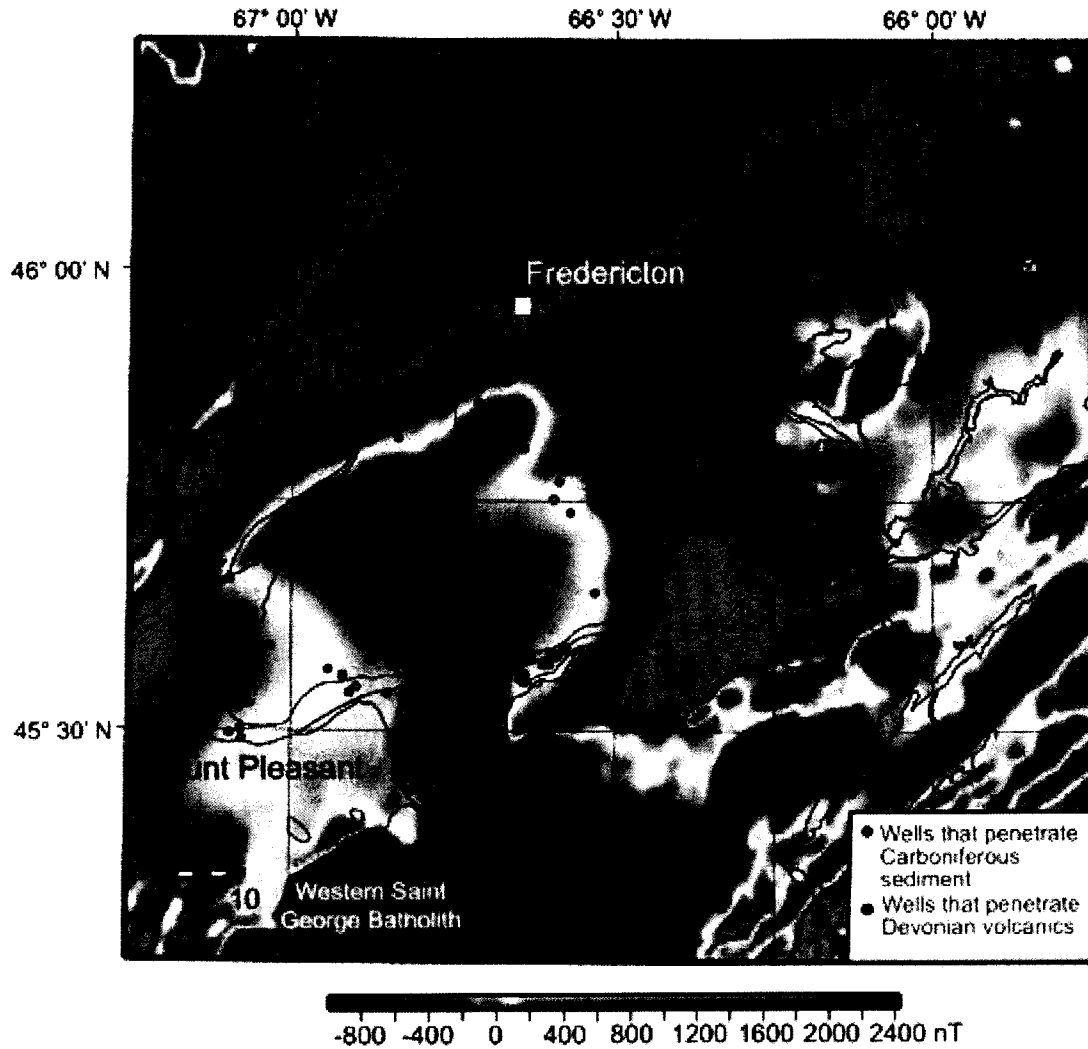


Figure 8.1.1. Residual total field magnetic survey of southwestern New Brunswick using 200m grid spacing. Data from Natural Resources Canada/ Geological Survey of Canada. Harvey and Mount Pleasant outcrop areas have associated, strong positive anomalies, as do the plutons to the south (i.e. Western Saint George Batholith and related, smaller plutons). Continuous positive anomalies between Harvey and Mount Pleasant

could hypothetically be caused by 1) Additional volcanic centers 2) Buried plutons beneath Carboniferous cover.

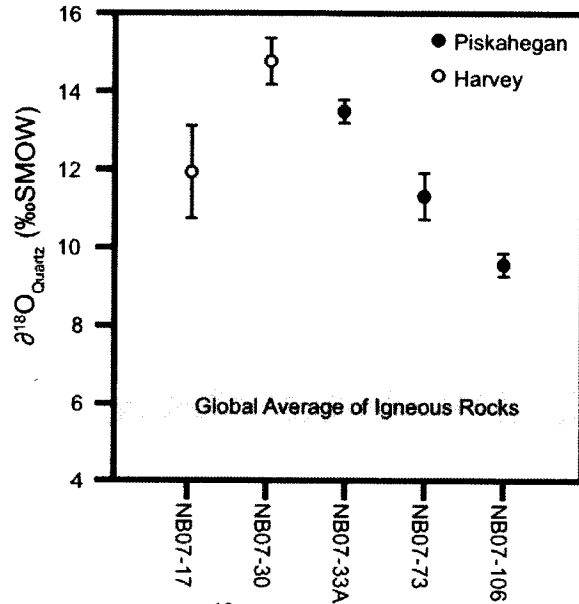


Figure. 8.1.2. $\delta^{18}\text{O}_{\text{Quartz}}$ (‰ SMOW) isotopic values of Harvey and Piskahegan compared to the global average of igneous rocks. Error bars represent 2σ of error.

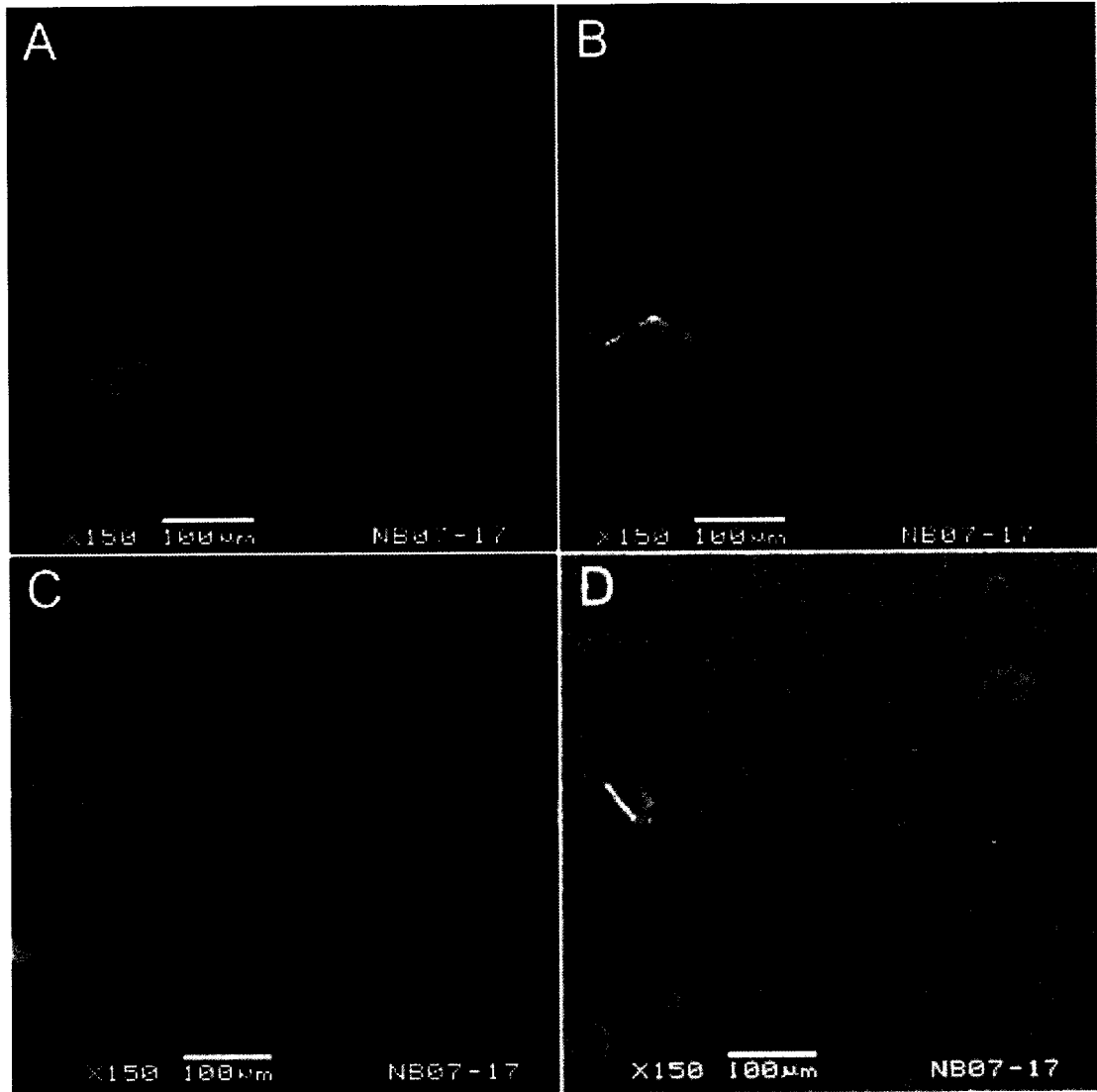


Figure 8.1.3. Cathode Luminescence (b, d) and Backscatter images (a, c) of zircons from Sample NB07-17.

8.2. Additional Tables

Formation	Unit	Sample	Coordinates	Description
Harvey	Cherry Hill	NB07-01	45 44' 02.3" N / 67 00' 40.5" W	pink flow banded (weak) ignimbrite, feldspar-phyric, cm size clasts
		NB07-02	45 44' 02.5" N / 67 00' 40.6" W	pink flow banded (weak) ignimbrite, feldspar-phyric, cm size clasts
		NB07-03	45 44' 03.8" N / 67 00' 41.9" W	pink flow banded (weak) ignimbrite, feldspar-phyric, cm size clasts
		NB07-04	45 44' 02.5" N / 67 00' 40.6" W	pink flow banded (weak) ignimbrite, feldspar-phyric, cm size clasts
		NB07-05	45 44' 02.3" N / 67 00' 40.5" W	pink flow banded (weak) ignimbrite, feldspar-phyric, cm size clasts
		NB07-06	45 44' 02.3" N / 67 00' 40.5" W	pink flow banded (weak) ignimbrite, feldspar-phyric, cm size clasts
		NB07-07	45 43' 57.4" N / 67 01' 07.4" W	ignimbrite and underlying red sediments/tuff, basal contact of ignimbrite exposed
		NB07-08	45 43' 57.4" N / 67 01' 07.4" W	ignimbrite and underlying red sediments/tuff, basal contact of ignimbrite exposed
		NB07-09	45 43' 58.1" N / 67 01' 05.5" W	pink-orange very fine grained rhyolite from projection at base
		NB07-10	46 43' 58.1" N / 67 01' 05.5" W	pink-orange very fine grained rhyolite from projection at base
		NB07-11	46 43' 58.1" N / 67 01' 05.5" W	pink-orange very fine grained rhyolite from projection at base
		NB07-12	46 43' 58.1" N / 67 01' 05.5" W	pink-orange very fine grained rhyolite from projection at base
		NB07-13	45 43' 59.5" N / 67 01' 01.7" W	red volcanogenic sediment
		NB07-14	45 43' 59.5" N / 67 01' 01.7" W	red volcanogenic sediment
		NB07-15	45 43' 59.3" N / 67 00' 51.8" W	pink ignimbrite with less feldspar
		NB07-16	45 43' 56.4" N / 67 00' 38.6" W	dark pink, weakly flow-banded rhyolite
		NB07-17	45 43' 51.4" N / 67 00' 30.5" W	quartz-feldspar porphyry, pink matrix, quartz and feldspars
		NB07-18	46 43' 51.4" N / 67 00' 30.5" W	extrusive rhyolite
		NB07-19	45 43' 51.4" N / 67 00' 29.4" W	rhyolite clasts up to 2-4 cm, less porphyritic (also other, smaller clasts (greenish) rare very fine grained)
		NB07-20	45 43' 51.4" N / 67 00' 29.0" W	rhyolite clasts up to 2-4 cm, less porphyritic (also other, smaller clasts (greenish) rare very fine grained)
	Harvey Mountain	NB07-21	45 44' 10.2" N / 66 59' 12.6" W	pink-white rhyolite, very fine grained and coarse grained
		NB07-21B	45 44' 10.2" N / 66 59' 12.6" W	pink-white rhyolite, very fine grained and coarse grained
		NB07-22	46 43' 33.7" N / 67 00' 31.3" W	rhyolite
		NB07-23	45 43' 32.7" N / 67 00' 30.6" W	flow banded
		NB07-24	46 43' 32.7" N / 67 00' 30.6" W	more massive
		NB07-25	45 40' 08.9" N / 67 05' 43.5" W	laminated rhyolite
		NB07-31	45 33' 21.5" N / 66 41' 48.0" W	rhyolite
	York Mills	NB07-26	45 40' 09.0" N / 67 05' 43.3" W	brecciated
		NB07-27	45 40' 09.4" N / 67 05' 41.6" W	brecciated
		NB07-28	45 40' 09.3" N / 67 05' 40.4" W	brecciated
		NB07-29	45 40' 03.8" N / 67 05' 45.9" W	outcrop of felsic volcanoclastic conglomerate, sand-pebble-boulder, sized clasts, poorly sorted and bedded, sub rounded to sub angular, one large boulder sized clast
NB07-30		45 42' 46.4" N / 67 01' 38.4" W	weakly flow-banded rhyolite, pinkdark purple-red, flow-banded rhyolite (flow banding nearly vertical), very vuggy, brecciated fracture fills, vugs and fractures filled with: druse quartz (dominant), and silica, barite, and purple and (rare) green fluorite, alteration is extensive, rare: 2.5cm sized basalt (dark grey), amygdaloidal, rounded inclusions	

Table 8.2.1. Sample locations and description of rocks from Harvey and Piskahegan

Formation	Unit	Sample	Coordinates	Description
Pekabegan	Big Seot Mountain	NB07-32A	45 33' 21.5" N / 66 41' 48.0" W	quartz-feldspar porphyry
		NB07-32B	45 33' 21.5" N / 66 41' 48.0" W	quartz-feldspar porphyry
		NB07-32C	45 33' 21.5" N / 66 41' 48.0" W	quartz-feldspar porphyry
		NB07-32D	45 33' 21.5" N / 66 41' 48.0" W	quartz-feldspar porphyry
		NB07-32E	45 33' 21.5" N / 66 41' 48.0" W	quartz-feldspar porphyry
		NB07-32F	45 33' 21.5" N / 66 41' 48.0" W	quartz-feldspar porphyry
		NB07-32G	45 33' 21.5" N / 66 41' 48.0" W	quartz-feldspar porphyry
		NB07-32H	45 33' 21.5" N / 66 41' 48.0" W	quartz-feldspar porphyry
		NB07-32I	45 33' 21.5" N / 66 41' 48.0" W	quartz-feldspar porphyry
		NB07-32J	45 33' 21.5" N / 66 41' 48.0" W	quartz-feldspar porphyry
		NB07-32K	45 33' 21.5" N / 66 41' 48.0" W	quartz-feldspar porphyry
		NB07-32L	45 33' 21.5" N / 66 41' 48.0" W	quartz-feldspar porphyry
		NB07-32M	45 33' 21.5" N / 66 41' 48.0" W	quartz-feldspar porphyry
		NB07-32N	45 33' 20.4" N / 66 41' 43.8" W	quartz-feldspar porphyry
		NB07-32O	45 33' 20.4" N / 66 41' 43.8" W	quartz-feldspar porphyry
		NB07-32P	45 33' 20.4" N / 66 41' 43.8" W	quartz-feldspar porphyry
		NB07-32Q	45 33' 20.4" N / 66 41' 43.8" W	quartz-feldspar porphyry
		NB07-33A	45 32' 39.2" N / 66 42' 16.8" W	feldspar and quartz porphyritic, med. Grey-pink with dark grey-green fine grained mafic inclusions, mid-way, brecciated quartz veins with embedded quartz crystals, clay alteration, more mafic
		NB07-33B	45 32' 39.2" N / 66 42' 16.8" W	feldspar and quartz porphyritic, med. Grey-pink with dark grey-green fine grained mafic inclusions, mid-way, brecciated quartz veins with embedded quartz crystals, clay alteration, more mafic
		NB07-33C	45 32' 39.2" N / 66 42' 16.8" W	feldspar and quartz porphyritic, med. Grey-pink with dark grey-green fine grained mafic inclusions, mid-way, brecciated quartz veins with embedded quartz crystals, clay alteration, more mafic
	NB07-33D	45 32' 38.3" N / 66 42' 18.3" W	rhyolite-more felsic and pink	
	McDougal Brook	NB07-34A	45 32' 38.3" N / 66 42' 18.3" W	rhyolite-more felsic and pink
		NB07-34B	45 32' 38.3" N / 66 42' 18.3" W	rhyolite-more felsic and pink
		NB07-34C	45 32' 38.3" N / 66 42' 18.3" W	rhyolite-more felsic and pink
		NB07-35A	45 32' 38.3" N / 66 42' 18.3" W	rhyolite-more felsic and pink
		NB07-35B	45 32' 38.3" N / 66 42' 18.3" W	rhyolite-more felsic and pink
		NB07-35C	45 33' 03.3" N / 66 41' 51.5" W	rhyolite
		NB07-35D	45 33' 03.3" N / 66 41' 51.5" W	rhyolite
		NB07-35E	45 34' 22.6" N / 66 34' 43.9" W	weakly vesicular dark grey andesite or basalt
		NB07-35F	45 34' 22.6" N / 66 34' 43.9" W	weakly vesicular dark grey andesite or basalt
		NB07-36	45 34' 22.6" N / 66 34' 43.9" W	weakly vesicular dark grey andesite or basalt
		NB07-37	45 34' 15.9" N / 66 36' 52.7" W	phyric rhyolite
		NB07-37A	45 34' 15.9" N / 66 36' 52.7" W	phyric rhyolite
		NB07-37B	45 34' 15.9" N / 66 36' 52.7" W	phyric rhyolite
NB07-101		45 28' 06.8" N / 66 46' 30.5" W	granite	
NB07-102	45 28' 06.8" N / 66 46' 30.5" W	granite		
NB07-103	45 28' 06.8" N / 66 46' 30.5" W	granite		

Table 8.2.1. Continued 1

Formation	Unit	Sample	Coordinates	Description
Pisakhegan	Soeth Oromocto	NB07-38A	45 34' 22.6" N / 66 34' 43.9" W	vesicular basalt
		NB07-38B	45 34' 22.6" N / 66 34' 43.9" W	vesicular basalt
		NB07-38C	45 34' 22.6" N / 66 34' 43.9" W	vesicular basalt
		NB07-71	45 33' 25.7" N / 66 36' 01.8" W	vesicular basalt -- deeply weathered reddish-brown
		NB07-72	45 33' 25.7" N / 66 36' 01.8" W	vesicular basalt -- deeply weathered reddish-brown
	Bailey Rock Rhyolite	NB07-39	45 34' 15.9" N / 66 36' 52.7" W	rhyolite
		NB07-73	45 34' 59.0" N / 66 35' 16.8" W	rhyolite
		NB07-77 ¹	45 33' 49.4" N / 66 40' 03.7" W	rhyolitic and basaltic boulders
		NB07-78 ¹	45 33' 49.4" N / 66 40' 03.7" W	rhyolitic and basaltic boulders
		NB07-79 ¹	45 33' 49.4" N / 66 40' 03.7" W	rhyolitic and basaltic boulders
	Albert	NB07-40	45 49' 29.2" N / 65 03' 12.3" W	shale with fish scales
		NB07-41	45 49' 29.2" N / 65 03' 12.3" W	siltstone
	Little Mount Pleasant	NB07-42	45 29' 34.6" N / 66 44' 23.9" W	porphyritic rhyolite
		NB07-43	45 29' 41.2" N / 66 44' 58.0" W	quartz-feldspar porphyry with flow-banded rhyolite
		NB07-97	45 25' 01.1" N / 66 47' 54.5" W	rhyolite
		NB07-98	45 25' 01.1" N / 66 47' 54.5" W	rhyolite
		NB07-99	45 25' 26.8" N / 66 46' 44.3" W	rhyolite
		NB07-100	45 25' 26.8" N / 66 46' 44.3" W	rhyolite
		NB07-104	45 28' 09.5" N / 66 44' 05.3" W	rhyolite
		NB07-105	45 28' 12.0" N / 66 44' 10.9" W	quartz-feldspar porphyry
		NB07-106	45 28' 12.0" N / 66 44' 10.9" W	quartz-feldspar porphyry
		NB07-107	45 27' 56.2" N / 66 44' 53.5" W	rhyolite
	Seelys	NB07-44	45 29' 52.5" N / 66 44' 58.0" W	rhyolitic boulders
		NB07-45	45 29' 52.5" N / 66 44' 58.0" W	rhyolitic boulders
		NB07-46	45 29' 54.0" N / 66 44' 57.7" W	rhyolitic boulders
		NB07-47	45 29' 57.8" N / 66 44' 58.1" W	rhyolitic boulders
		NB07-49	45 30' 30.0" N / 66 42' 25.1" W	rhyolitic boulders
		NB07-50	45 30' 36.3" N / 66 43' 12.2" W	rhyolitic boulders
		NB07-51	45 30' 36.3" N / 66 43' 12.2" W	rhyolitic boulders
		NB07-52 ¹	45 30' 31.3" N / 66 42' 03.0" W	rhyolitic boulders
		NB07-80	45 32' 33.9" N / 66 42' 28.9" W	rhyolitic boulders
		NB07-81	45 32' 33.9" N / 66 42' 28.9" W	rhyolitic boulders
		NB07-82	45 32' 17.1" N / 66 42' 44.3" W	rhyolitic boulders
		NB07-83	45 32' 15.5" N / 66 42' 45.7" W	rhyolitic boulders
		NB07-84	45 32' 15.5" N / 66 42' 45.7" W	rhyolitic boulders
		NB07-85	45 31' 44.2" N / 66 43' 36.1" W	rhyolitic boulders
NB07-86		45 29' 35.8" N / 66 46' 27.5" W	rhyolitic boulders	
NB07-87	45 29' 35.8" N / 66 46' 27.5" W	rhyolitic boulders		
NB07-89	45 28' 49.7" N / 66 50' 34.7" W	rhyolitic boulders		
NB07-90	45 28' 49.7" N / 66 50' 34.7" W	rhyolitic boulders		

Table 8.2.1. Continued 2

Formation	Unit	Sample	Coordinates	Description	
Paskabegan	Souiliar Mountain	NB07-48	45 30' 31.3" N / 66 40' 54.2" W	rhyolite	
		NB07-53	45 30' 42.4" N / 66 40' 42.7" W	rhyolite	
		NB07-54	45 30' 42.4" N / 66 40' 42.7" W	rhyolite	
		NB07-55	45 31' 14.2" N / 66 40' 16.6" W	basalt / andesite	
		NB07-56	45 31' 14.2" N / 66 40' 16.6" W	basalt / andesite	
		NB07-57	45 31' 14.2" N / 66 40' 16.6" W	basalt / andesite	
		NB07-58	45 31' 14.2" N / 66 40' 16.6" W	basalt / andesite	
		NB07-59	45 31' 14.2" N / 66 40' 16.6" W	basalt / andesite	
		NB07-60	45 31' 14.2" N / 66 40' 16.6" W	basalt / andesite	
		NB07-61	45 31' 14.2" N / 66 40' 16.6" W	basalt / andesite	
		NB07-62	45 31' 06.4" N / 66 40' 18.5" W	basalt / andesite with sulphides	
		NB07-63	45 31' 06.4" N / 66 40' 18.5" W	basalt / andesite with sulphides	
		NB07-64	45 30' 47.7" N / 66 40' 36.5" W	rhyolite	
		NB07-65	45 30' 29.3" N / 66 40' 31.7" W	rhyolite	
		NB07-66	45 30' 28.4" N / 66 40' 33.9" W	rhyolite	
		NB07-67	45 30' 07.7" N / 66 40' 20.4" W	basalt / andesite rubble	
		NB07-68	45 30' 04.6" N / 66 40' 11.5" W	basalt / andesite boulders	
		NB07-69	45 30' 05.4" N / 66 40' 11.1" W	basalt / andesite boulders	
		NB07-70	45 30' 02.6" N / 66 40' 09.5" W	basal unconformity-related slate/rhyolite conglomerate	
		NB07-91	45 28' 17.0" N / 66 50' 17.4" W	basaltic stream boulder	
	NB07-92	45 28' 00.4" N / 66 49' 59.2" W	rhyolite		
	NB07-93	45 28' 00.4" N / 66 49' 59.2" W	rhyolite / andesite (dark)		
	NB07-94	45 27' 50.4" N / 66 50' 01.8" W	rhyolite? subcrop / boulders		
	NB07-95	45 27' 50.4" N / 66 50' 01.8" W	rhyolite? subcrop / boulders		
	NB07-96	45 27' 50.4" N / 66 50' 01.8" W	rhyolite? subcrop / boulders		
		Kleef	NB07-74	45 33' 59.4" N / 66 40' 35.7" W	basaltic boulders
			NB07-75	45 34' 02.7" N / 66 40' 31.1" W	basaltic, feldspar-phyrnic boulders
			NB07-76	45 34' 02.7" N / 66 40' 31.1" W	basaltic, feldspar-phyrnic boulders
		Rothea*	NB07-108	45 34' 48.3" N / 66 33' 23.2" W	highly altered rhyolite, pyroclastics, or basalt?

Table 8.2.1. Continued 3.

Albert (n=2)		Big Scott Mountain/ Seebys (n=16)																
	40	41	32a	32b	32c	32d	32f	32k	32l	32m*	32n	32o	32p	32q	33a*	33b	33c	33d
SiO ₂ (wt. %)	35.54	31.13	74.24	73.73	73.80	72.43	72.86	73.63	74.92	74.00	73.42	73.60	73.96	72.92	74.45	73.11	73.82	73.83
TiO ₂	0.42	0.47	0.32	0.36	0.36	0.37	0.36	0.35	0.34	0.37	0.37	0.35	0.34	0.35	0.30	0.32	0.31	0.37
Al ₂ O ₃	7.89	8.33	12.39	12.54	12.70	12.27	13.06	12.21	11.95	12.11	12.62	12.68	12.91	12.84	12.52	12.79	13.11	12.58
Fe ₂ O ₃	4.44	3.61	2.34	2.50	2.62	2.51	2.46	2.55	2.49	1.81	2.61	2.34	2.40	2.42	2.33	2.33	2.33	2.43
MnO	0.14	0.08	0.03	0.03	0.03	0.03	0.03	0.03	0.03	0.03	0.04	0.03	0.04	0.03	0.03	0.03	0.03	0.03
MgO	7.14	3.46	0.41	0.49	0.49	0.50	0.46	0.46	0.42	0.32	0.63	0.41	0.49	0.45	0.38	0.42	0.43	0.45
CaO	20.90	15.88	0.50	0.62	0.57	0.64	0.54	0.57	0.53	0.54	0.64	0.51	0.59	0.55	0.46	0.34	0.32	0.44
Na ₂ O	1.26	1.93	1.64	1.62	1.78	1.92	1.25	1.81	2.09	1.55	1.88	1.58	1.49	1.31	1.53	1.26	1.20	1.54
K ₂ O	1.41	1.30	6.13	6.29	5.85	5.39	7.12	5.60	5.30	6.79	5.63	6.69	6.88	7.29	6.55	7.25	7.45	6.36
P ₂ O ₅	0.15	0.10	0.06	0.07	0.08	0.06	0.07	0.07	0.06	0.07	0.07	0.07	0.06	0.07	0.05	0.06	0.06	0.08
F										0.05					0.03			
LOI	23.90	15.10	1.40	1.60	2.10	1.80	1.80	1.80	1.70	1.10	1.90	1.50	1.90	1.60	1.50	1.50	2.10	2.00
Total	103.19	101.38	99.47	99.85	100.40	97.91	100.01	99.08	99.83	99.73	99.81	99.85	100.06	99.83	99.93	99.43	100.36	100.11
Cr(ppm)	44	45	1.0	1.0	8.0	1.0	7.0	9.0	4.0	-	7.0	5.0	5.0	-	-	-	2.0	3.0
Ni	29	24	-	-	1.0	-	20	21	7.0	-	2.0	-	2.0	-	-	1.0	1.0	6.0
Co	7.0	3.0	92	91	118	102	144	78	68	2.0	118	95	63	141	2.0	122	98	113
V	65	45	12	13	11	16	14	11	16	15	16	18	8.0	18	9.0	15	16	18
Pb	-	1.0	25	24	26	26	33	24	23	16	32	27	27	28	16	27	29	30
Zn	50	42	43	42	48	47	45	43	41	50	44	42	42	42	50	43	40	41
Sn										5.0					6.0			
W										3.1					4.4			
Sb										7.0					8.5			
Rb	45	40	290	311	290	278	348	272	267	314	297	313	353	360	318	352	365	312
Cs			14	9.0	10	3.0	7.0	7.0	11	20	12	10	9.0	13	20	12	10	12
Ba	615	619	514	513	486	411	609	460	433	634	475	563	553	610	537	582	588	499
Sr	684	714	150	144	168	167	141	164	154	132	160	146	135	148	133	138	135	143
Tl										4.0					3.5			
Ga	9.0	8.0	15	15	17	19	19	16	16	15	16	15	15	16	15	16	15	15
Ta										2.14					2.24			
Nb	7.00	8.00	21.0	23.0	22.0	22.0	24.0	21.0	21.0	20.8	21.0	22.0	22.0	22.0	20.7	22.0	23.0	22.0
Hf										7.9					7.6			
Zr	98.0	133	281	299	308	310	317	297	287	306	274	298	288	300	293	280	282	308
Y	27.0	29.0	43.0	46.0	43.0	45.0	50.0	46.0	43.0	45.1	43.0	45.0	48.0	44.0	49.8	48.0	45.0	47.0
Th	-	-	31.0	35.0	35.0	30.0	36.0	33.0	35.0	28.5	34.0	32.0	33.0	31.0	30.0	33.0	34.0	34.0
U	-	-	10.0	13.0	14.0	10.0	14.0	13.0	11.0	5.25	13.0	10.0	14.0	13.0	4.55	13.0	12.0	14.0
La	-	34.0	38.0	76.0	60.0	48.0	105.0	38.0	56.0	51.0	38.0	38.0	42.0	56.0	60.6	45.0	62.0	84.0
Ce	54.0	71.0								101					106			
Pr										11.5					12.8			
Nd	31.0	43.0	45.0	36.0	54.0	52.0	53.0	38.0	32.0	42.5	43.0	46.0	43.0	44.0	45.0	50.0	42.0	52.0
Sm										8.59					9.05			
Eu										1.03					1.12			
Gd										7.48					8.24			
Tb										1.33					1.50			
Dy										8.21					9.16			
Ho										1.64					1.82			
Er										4.89					5.39			
Ym										0.755					0.799			
Yb										4.79					5.13			
Lu										0.706					0.745			

Table 8.2.2. Major and trace element whole-rock data from Piskahegan. Major elements and compounds were analyzed using XRF. * Representative samples were analyzed for trace elements concentrations via ICP-MS. Values are not normalized to 100%, - symbol indicates no data available or below detection limits.

	KleeF (n=3)			McDougall Brook Granite (n=20)															
	Y4*	Y5	Y6*	34a	34b	34c	35a*	35b	35c	35d	35e	36	37	37a	37b	38a	38b		
SiO ₂ (wt. %)	47.87	47.57	45.45	68.14	66.78	67.70	75.73	74.79	76.85	74.91	75.84	68.47	66.21	66.20	66.31	55.91	55.84		
TiO ₂	3.12	3.04	2.79	0.54	0.64	0.53	0.17	0.18	0.18	0.19	0.19	0.58	0.77	0.79	0.77	1.51	1.52		
Al ₂ O ₃	14.65	14.53	16.49	13.61	13.68	13.53	11.80	11.93	11.89	12.01	11.95	13.31	13.29	13.42	13.37	15.70	15.79		
Fe ₂ O ₃	13.90	14.71	13.41	4.18	4.68	4.14	1.64	1.60	1.33	1.59	1.37	4.28	5.13	4.75	4.62	8.42	8.24		
MnO	0.18	0.28	0.26	0.10	0.10	0.11	0.05	0.05	0.04	0.06	0.04	0.10	0.09	0.08	0.08	0.14	0.13		
MgO	3.92	3.82	4.33	0.83	0.84	0.88	0.33	0.32	0.30	0.30	0.28	0.75	1.54	1.50	1.49	3.46	3.35		
CaO	7.99	7.35	7.03	1.75	2.24	2.23	0.81	1.33	0.38	1.13	0.86	1.71	1.99	2.18	2.41	5.48	4.89		
Na ₂ O	3.33	3.03	3.81	2.86	2.70	2.28	1.57	1.65	1.32	1.48	1.34	1.23	1.01	2.62	2.65	3.24	3.83		
K ₂ O	1.26	1.18	0.98	5.56	5.17	5.36	6.02	5.72	5.76	5.79	5.93	5.82	6.03	4.31	4.42	2.99	3.10		
P ₂ O ₅	1.01	1.13	1.14	0.14	0.19	0.14	0.02	0.03	0.03	0.03	0.03	0.17	0.20	0.20	0.19	0.50	0.50		
F							0.03												
LOI	2.40	3.50	4.20	2.40	3.00	3.50	1.70	2.50	1.60	2.30	1.80	3.70	4.00	4.20	4.00	2.70	2.70		
Total	99.63	100.13	99.89	100.10	100.02	100.39	99.87	100.10	99.68	99.79	99.63	100.12	100.26	100.24	100.30	100.05	99.89		
Cr (ppm)	30	6.0	20	3.0	8.0	5.0	-	-	5.0	2.0	1.0	6.0	13	10	11	20	22		
Ni	-	17	-	5.0	-	3.0	-	4.0	-	3.0	-	2.0	7.0	8.0	3.0	24	20		
Co	29	32	31	164	131	160	1.0	178	180	184	151	143	118	118	110	107	125		
V	245	205	195	31	25	32	-	12	12	7	9	33	59	65	69	140	142		
Pb	13	12	30	28	23	31	19	39	27	28	27	39	15	11	14	3.0	-		
Zn	130	162	200	77	83	76	40	47	44	54	46	78	71	62	60	95	94		
Sm	2.0		2.0				3.0												
W	0.70		1.00				1.2												
Sb	8.0		3.4				3.4												
Rb	30	29	24	163	154	175	203	200	203	208	210	215	309	213	212	62	66		
Cs	2.0		3.9	14	10	12	12	14	15	16	17	8.0	14	13	8.0	21	24		
Ba	488	672	449	678	733	563	119	130	144	133	175	731	562	396	427	713	737		
Sr	640	555	629	161	132	117	67	78	76	83	80	90	126	127	130	805	950		
Tl	0.23		0.31				1.6												
Ga	25	21	27	17	18	17	15	17	16	17	14	14	18	18	17	17	19		
Ta	2.27		2.32				1.32												
Nb	34.7	38.0	37.4	18.0	19.0	18.0	15.3	17.0	16.0	18.0	16.0	18.0	19.0	19.0	18.0	18.0	18.0		
Hf	9.8		10.5				6.20												
Zr	478	477	531	480	499	463	213	218	217	225	229	481	271	269	271	339	343		
Y	57.4	64.0	62.7	39.0	39.0	41.0	34.9	40.0	38.0	39.0	36.0	37.0	46.0	54.0	60.0	39.0	38.0		
Th	3.85	9.00	4.65	26.0	30.0	28.0	21.9	28.0	28.0	30.0	30.0	31.0	26.0	28.0	30.0	-	-		
U	1.20		0.850	9.00	13.0	13.0	5.31	12.0	10.0	12.0	10.0	14.0	12.0	14.0	13.0	-	-		
La	43.6	83.0	48.3	61.0	57.0	81.0	88.8	73.0	101.0	81.0	96.0	70.0	57.0	43.0	84.0	48.0	44.0		
Ce	91.6	117	101				178												
Pr	12.1		13.4				19.2												
Nd	51.2	60.0	56.9	64.0	59.0	57.0	62.2	69.0	72.0	75.0	59.0	62.0	46.0	61.0	53.0	49.0	63.0		
Sm	13.0		14.1				11.5												
Eu	4.29		4.42				0.603												
Gd	12.7		13.8				8.92												
Tb	1.95		2.20				1.31												
Dy	10.7		11.9				7.21												
Ho	2.04		2.25				1.36												
Er	5.87		6.54				4.00												
Tm	0.844		0.927				0.594												
Yb	5.14		5.60				3.75												
Lu	0.748		0.807				0.542												

Table 8.2.2. Continued 1.

	McDougall Brook Granite (n=20)					Mount Pleasant Mine Site (n=1)*	Scoullar Mountain (n=19)								
	38c	38c2	39	01	102	103	48*	53*	54	55	56*	57	58	60	61*
							88								
SiO ₂ (wt %)	55.15	55.05	52.01	69.00	68.60	74.88	75.44	75.18	74.75	56.35	56.65	51.41	56.33	56.43	55.60
TiO ₂	1.53	1.53	0.41	0.51	0.53	0.04	0.16	0.16	0.16	1.26	1.26	1.65	1.24	1.27	1.28
Al ₂ O ₃	15.85	15.85	12.92	13.73	14.01	12.73	12.21	12.11	12.09	15.04	15.02	14.92	14.91	15.03	15.06
Fe ₂ O ₃	8.53	8.53	3.13	2.99	3.13	1.68	1.85	1.63	1.64	7.68	7.55	9.79	7.77	7.75	7.78
MnO	0.14	0.14	0.03	0.07	0.07	0.04	0.05	0.05	0.05	0.14	0.13	0.16	0.12	0.13	0.12
MgO	3.43	3.55	0.30	0.71	0.65	0.05	0.28	0.29	0.29	3.08	3.17	4.46	3.57	3.05	3.38
CaO	5.78	5.75	0.43	1.88	1.78	0.37	0.54	0.80	1.01	6.57	6.51	6.24	5.95	6.58	6.25
Na ₂ O	3.48	3.44	3.02	3.11	2.97	3.34	2.73	2.25	2.55	2.10	2.17	2.41	2.15	2.09	1.92
K ₂ O	3.01	2.90	5.40	4.99	5.26	4.95	5.10	5.36	5.24	2.96	2.94	2.49	3.00	2.91	3.16
P ₂ O ₅	0.50	0.50	0.11	0.14	0.14	0.01	0.03	0.03	0.03	0.30	0.30	0.48	0.30	0.31	0.31
F						0.52	0.09	0.07							
LOI	3.00	2.50	2.20	2.10	2.10	0.80	1.20	2.20	1.70	5.30	4.80	6.80	4.80	5.00	5.40
Total	100.40	99.75	99.96	99.23	99.24	99.41	99.67	100.14	99.51	100.78	100.50	100.81	100.15	100.55	100.25
Cr(ppm)	26	25	5.0	20	8.0	30	20	30	12	78	90	58	81	79	80
Ni	20	23	2.0	7.0	3.0	-	-	-	-	17	-	29	15	20	-
Co	102	92	138	8.0	6.0	-	1.0	1.0	-	22	23	27	24	25	23
V	145	150	15	26	33	-	7.0	6.0	8.0	156	165	165	147	150	159
Pb	4.0	5.0	44	24	27	19	10	20	18	16	12	11	17	21	12
Zn	95	94	49	64	60	50	50	50	48	78	80	102	79	80	80
Sn						22	5.0	5.0			2.0				2.0
W						7.1	3.5	1.1			1.1				2.3
Sh						1.9	2.4	2.7			2.0				2.4
Rb	61	58	226	182	197	-	253	283	259	84	76	123	88	81	97
Cs	24	18	5.0			20	6.0	7.3			4.8				8.7
Ba	751	716	495	667	787	17	85	87	81	567	544	549	606	568	572
Sr	835	833	102	109	105	6	20	19	30	347	301	360	359	352	281
Tl						9.4	2.3	2.8			0.87				1.2
Ga	20	19	20	18	18	35	21	21	18	18	20	19	18	18	20
Ta						17.2	2.24	2.14			0.990				1.02
Nb	21.0	18.0	21.0	15.0	16.0	67.5	23.8	23.7	23.0	14.0	13.3	20.0	13.0	12.0	13.4
Hf						9.30	6.70	6.60			6.10				6.10
Zr	341	337	354	340	363	130	213	213	194	255	272	304	248	254	272
Y	38.0	38.0	69.0	35.0	37.0	159.0	79.5	67.2	61.0	37.0	33.9	43.0	36.0	35.0	34.8
Th	2.00	-	32.0	23.0	29.0	47.4	28.4	28.1	35.0	9.00	9.40	9.00	11.0	11.0	9.41
Li	-	-	15.0	10.0	12.0	31.9	5.10	5.10	15.0	4.00	2.91		3.00	4.00	2.80
La	50.0	53.0	117	66.0	61.0	51.6	107	101	89.0	40.0	39.5	19.0	48.0	66.0	39.9
Ce				139	144	123	160	147	146	120	78.2	76.0	106	91.0	79.1
Pr						14.9	22.1	21.6			9.42				9.36
Nd	52.0	44.0	85.0	53.0	58.0	57.9	77.4	73.6	68.0	64.0	35.7	45.0	49.0	37.0	34.7
Sm						13.9	15.9	14.9			7.67				7.61
Eu						0.049	0.616	0.546			1.97				2.11
Gd						13.3	14.9	13.4			7.05				7.25
Tb						2.87	2.44	2.12			1.08				1.16
Dy						21.3	14.1	11.9			6.15				6.62
Ho						5.21	2.74	2.29			1.18				1.27
Er						18.6	7.88	6.72			3.53				3.74
Tm						3.26	1.14	1.00			0.512				0.541
Yb						23.2	6.93	6.29			3.22				3.37
Lu						3.72	0.984	0.906			0.505				0.490

Table 8.2.2. Continued 2.

	Secullar Mountain (n=19)							South Oromocto Andesite (n=2)	
	62	63	64	66*	67	94	96	71	72
SiO ₂ (wt %)	61.32	41.54	73.82	75.63	60.02	62.51	60.21	53.73	52.37
TiO ₂	0.50	1.31	0.16	0.17	1.26	1.22	1.21	1.52	1.52
Al ₂ O ₃	11.06	15.75	11.86	11.86	14.77	14.76	14.85	15.91	15.94
Fe ₂ O ₃	7.25	7.73	1.76	1.84	7.09	6.13	6.83	7.96	7.89
MnO	0.17	0.17	0.05	0.07	0.13	0.11	0.13	0.16	0.17
MgO	2.66	1.94	0.26	0.32	2.77	1.74	2.16	5.12	4.70
CaO	6.59	7.44	0.86	0.47	3.24	3.22	3.13	5.60	8.36
Na ₂ O	0.77	4.83	2.92	3.15	3.33	3.47	3.86	3.84	3.03
K ₂ O	2.24	2.19	5.05	4.70	3.71	4.03	3.73	2.33	1.57
P ₂ O ₅	0.10	0.48	0.03	0.03	0.33	0.47	0.44	0.49	0.49
F				0.02					
LOI	8.50	-	1.20	0.90	3.00	1.00	2.70	3.20	3.80
Total	101.17	83.39	97.97	99.15	99.64	98.66	99.25	99.86	99.83
Cr(ppm)	68	82	26	30	24	19	26	58	61
Ni	45	15	2.0	-	7.0	7.0	8.0	42	38
Co	29	31	1.0	1.0	20	15	13	24	24
V	116	150	8.0	9.0	129	91	98	162	163
Pb	39	31	33	14	8.0	18	17	-	13
Zn	112	101	51	60	80	88	91	95	92
Sn				5.0					
W				1.3					
Sb				2.5					
Rb	134	112	246	251	126	183	147	39	25
Cs				5.0					
Ba	281	701	85	96	759	901	899	659	388
Sr	105	359	44	28	407	223	360	936	707
Tl				2.7					
Ga	21	19	16	19	18	17	18	17	19
Ta				2.14					
Nb	15.0	15.0	23.0	23.3	16.0	19.0	19.0	20.0	20.0
Hf				6.40					
Zr	142	142	184	209	305	448	435	300	298
Y	29.0	47.0	65.0	75.9	38.0	43.0	46.0	35.0	34.0
Th	19.0	12.0	32.0	27.5	12.0	20.0	14.0	-	3.00
U	7.00	17.0	12.0	5.31	3.00	12.0	6.00	-	-
La	48.0	37.0	92.0	109	48.0	83.0	71.0	42.0	58.0
Ce	56.0	106	165	157	83.0	109	127	72.0	81.0
Pr				22.9					
Nd	23.0	49.0	66.0	80.2	49.0	44.0	59.0	37.0	39.0
Sm				16.7					
Eu				0.583					
Gd				15.1					
Tb				2.41					
Dy				13.4					
Ho				2.52					
Er				7.40					
Tm				1.09					
Yb				6.76					
Lu				0.991					

Table 8.2.2. Continued 3.

	Cherry Hill NB07-18 (n=11)											Harvey Mountain- NB07-31(n=13)							
	1	2	3	4	5	6	7	8	9	10	11	1	2	3	4	5	6	7	8
K ₂ O	6.3	6.0	6.4	6.2	6.6	5.9	6.8	6.3	6.4	6.4	6.1	6.5	6.6	6.9	5.6	6.7	6.5	6.4	7.0
Na ₂ O	3.1	2.9	3.3	0.66	3.0	3.1	3.1	3.2	3.3	3.1	3.2	2.5	2.7	2.6	2.5	2.8	2.7	2.6	3.4
Al ₂ O ₃	15	14	15	15	15	14	15	15	16	15	15	15	15	15	13	14	14	14	17
MnO	0.02	-	-	0.01	0.03	0.01	0.02	0.01	0.01	-	-	0.06	0.06	0.04	0.09	0.05	0.03	0.04	0.03
CaO	0.38	0.22	0.40	0.42	0.26	0.32	0.40	0.32	0.47	0.18	0.37	0.21	0.33	0.39	0.31	0.15	0.17	0.18	0.88
TiO ₂	0.10	0.02	0.11	0.02	0.04	0.11	0.02	0.01	0.07	0.06	0.12	0.04	0.03	-	0.04	0.01	0.04	0.05	0.08
SrO ₂	75	76	74	77	74	75	74	74	73	75	75	75	75	74	78	75	76	76	71
FeO	0.30	0.54	0.30	0.34	1.07	0.64	1.10	0.27	0.15	0.54	0.37	0.71	0.58	0.82	0.88	0.97	0.72	0.95	0.66
SO ₃	0.01	0.01	0.01	0.01	-	0.02	0.01	0.01	0.04	-	0.01	0.01	0.01	0.04	0.04	-	0.03	-	0.03
Cr ₂ O ₃	-	-	-	-	-	-	-	-	-	-	-	-	0.02	-	-	-	-	-	-
MgO	-	-	-	-	-	-	-	-	-	-	-	-	0.01	0.01	-	-	-	-	-
NiO	0.01	-	0.01	0.02	-	0.02	-	-	0.01	-	0.02	-	-	-	-	0.02	0.01	-	0.01
Total	100	100	100	100	100	100	100	100	100	100	100	100	100	100	100	100	100	100	100
Cl	0.16	0.17	0.17	0.18	0.22	0.14	0.21	0.21	0.18	0.18	0.15	0.05	0.02	0.07	0.01	0.01	0.02	0.02	0.19
Al	0.10	0.09	0.10	0.09	0.09	0.09	0.09	0.10	0.10	0.10	0.10	0.10	0.10	0.09	0.08	0.09	0.09	0.09	0.11
Mn	-	-	-	-	-	-	-	-	-	-	-	-	-	-	-	-	-	-	-
Ca	-	-	-	-	-	-	-	-	-	-	-	-	-	-	-	-	-	-	0.01
Ti	-	-	-	-	-	-	-	-	-	-	-	-	-	-	-	-	-	-	-
F	-	-	-	-	0.01	-	-	0.01	-	-	-	0.02	0.02	0.02	0.02	0.03	0.03	0.03	0.03
Si	0.41	0.41	0.40	0.41	0.41	0.41	0.41	0.40	0.40	0.41	0.41	0.41	0.41	0.41	0.42	0.41	0.41	0.41	0.39
Fe	-	-	-	0.01	-	-	-	-	-	-	-	-	-	-	-	-	-	-	-
S	-	-	-	-	-	-	-	-	-	-	-	-	-	-	-	-	-	-	-
Cr	-	-	-	-	-	-	-	-	-	-	-	-	-	-	-	-	-	-	-
Mg	-	-	-	-	-	-	-	-	-	-	-	-	-	-	-	-	-	-	-
Ni	-	-	-	-	-	-	-	-	-	-	-	-	-	-	-	-	-	-	-
Total	0.58	0.58	0.59	0.59	0.59	0.58	0.59	0.59	0.59	0.56	0.58	0.58	0.58	0.59	0.57	0.58	0.58	0.58	0.60

Table 8.2.3. Harvey major and trace element data analyzed by electron microprobe of melt inclusions hosted in quartz phenocrysts. – symbol indicate no data available.

Harvey Mountain- NB07-31(n=13)						York Mills NB07-30 (n=7)						
	9	10	11	12	13	1	2	3	4	5	6	7
K ₂ O	6.6	4.9	2.6	0.12	0.25	6.1	5.0	6.0	6.2	6.0	6.5	9.3
N ₂ O	2.7	2.3	0.03	0.05	0.13	3.3	4.3	3.3	3.4	3.3	3.4	3.5
Al ₂ O ₃	15	12	3.3	0.6	1.0	15	19	15	15	15	16	18
MnO	0.07	0.17	-	-	0.02	-	0.06	0.02	-	0.02	0.04	0.01
CaO	0.19	0.27	0.01	0.01	0.01	0.69	2.9	0.53	0.35	0.48	0.70	1.6
TiO ₂	-	-	-	-	0.04	0.06	0.31	0.05	0.00	0.07	0.08	0.02
SiO ₂	75	78	94	99	98	73	66	74	74	73	73	66
FeO	0.71	2.03	0.06	0.03	0.17	1.3	1.9	1.3	0.31	1.43	0.36	0.16
SO ₃	0.01	0.01	-	0.02	-	0.01	0.11	0.02	0.03	-	0.02	0.57
Cr ₂ O ₃	0.01	-	-	-	0.01	0.01	0.01	-	-	-	-	-
MgO	-	-	-	-	-	0.01	0.11	0.01	-	0.02	-	0.02
NiO	0.01	0.02	-	0.13	-	0.01	-	0.03	0.01	-	0.04	-
Total	100	100	100	100	100	100	-	100	100	100	100	100
Cl	0.03	0.12	0.00	-	-	0.16	0.73	0.15	0.15	0.15	0.16	0.28
Al	0.10	0.08	0.02	-	0.01	0.10	0.13	0.10	0.10	0.10	0.10	0.12
Mn	-	-	-	-	-	-	-	-	-	-	-	-
Ca	-	-	-	-	-	-	0.02	-	-	-	-	0.01
Ti	-	-	-	-	-	-	-	-	-	-	-	-
F	0.02	0.02	-	-	-	-	0.03	0.01	0.01	-	0.02	0.01
Si	0.41	0.42	0.48	0.50	0.49	0.40	0.37	0.40	0.41	0.40	0.40	0.37
Fe	-	0.01	-	-	-	0.01	0.01	0.01	-	0.01	-	-
S	-	-	-	-	-	-	-	-	-	-	-	-
Cr	-	-	-	-	-	-	-	-	-	-	-	-
Mg	-	-	-	-	-	-	-	-	-	-	-	-
Ni	-	-	-	-	-	-	-	-	-	-	-	-
Total	0.58	0.57	0.52	0.50	0.50	0.59	0.61	0.59	0.59	0.59	0.59	0.62

Table 8.2.3. Continued 1.

Piskahegan																				
	Bailey Rock- NB07-39 (n=12)												Bailey Rock NB07-78 (n=8)							
	1	2	3	4	5	6	7	8	9	10	11	12	1	2	3	4	5	6	7	8
K ₂ O	6.3	6.4	6.8	6.3	6.5	6.5	7.0	7.4	6.3	6.5	6.5	2.2	4.4	7.4	6.1	6.0	6.6	6.3	6.1	5.9
Na ₂ O	2.9	2.9	2.9	2.9	2.7	3.2	2.9	2.8	2.7	2.7	2.7	0.42	1.3	3.0	2.8	3.8	3.1	3.1	3.1	3.1
Al ₂ O ₃	15	14	14	14	14	15	14	15	14	14	14	15	15	15	14	14	15	15	15	15
MnO	0.02	0.01	0.04	0.02	0.03	0.03	0.03	0.03	0.02	0.05	0.01	0.03	0.06	0.03	0.03	0.01	0.03	0.01	0.02	0.05
CaO	0.42	0.40	0.41	0.32	0.32	0.08	0.06	0.08	0.35	0.42	0.20	0.23	1.6	0.86	0.42	0.61	0.82	0.31	0.42	0.81
TiO ₂	0.21	0.12	0.12	0.16	0.23	0.08	0.14	0.24	0.17	0.13	0.17	0.11	0.27	0.12	0.11	0.13	0.17	0.18	0.14	0.15
SiO ₂	75	76	75	75	76	75	74	74	77	75	76	82	74	73	77	74	74	75	75	75
FeO	0.39	0.28	0.28	1.4	0.28	0.21	0.86	0.72	0.29	0.31	0.31	0.31	3.15	0.61	0.15	0.39	0.26	0.25	0.32	0.25
SO ₃	0.01	-	-	0.02	-	0.01	-	0.01	-	0.03	0.01	0.01	-	0.03	0.04	-	0.04	0.02	0.01	0.01
Cr ₂ O ₃	-	-	-	-	-	-	-	-	-	-	-	-	-	-	0.01	0.01	-	-	-	-
MgO	-	-	-	0.03	-	-	0.25	0.06	0.01	-	-	-	0.18	0.01	-	0.02	-	-	-	-
NiO	0.04	-	-	-	0.02	-	-	0.02	-	0.02	0.03	-	-	0.02	0.01	0.02	0.03	0.01	-	0.02
Total	100	100	100	100	100	100	100	100	100	100	100	100	100	100	100	100	100	100	100	100
Cl	0.11	0.08	0.12	0.15	0.10	0.14	0.13	0.11	0.10	0.10	0.07	0.08	0.13	0.14	0.14	0.14	0.17	0.13	0.12	0.14
Al	0.09	0.09	0.09	0.09	0.09	0.09	0.09	0.09	0.09	0.09	0.09	0.09	0.10	0.10	0.09	0.09	0.10	0.10	0.10	0.10
Mn	-	-	-	-	-	-	-	-	-	-	-	-	-	-	-	-	-	-	-	-
Ca	-	-	-	-	-	-	-	-	-	-	-	-	0.01	0.01	-	-	-	-	-	-
Ti	-	-	-	-	-	-	-	-	-	-	-	-	-	-	-	-	-	-	-	-
F	0.02	0.00	0.01	-	-	0.02	0.01	0.02	0.02	0.01	0.00	0.01	0.01	0.02	0.01	-	0.02	0.01	0.01	0.02
Si	0.41	0.41	0.41	0.41	0.41	0.41	0.41	0.41	0.42	0.41	0.41	0.43	0.40	0.40	0.41	0.41	0.40	0.41	0.41	0.41
Fe	-	-	-	0.01	-	-	-	-	-	-	-	-	0.01	-	-	-	-	-	-	-
S	-	-	-	-	-	-	-	-	-	-	-	-	-	-	-	-	-	-	-	-
Cr	-	-	-	-	-	-	-	-	-	-	-	-	-	-	-	-	-	-	-	-
Mg	-	-	-	-	-	-	-	-	-	-	-	-	-	-	-	-	-	-	-	-
Ni	-	-	-	-	-	-	-	-	-	-	-	-	-	-	-	-	-	-	-	-
Total	0.58	0.58	0.58	0.58	0.58	0.58	0.59	0.59	0.58	0.58	0.58	0.54	0.57	0.59	0.58	0.59	0.59	0.58	0.58	0.58

Table 8.2.4. Piskahegan major and trace element data analyzed by electron microprobe of

melt inclusions hosted in quartz phenocrysts. – symbol indicate no data available.